



**POLITECNICO
DI TORINO**



MASTER'S DEGREE IN AEROSPACE ENGINEERING

MASTER THESIS

IFS OPTIMIZATION FOR JET FUEL'S SURROGATE

INTERNAL SUPERVISOR:

PROF. PASTRONE, DARIO GIUSEPPE

DIMEAS, Politecnico di Torino

EXTERNAL SUPERVISORS:

PROF. DR.-ING. HAIDN, OSKAR J.

LTF, Technische Universität München

DR. PH.D. SLAVINSKAYA, NADEZHDA A.

Gesellschaft für Anlagen- und Reaktorsicherheit

CANDIDATE:

FREILINO LUCA

student ID: s240131

Politecnico di Torino

17JULY 2019

MASTERARBEIT

Student: Freilino Luca

Supervisors: Prof. Dr.-Ing. Haidn, Oskar J.
Dr. Ph.D. Slavinskaya, Nadezhda A.

Issued: October 1, 2018

Submitted: March 31, 2019

Für diese technische Unterlage wird jeglicher Rechtsschutz in Anspruch genommen. Die dadurch begründeten Rechte, insbesondere der Vervielfältigung und Speicherung in Datenverarbeitungsanlagen bleiben, auch bei nur auszugsweiser Verwertung, vorbehalten

For this technical document any legal protection is claimed. The rights thereby justified, in particular duplication and storage in data processing systems, remain reserved, even if only for a few seconds recycling

STATEMENT OF AUTHORSHIP

I HEREBY DECLARE THAT I HAVE AUTHORED THIS THESIS INDEPENDENTLY, THAT I HAVE NOT USED OTHER THAN THE DECLARED SOURCES/RESOURCES AND THAT I HAVE EXPLICITLY MARKED ALL MATERIAL WHICH HAS BEEN QUOTED EITHER LITERALLY OR BY CONTENT FROM THE USED SOURCES. ACCORDING TO MY KNOWLEDGE, THE CONTENT OR PARTS OF THIS THESIS HAVE NOT BEEN PRESENTED TO ANY OTHER EXAMINATION AUTHORITY AND HAVE NOT BEEN PUBLISHED. I AM FULLY AWARE THAT THE WORK CAN BE CONSIDERED AS A "FAIL" IN THE EVENT OF A FALSE DECLARATION. IN CASE OF JUSTIFIED SUSPICION, THE THESIS IN DIGITAL FORM CAN BE EXAMINED WITH PROPER SOFTWARES. FOR THE COMPARISON OF MY WORK WITH EXISTING SOURCES:

☒ I AGREE TO STORAGE IN THE INSTITUTIONAL REPOSITORY TO ENABLE COMPARISON WITH FUTURE THESES SUBMITTED

☐ I DO NOT AGREE TO STORAGE IN THE REPOSITORY

FURTHER RIGHTS OF REPRODUCTION AND USAGE, HOWEVER, ARE NOT GRANTED HERE. IN ANY CASE, THE EXAMINATION AND EVALUATION OF MY WORK HAS TO BE CARRIED OUT INDIVIDUALLY AND INDEPENDENTLY FROM THE RESULTS OF THE PLAGIARISM DETECTION SERVICE.

NAME IN CAPITALS: _____

SIGN: _____

DATE AND PLACE: _____

... a chi sa di esserci stato...

URheberRECHTE ©2019
FREILINO LUCA
ALLE RECHTE VORBEHALTEN

ACKNOWLEDGMENTS

Fully aware that few lines cast out at the beginning of this work are not sufficient to summarize my period of Master Thesis and, more generally, my University's life, the idea of returning all the support I received in these years moved me to thank all the people who have manifested, in one way or another, their closeness to me. Being the acknowledgments paragraph the most personal part of a thesis, my previous idea of a detached work will be temporarily abandoned in favour of a most emotional one. Then, starting with the working sphere, my first thank goes to Dr. Nadezhda "Nadja" Slavinskaya for her closeness and her constant support, from both the academic and the personal point of view. Additionally, my personal thanks go to Prof. Dario Pastrone, who helped me in many ways during this period. Firstly, he allowed to live my German experience, which enabled me to grow as a person, and then helped me directly with the thesis drafting. Similarly, I would like to thank Prof. Dr.-Ing. Oskar Haidn, who helped me in the settling-in period at TUM university and for his precious advices. In the end, a special thank goes to the M.Sc. student Ye Hong and to the Ph.D. student Filippo Masseni. Without your precious help this thesis would not have been the same. Turning to my private sphere, I usually think that common thankful sentences may end up in the ordinary, but this time I have to disagree with myself. I do not often show my gratitude to my relatives, wrongly used to think it as granted, but I just want to say that this thesis is mostly yours. I am only a vessel driven by your sacrifices and by your aspirations. Similarly, special thanks go to my friends, to every single word, message, coffee and beer we shared in these years. In summary, I know, or better, we know, what I have been through, and I am sure I would have never got over everything without your aid and your faith. I wish you would be so kind to welcome this text as a partial compensation for everything.

ABSTRACT

In the last decades, the increasing demand for air transport, both in the military and in the civil field, has led to an exponential growth of greenhouse gases emission, which are rationally thought to play an active role in climate change. One of the most important (and promising) solution proposed to counter this notoriuos problem is the replacement of current fuels with less pollutant ones. In this perspective, the Technical University of Munich (TUM), under the exclusive patronage of DLR centre (Deutsches Zentrum für Luft- und Raumfahrt, the German Aerospace Center), has started a new research project whose purpose is to find reliable alternatives to the existent petroleum fuels. Since no such promising improvement would be achieved if the research was focused on current feedstocks, the interest is centered on renewable energy sources, whose products, even if after many different chemical processes, are the main hydrocarbons directly involved in the fuel combustion, reducing as much as possible the presence of other polluting agents, such as sulfur oxide (SO_x) and nitrogen oxide (NO_x). From this alarming context immediately flows the necessity to find a well founded solution (matematically speaking, a numerical model) to forecast the chemical and physical properties of hydrocarbons' surrogate, in order to validate them against the reference petroleum fuel's properties. In this regard, the collaboration between Polytechnic University of Turin and TUM has made possible the development of this Master Thesis, whose main aim is to find the optimal IFS (Input Formula of Surrogate) for given petroleum fuel. The strategy of IFS construction is based on the direct correlation between the synthetic petroleum fuel's specifications and the hydrocarbons' model's ones and it is used to reproduce the real fuel combustion properties. The IFS is intended to include adequate fractions of four different chemical families of hydrocarbons, i.e. normal/iso-paraffins, naphthenes (also known as cycloparaffins) and aromatics. Thanks to previous studies and with an huge bibliography effort, researchers succedeed in completing a full properties table for the forty-seven (47) hydrocarbons, which are supposed to be the starting point for future developments. Going into the specifics of this thesis, the first pages are dedicated to a general introduction of the main problem, trying to get the reader on the path of the reference topic. Then, after a brief presentation of many important civil and military fuels, paying attention to adding specific information about the reasons for their current utilization or their past dereliction, some historical kerosene models are shown, with the aim of introducing the general iter for jet fuel modelling. In the same pages, their properties are also shown in order to make the reader more aware about their general meaning (and also their normal magnitude and operative range). After a brief treatise about the main chemical and physical properties of jet fuels, the indirectly optimized MATLAB code for the IFS is introduced. It consists of three main parts, each of them dedicated to a particular output. While the first two are independent from each other, the third one leans on them, giving the IFS as direct output.

Then, a second possible code is introduced. This time, the code is characterized by a robust strategy of optimization through the use of the PSO algorithm (Particle Swarm Optimization) and it returns the same outputs of the previous attempt's code. These data are validated against a reference model, obtained from previous researches. In the end, potential future developments are hypothesized, in order to further validate the numerical model proposed in this work. However, regardless any possible future advancement, this thesis, since supported by a broad theoretical discussion, is thought to be a valid starting point for the course of research, giving forthcoming insiders a well founded basis where to begin their work.

Keywords: air transport growth, aromatics, cyclo-paraffins, development, greenhouse gases, hydrocarbons, IFS, iso/normal paraffins, jet fuels, numerical model, optimization, petroleum, PSO, research, surrogate

Index

1	Introduction	1
1.1	Overview	11
2	Literature Overview	12
2.1	Jet Fuels	12
2.1.1	Alternative jet fuels	12
2.1.2	General compositions of jet fuels	18
2.2	Kerosene	23
2.2.1	Kerosene types	23
2.2.2	Kerosene modelling	33
3	Fuel Properties	45
3.1	Physical properties	46
3.2	Chemical properties	53
3.3	Experimental estimation methods of fuel properties	58
4	Brute-Force Search Algorithm	65
4.1	Interface	67
4.2	Database	69
4.3	Software	73
4.3.0	MATLAB's version conformity check	74
4.3.1	First sub-module	74
4.3.2	Second sub-module	75
4.3.3	Third sub-module	78
4.4	Output	80
5	PSO Directly Optimized Algorithm	83
5.1	Particle Swarm Optimization	84
5.2	Software	88
6	Results	89
6.1	Saibov's Thesis Validation	89
6.2	Saibov's Thesis Continuation	92
6.2.1	Premise	93
6.3	Results	93

7 Further Developments	94
Appendix A Physics of Aircraft Engine	101
Appendix B Particle Swarm Optimization Example	106
Appendix C MATLAB functions	108
C.1 <i>nchoosek</i>	108
C.2 <i>ndgrid</i>	109
C.3 <i>parfor</i>	110
C.4 <i>fmincon</i>	112
C.5 <i>particleswarm</i>	114

List of Figures

1.1	Forecast of emissions in equivalent CO_2 [6]	1
1.2	GAFT value chain model [7]	3
1.3	CTL processes	3
1.4	ATJ process	4
1.5	Readiness level	4
1.6	NJFCP integration into the ASTM process	6
1.7	Available range	7
1.8	Average composition	8
1.9	GCxGC	8
1.10	density-T curve	9
1.11	viscosity-T curve	9
1.12	Cp-T curve	10
1.13	h-T curve	10
1.14	surface tension-T curve	10
1.15	vapor pressure-T curve	10
2.1	Different paths	13
2.2	Evolution of cryogenic and Jet-A fuel cost	13
2.3	FT process	14
2.4	GTL process using the FT method	15
2.5	BTL process	16
2.6	n-pentane	18
2.7	i-pentane	18
2.8	Cyclohexane structures	19
2.9	Unsubstituted PAHs	20
2.10	Substituted PAHs	20
2.11	Soot formation	21
2.12	Typical hydrocarbon distribution for kerosene-type jet fuel	23
2.13	A Pratt&Whitney J58 burning off JP-7 fuel	27
2.14	JP-8 strip	28
2.15	Saturn V	31
2.16	TH-dimer	31
2.17	Distillation curve	34
2.18	Surface regression rate	34
2.19	Hex-12 heat flux	34
2.20	Predicted and measured intermediate species profiles	35
2.21	Experimental and model data for ignition delay	36
2.22	Counterflow	36

2.23	Surrogate burning velocity	36
2.24	Fuel mass fraction	37
2.25	TSI	37
2.26	n-decane's ignition delay times	37
2.27	Ignition delay times	38
2.28	Effect of Φ and dilution on ignition-delay times	39
2.29	Extinction strain rate	40
2.30	Laminar flame speed	40
2.31	NO_x ppm	40
2.32	Ignition delay times	40
2.33	Ignition delay times	41
2.34	Strain rates of extinction for counter flow diffusion flames	41
2.35	Surrogates density	42
2.36	Surrogates viscosity	42
2.37	Flames reconstituted 2D-images	43
2.38	Radial profiles at different HAB	43
2.39	Reactivity map	44
3.1	3D distillation curve	48
3.2	Phase diagram	49
3.3	Molecular structure of the three pentane isomers	53
3.4	Temperature history for pentane isomers	53
3.5	Delay times for iso/neo/n-pentane	53
3.6	Pure-component CNs for different hydrocarbon classes	55
3.7	Ignition delay time and PM emissions as a function of CN [75]	55
3.8	Mixture's TSI evaluation	57
3.9	CH ratio effect of smoke point	57
4.1	Block scheme of the algorithm	66
4.2	First block of the scheme	67
4.3	Second block of the scheme	69
4.4	IUPAC logo	72
4.5	Third block of the scheme	73
4.6	First sub-module of the algorithm	75
4.7	First refinement of percentages	76
4.8	Final distribution of percentages	76
4.9	Colormap of figure 4.8	77
4.10	Second sub-module of the algorithm	77
4.11	Last block of the algorithm	79
4.12	Last block of the scheme	80
4.13	Output: compared magnitude	81
4.14	Output: relative magnitude	81
5.1	Bird flock	84
5.2	Fish school	84
5.3	Basic PSO block diagram	86
5.4	Spaced region by particle's velocity	87
5.5	Example of iteration-objective function curve	88

A.1	Fuel properties evolution	101
A.2	Control volume	102
B.1	Function 3D curve	106
B.2	Contour lines	106
B.3	First PSO iteration	107
B.4	Second PSO iteration	107
B.5	Eighth PSO iteration	107
B.6	Last PSO iteration	107
C.1	Input arguments	109
C.2	<i>parfor</i> function	111

List of Tables

1.1	Specification test results for category A fuels	7
2.1	Fuel characteristics for different aviation fuels	24
2.2	Main properties of T-family jet fuels	25
2.3	Properties of the previous jet fuel	26
2.4	Sum up of JPs properties	29
2.5	Comparison between Jet A-1, Jet A and Jet B properties	30
2.6	Comparison between some missiles fuels properties	32
2.7	Composition of tested surrogate blends	33
2.8	Surrogates properties	33
2.9	Fuels' properties	39
2.10	Fuels' properties	42
3.1	Empirical constant for each compound class [15]	47
3.2	Structural contribution for b_i [15]	47
3.3	Enthalpies table [67]	52
3.4	Parameter value β the pure-component structure parameter	55
3.5	Physical properties of the main hydrocarbons	64
4.1	Clusters features	65
4.2	Example	67
4.3	Simplified algorithm depiction. Model design 1	68
4.4	Simplified algorithm depiction. Model design 2	68
4.5	Simplified algorithm depiction. Model design 3	68
4.6	Input file	71
4.7	Input data	71
4.8	Family division of hydrocarbons	72
4.9	Models design	73
4.10	Brief depiction of main algorithm	78
4.11	Brief sum up of the output files	80
5.1	Brief sum up of the output files	83
6.1	SPK composition	89
6.2	Check SPK full	90
6.3	Check SPK-1	90
6.4	Check SPK-2	90
6.5	CN calculation table as shown in [86]	91
6.6	Uncertainty errors	93

B.1	Input parameters	107
C.1	<i>exit flag</i> table	114

Nomenclature

List of Abbreviations

[A]	ACI	Airports Council International
	AFOSR	Air Force Office of Scientific Research
	AFR	Air-to-Fuel Ratio
	AFRL	Air Force Research Laboratory
	ASTM	American Society for Testing and Materials
	ATJ	Alcohol to Jet
[B]	BTL	Biomass to Liquid
[C]	C/H	Carbon-to-Hydrogen
	CFD	Computational Fluid Dynamics
	CFR	Cooperative Fuel Research
	CIS	Commonwealth of Independent States
	CL	Check List
	CMO	Commercial Market Outlook
	CN	Cetane Number
	CRC	Chemical Rubber Company
	CTL	Coal to Liquid
[D]	DCL	Direct Coal to Liquid
	DSHC	Direct Sugar to Hydrocarbons
[F]	FAA	Federal Aviation Administration
	FBP	Final Boiling Point
	FT	Fischer-Tropsch
[G]	GAFT	Gasification and FT-Synthesis of Lignocellulosic Feedstocks
	GC	Gas Chromatography
	GLCM	Ground Launched Cruise Missile
	GOST	<i>Gosudarstvennyy Standart</i> , Russian State Standard
	GTL	Gas to Liquid

[H]	HAB	Heights-Above-Burner
	HEFA	Hydroprocessed Esters and Fatty Acids
	HHV	Higher Heating Value
	HMN	2,2,4,4,6,8,8-Heptamethylnonane
	HPAH _s	High Molecular Weight PAHs
[I]	IATA	International Air Transport Association
	IBP	Initial Boiling Point
	ICL	Indirect Coal to Liquid
	IDEA	Integrated Diesel European Action
	IDT	Ignition Time Delay
	IUPAC	International Union of Pure and Applied Chemistry
[J]	JP	Jet Propellant
	JSR	Jet Stirred Reactor
[L]	LHV	Lower Heating Value
	LII	Laser Induced Incandescence
	LNG	Liquefied Natural Gas
	LPAH _s	Low Molecular Weight PAHs
[M]	MAH _s	Monocyclic Aromatic Hydrocarbons
	MIL-DTL	Military Detail Specification
	MW	Molecular Weight
[N]	NASA	National Aeronautics and Space Administration
	NATO	North Atlantic Treaty Organization
	NIL	National Information Library
	NJFCP	National Jet Fuels Combustion Program
[P]	PAH _s	Polycyclic Aromatic Hydrocarbons
	PM	Particulate Matter
[R]	RCM	Reliability Centered Maintenance
	RP	Refined Petroleum / Rocket Propellant
[S]	SP	Smoke Point
	SPK	Synthetic Paraffinic Kerosene
	SRK	Soave-Redlich-Kwong
[T]	TH	Tetrahydromethylcyclopentadiene
	TS	<i>Toplivo Samolet</i> , Jet Fuel
	TSI	Threshold Sooting Index
[U]	USAF	United States Air Force
[V]	VABP	Volumetric Average Boiling Point

List of Symbols & Variables

GENERAL

a, b, c, d		generic constant
b_i		contribution of the i-th chemical group to the compound's viscosity
C_p	$\left[\frac{J}{K}\right]$	heat capacity at constant pressure
$E_{S,mix}$	$\left[\frac{kJ}{kg}\right]$	specific energy
g	$\left[\frac{m}{s^2}\right]$	gravity acceleration
h	$[m], [mm]$	height
MW	$\left[\frac{g}{mol}\right]$	molecular weight
n_i		number of times that the i-th group appears in the molecule
p_{crit}	$[Pa]$	critical pressure
R	$\left[\frac{J}{Kmol}\right]$	ideal gas constant
s^0	$\left[\frac{J}{K}\right]$	standard normal entropy
T_{crit}	$[K]$	critical temperature
T_{boil}	$[K]$	boiling temperature
T_0	$[K]$	standard temperature
T_r	$[K]$	reduced temperature
V_m	$\left[\frac{m^3}{mol}\right]$	molar volume
x		calculated value
\bar{x}		input value
Z		compound's atomic-number sum

GREEK LETTERS

β_i		pure i-th component structure parameter
χ_i		mole fractions of the i-th components
$\Delta_c H^0$	$\left[\frac{kJ}{mol}\right]$	combustion enthalpy
Δh_f^0	$\left[\frac{kJ}{mol}\right]$	formation enthalpy
ϵ_{rel}		relative error
η	$\left[\frac{kg}{ms}\right]$	dynamic viscosity
η^+	$\left[\frac{kg}{ms}\right]$	empirical constant for each chemical compound class
ν	$\left[\frac{m^2}{s}\right]$	kinematic viscosity
ν_i		volume fraction of the i-th molecule
ω_i		stoichiometric coefficient of the i-th reactant in a reaction
Φ_c		critical equivalence ratio
ρ	$\left[\frac{kg}{m^3}\right]$	liquid density
θ		constant function of chemical compound's structure

Chapter 1

Introduction

Nowadays, air traffic is an essential part of our modern society, helping people to feel more comfortable about the progressive reduction of physical distances between different countries and places. This new outlook, despite numerous external upheavals over the years, created an increasing demand for air transport which has spread all over the world, from the poorest countries to the richest ones; according to the Airports Council International Forecast [1], in the next 20 years the world air traffic is expected to double or even to triple. This remarkable trend is confirmed even by the last Commercial Market Outlook of the main aircraft companies, such as Boeing, Airbus, Embraer and Bombardier [2]-[5]. If these previsions revealed themselves to be true, the progressive increase of air traffic would provoke a significant and growing contribution to the global inventory of greenhouse gases, which are rationally thought to be implicated in climate change. Over the years, many different (and sometimes hasty) solutions have been proposed to limit this pessimistic future, from new aerodynamics and structural concepts for wings and fuselage (able to act in an indirect way to the increase of the aerodynamic efficiency) to new flight pats, chosen to take advantage of favorable winds. But these possibilities, which entail a reduction of the fuel's consumption, are defined not to be enough to counter the problem. In this regard, a more promising road to limit the greenhouse gases emission is thought to be the sostitution of actual fuels with other less polluting (see figure 1.1), acting directly on the fuel's chemistry.

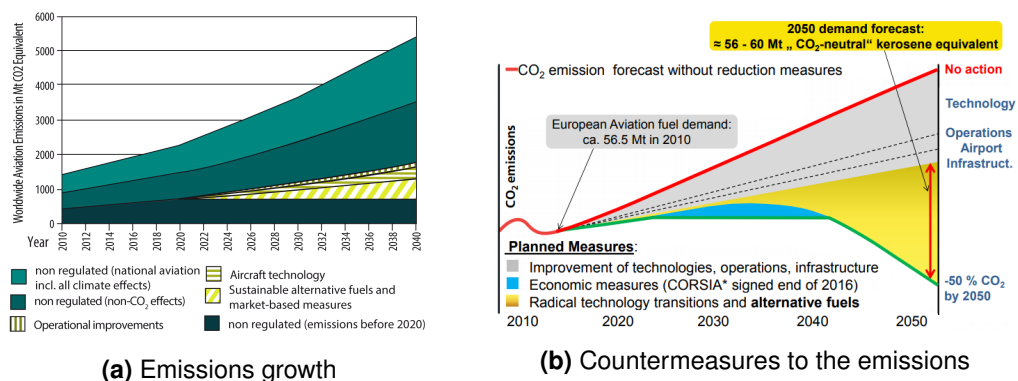


Figure 1.1 Forecast of emissions in equivalent CO_2 [6]

In addition, the aviation sector has a high demand for fossil fuels; in this context, the investigation for new alternative fuels (non-petroleum based) for aircrafts occurs to be more indispensable than ever. Moreover, the incessant growth of fossil fuels' costs has prompted the industry to look for alternative (and cheaper) combustibles which should be able to provide the required service features with a mixture of crude oil based kerosene and alternative fuels. They could have different origin, most of which are summed up in the following list, trying to show at the same time their main features:

- **Hydroprocessed Esters and Fatty Acids (HEFA):** for the production of sustainable fuels based on esters and fatty acids, all forms of native fat or oil could be used. In addition to fats and wastes from the food industry, mainly vegetable oils and fatty acids from the refining process are used. The manufacturing process is based on their hydrogenation and then on their refining, similarly to fossil fuels. This process is already mature and has been approved by the ASTM since 2011. HEFA kerosene has been used in thousands of test flights and in regular service. However, HEFA biojet historically costs more than fossil-derived jet fuels (and a similar prospect afflicts their feedstocks).
- **Fischer-Tropsch (FT):** in the Fischer-Tropsch synthesis, long-chain hydrocarbons are generated from a synthesis gas (carbon monoxide and hydrogen) in a reactor. Thereafter, these syngas must be further processed into kerosene (by hydrocracking and/or isomerization). Since 2009, the original process is certified by the ASTM for aviation, but the technology as a whole is extremely demanding. The Fischer-Tropsch process produces high value, clean-burning fuels and a wide range of biomass is suitable as its starting feedstocks. The resulting fuels are colorless, odorless and low in toxicity. FT fuels have less sulfur, nitrogen oxide, carbon monoxide and particulate matter emissions than petroleum fuels.
- **Gas to liquid (GTL):** biomasses of different origin and composition are first converted into biogas via biochemical processes. In addition to wood, almost all available biomass (including waste) can be used. Also, in terms of techno-economic aspects, the production can be realized in a comparatively small-scaled way. As a result, biomass resources with a relatively low energy content, such as liquid manure, can be opened up, which would be uneconomical to transport over long distances. However, this can only be achieved by feeding the biomethane into the existing natural gas network. The collected biomethane can be fed to refineries. In the subsequent GTL process, this biomethane is converted into carbon monoxide (CO) and hydrogen (H_2). CO and H_2 are then converted by FT synthesis in long-chain hydrocarbons - and thus ultimately in sustainable kerosene. So far, no sustainable aviation fuel has been generated via the GTL process. Since biomethane and fossil methane are chemically identical and the technology for natural gas is already used on a large scale, production is considered to be problem-free. However, there are high costs for fuel production from renewable resources via the GTL process.

- **Biomass to Liquid (BTL):** for the production of biomass-to-liquid fuels, solid biomass is converted directly via thermochemical gasification into a synthesis gas which consists primarily of CO and H_2 . For this purpose, lignocellulosic biomass is used. After a purification by FT synthesis, the gas produced from the biomass is relocated in hydrocarbon chains. Subsequently, kerosene is separated from the resulting hydrocarbon mixture by means of the refinery processes. A typical production scheme for BTL fuel is shown in the next figure, which refers to the GAFT¹ value chain model:

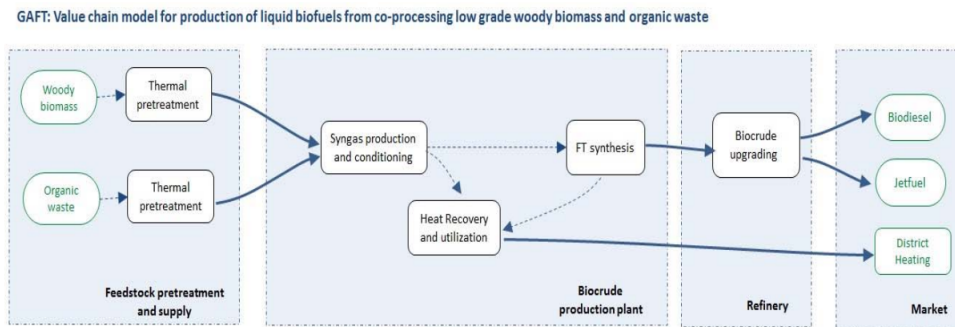


Figure 1.2 GAFT value chain model [7]

- **Coal to Liquid (CTL):** coal liquefaction is a process of converting coal into liquid fuels. Specific liquefaction technologies generally divide into two categories: direct liquefaction (DCL) and indirect liquefaction (ICL) processes. Direct processes are based on approaches such as carbonization, pyrolysis and hydrogenation. Indirect liquefaction processes generally involve gasification of coal to a mixture of carbon monoxide and hydrogen and then, using a suitable process, conversion of the syngas mixture into liquid hydrocarbons. In contrast, direct liquefaction processes convert coal into liquids directly.

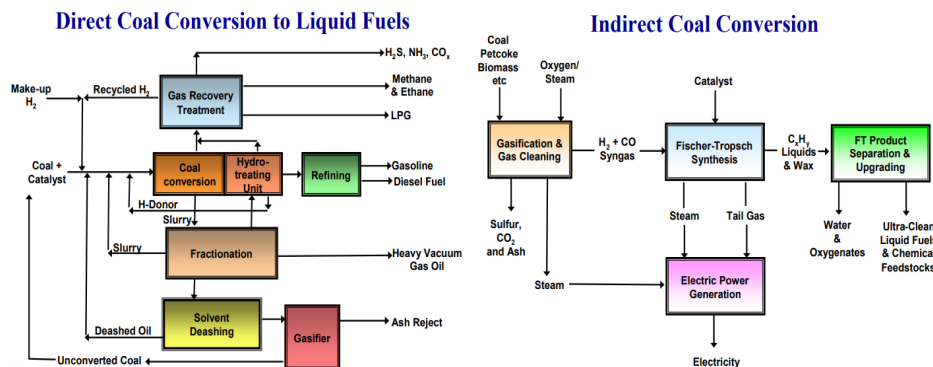


Figure 1.3 CTL processes

¹ GAFT is a Norwegian project, whose overall objective is to accelerate the implementation of liquid biofuels production in Norway guaranteeing alternative sources for the jet fuel's refining.

- **Direct Sugar to Hydrocarbons (DSHC):** in DSHC technology, sugar is firstly converted directly into pure unsaturated hydrocarbons by aerobic fermentation of genetically modified yeasts and subsequently the output products must be hydrogenated. In principle, even higher sugars (polysaccharides such as cellulose) can be metabolized after digestion. While the fermentation of simple sugars to hydrocarbons has already reached industrial scale, the fermentation of higher sugar still needs some development work. By the way, some specific tests have already been made by the American Pratt & Whitney [8] with a 20-80% fuel blend of Amyris Farnesane-Jet A and no difference was observed in engine operability.
- **Alcohol to Jet (ATJ):** in alcohol-to-jet technology, hydrocarbons are produced from alcohols, mainly derived from lignocellulosic biomasses and sugar. The actual conversion of the alcohol takes place in three steps:
 1. *O* is removed by dehydration and short-chain alkenes are formed
 2. their oligomerization to long-chain alkenes takes place
 3. they are hydrogenated to alkanes

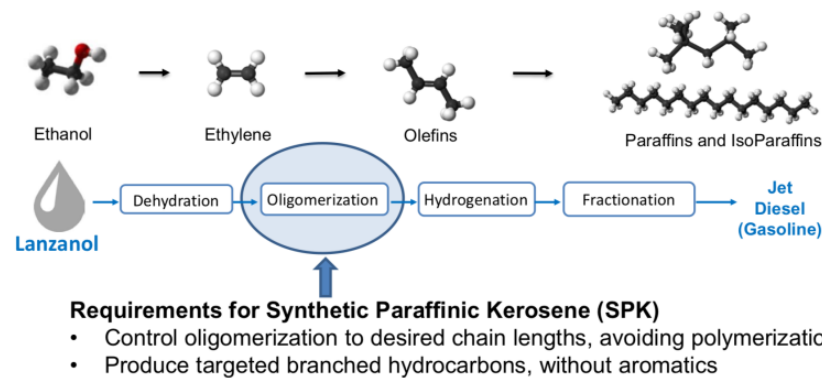


Figure 1.4 ATJ process

The readiness level of some of them is shown in the following figure:

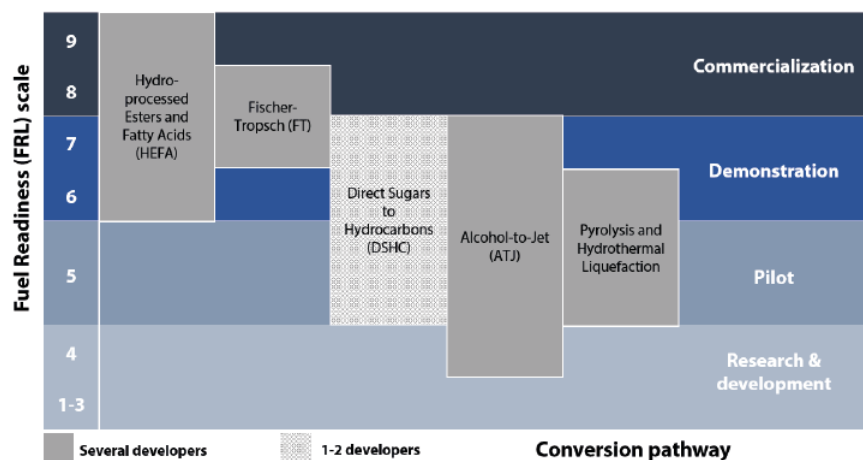


Figure 1.5 Readiness level

However, there are several requirements to observe; as for any other jet fuel, the most important one is not to compromise the safety of the equipped aircraft in any way. In addition, the fuel developed must have:

- good atomization, evaporation and burning characteristics
- good thermal and chemical stability
- low viscosity and explosion risk
- high lubricity and specific heat capacity
- good storage and handling characteristics

These requirements reflect the actual complexity of the situation. The aviation industry also presents far greater restrictions on any candidate fuel due to several factors that could undermine the operations' safety:

- i. the extreme conditions under which combustion must reliably and safely take place demand a limited range of potential liquid fuels
- ii. any product must be fully interchangeable with the current jet fuel product to avoid the logistic problems of airports handling multiple fuels of varying qualities and the commercial limitations this would impose
- iii. the long life of a commercial jet imposes on any candidate fuel to be "backwards compatible" for use in existing engine technology

Thence, aviation's current focus is on the development of "drop-in fuels", which are alternative jet fuels composed solely of hydrocarbons (but produced from alternative sources such as bioderived feed stocks), and that could provide essentially identical performance to that from petroleum-derived jet fuels. These drop-in fuels may be more appropriately considered the same as jet fuel, but produced from alternative raw materials. Drop-in fuels do not require engine/airplane redesign, nor new fuel systems/components on ground or in flight. Furthermore, hydrocarbon drop-in fuels undergo rigorous evaluation to ensure that they do not degrade margins for safety, operability, performance or durability. The desire for hydrocarbon drop-in fuels is primarily due to the very high energy density of liquid hydrocarbon fuels and the enormous cost of converting aircraft and infrastructure to accommodate not drop-in fuels. Nevertheless, it's important to remind that the certification is costly, requiring significant resources (including fuel intensive tests that are variable in scope) and lengthy times required for certification. As a result, the FAA, NASA, AFRL and AFOSR established an international joint federal, academic and industrial program called the National Jet Fuels Combustion Program (NJFCP), with a view to develop combustion-related generic test and modeling capabilities that could improve the understanding of the impact of fuel chemical composition and physical properties on combustion, leading to speeding the approval process of new alternative jet fuels [9]. This program intervenes in the last steps of the generalized certifications process of ASTM (American Society for Testing and Materials)² (figure 1.6).

² ASTM International, acronym of American Society for Testing and Materials, is an international standards organization that develops and publishes technical standards for a wide range of materials, products, systems and services.

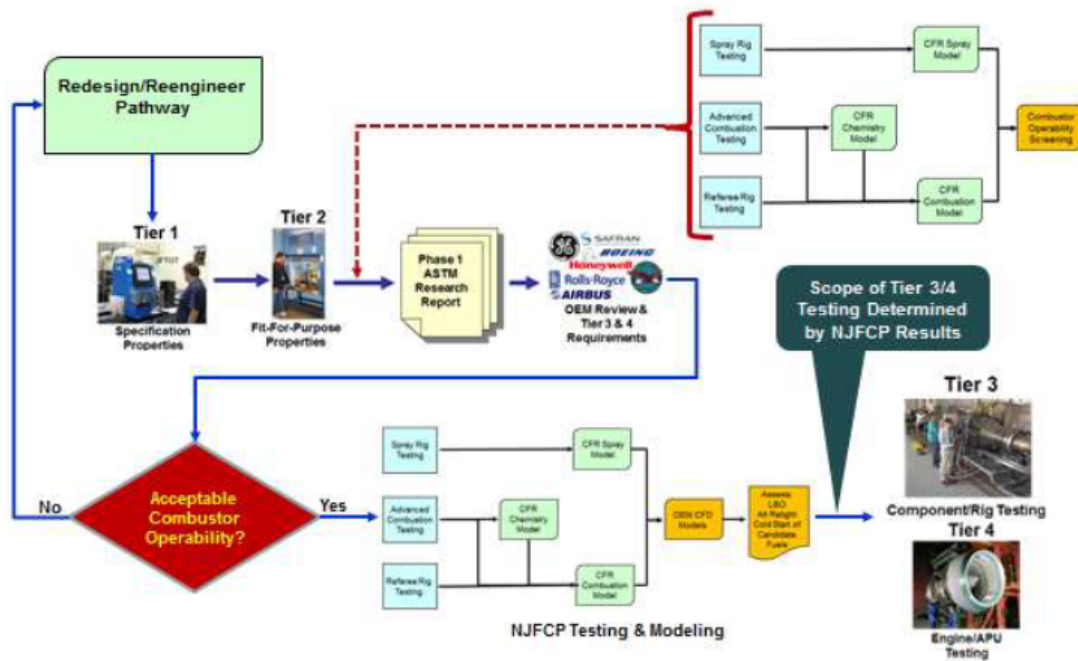


Figure 1.6 NJFCP integration into the ASTM process

The NJFCP incorporates efforts from a large number of academic institutions, US government laboratories, original equipment manufacturers of gas turbine jet engines, individual contractors and international partners, as well as US Federal agencies that provide funding and oversight of the program. To succeed in the validation of these alternative fuels, one of the strongest and most efficient NJFCP's instrument is the CFD (Computational Fluid Dynamic) simulation of the proposed fuel's model. One of the most important and used software for the chemical research is CHEMKIN, developed by ANSYS. CHEMKIN is a software tool for solving complex chemical kinetics problems and it is used worldwide in the combustion, chemical processing, microelectronics and automotive industries. CHEMKIN solves thousands of reaction combinations to develop a comprehensive understanding of a particular process, which might involve multiple chemical species, concentration ranges and gas temperatures. However, because of the outstanding complexity of traditional jet fuels (each of them is a mixture of several thousands of hydrocarbons such as paraffines, cycloalkanes, aromatics and olefins), the processing of actual chemical kinetic data of these blends is something currently utopian. Therefore, only simplified chemical kinetic models of practical fuels such as surrogate mixtures can be used to develop alternative fuel types. General formulae or standard rules for the construction of such surrogate mixtures are not established yet, but common principles of such construction are clear and require that the surrogate mixture must have similar physical and chemical characteristics of the target fuel [10]. The physical properties can be summarised in density, fuel energy content, evaporation characteristics (boiling range, flash point, vapour pressure), thermal conductivity, surface tension and viscosity. On the other hand, chemical properties (which are related to the chemical composition) are mainly C/H ratio, flame speeds, ignition delays and sooting tendency.

These properties, in case of conventional fuels, are summed up by NJFCP in the category A paper. This document also includes the following data:

- **Specification properties:** the specification properties are features important to combustion and could be summed up in: flash point, viscosity, aromatic content, hydrogen content, ASTM D86 distillation, smoke point, measured heat of combustion and measured cetane number. A summary of key properties of the fuels is given in figure 1.7 and in table 1.1, which show that the fuels do indeed encompass a wide range of properties within the jet fuel experience base. Density was not a criteria for the Category A fuels, but the viscosity and aromatic requirements also effectively drove the density of the fuels to the edges of the distribution.

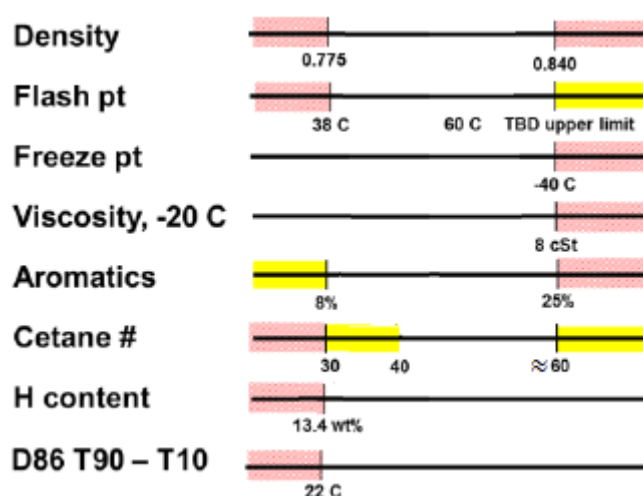


Figure 1.7 Available range

Property	Test method	Limits
Density, $\frac{kg}{m^3}$	D4052	0.775-0.84
Flash point, $^{\circ}C$	D93	> 38
Viscosity at -20 $^{\circ}C$, [cSt]	D445	< 8
Aromatics, vol [%]	D1319	< 25
Heat of combustion, $\frac{kJ}{kg}$	D4809	> 42800
H content, mass [%]	D3701	> 13.4
H content, mass [%]	D7171	> 13.4
H content, mass [%]	GCxGC (UDRI)	> 13.4
H/C ratio, [-]	D3701	n/a
Molecular formula	GCxGC	n/a
Derived Cetane Number	D6890	n/a
Distillation, $^{\circ}$	D86	
IBP		
10 %		< 205
20 %		
50 %		
90 %		
FBP		< 300
Engine Cetane Number	D613	n/a
Smoke pt, [mm]	D1322	> 18
Freeze pt, $^{\circ}C$	D5972	> -47

Table 1.1 Specification test results for category A fuels

- **Composition:** thanks to GCxGC³ system, it is possible to evaluate the distribution of major hydrocarbon classes across carbon number and the average molecular weight. The fuel specification properties don't control the fuel composition directly, aside from the 25% (vol) limit on total aromatics by ASTM D1319. The indirect effect of the specification limits lead to the (average) distribution of hydrocarbons shown in figure 1.8. The lack of hydrocarbons below about C₈ is due to the flash point limit (> 38 °C); while the lack above about C₁₇ is due to the freeze point limit (< -40 °C). In general, typical jet fuels have four classes of hydrocarbons (olefins are low in jet fuels) distributed across many carbon numbers.

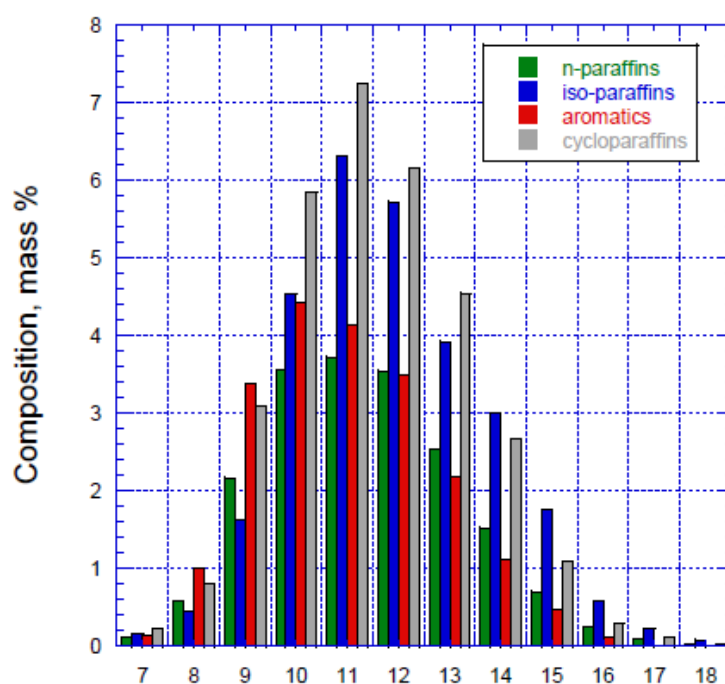


Figure 1.8 Average composition

3

GC is the acronym for comprehensive two-dimensional Gas Chromatography, which is a multidimensional gas chromatography technique that was described in 1991. GCxGC utilizes two different columns with two different stationary phases. In GCxGC, the effluent from the first dimension column is diverted to the second dimension column via a modulator. Then, the modulator traps and injects the effluent from the first dimension column onto the second dimension. This process creates a retention plane of the 1st dimension separation x 2nd dimension separation.

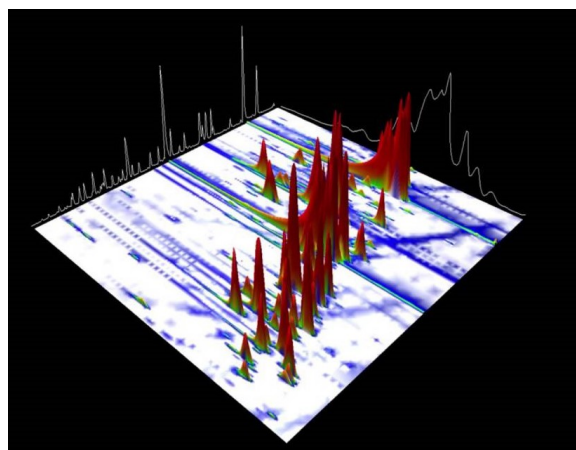


Figure 1.9 GCxGC

- **Fit-for-purpose properties:** the alternative fuel approval process (ASTM D4054) defines this class of properties that are not limited by the specification, but are limited to an expected range for fuels that are acceptable (“fit-for-purpose”). They can be summed up in the density-T curve, viscosity-T curve, C_p -T curve, surface tension-T curve and vapor pressure-T curve:

- density-T curve: density is a linear function of temperature in the range shown, which is significantly below the jet fuel critical temperature ($\approx 400^\circ\text{C}$). For the temperature range shown, it would seem reasonably accurate to extrapolate density of an unknown jet fuel based on this slope and the 15°C specification density.
- viscosity-T curve: given the strong temperature dependence of viscosity, measurements at -20°C appear to be warranted for any new fuel, rather than an estimate based on ambient temperature viscosity or based on correlations with other properties. ASTM D7566 has started using a 12 cSt limit at -40°C for alternative fuels. The data in figure 1.11 have been linearized for ASTM D341 using the correlation: $\log(v + 0.7) = a - b \cdot \log(T)$, where a and b are fuel constants.

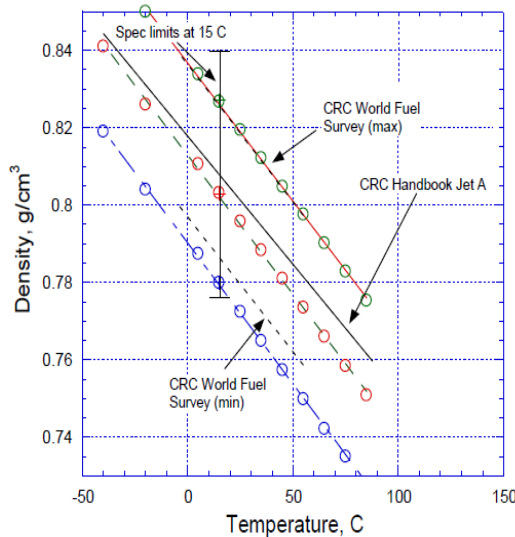


Figure 1.10 density-T curve

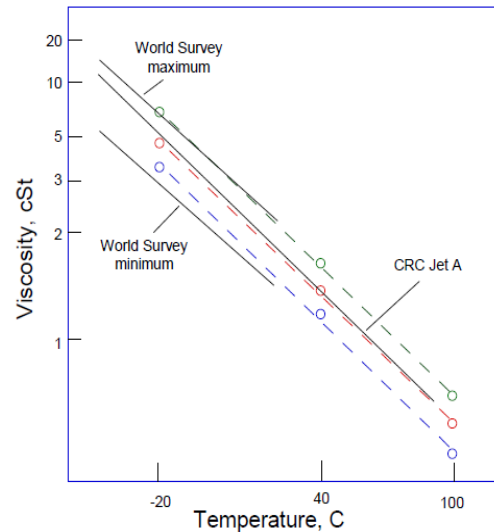


Figure 1.11 viscosity-T curve

- heat capacity-T (C_p -T): heat capacity is a fit-for-purpose property which is evaluated using ASTM E1269. The results are shown in figure 1.12. There is some spread in the data which shows differences among fuels, probably due to density’s differences. The heat capacity can also be calculated from enthalpy data since C_p is the slope of the h-T curve at a given temperature (figure 1.13):

$$C_p = \left(\frac{\partial h}{\partial T} \right)_{p=\text{const}}$$

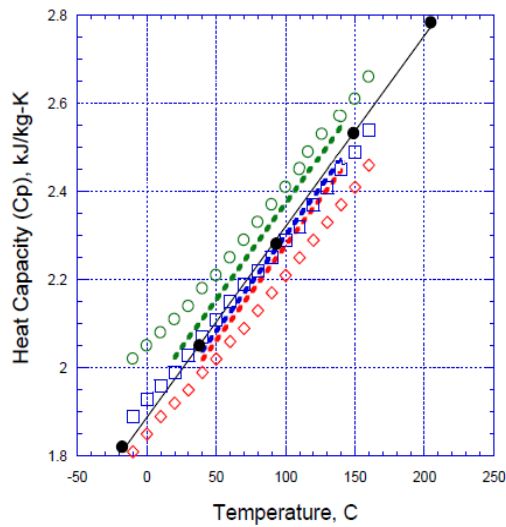


Figure 1.12 Cp-T curve

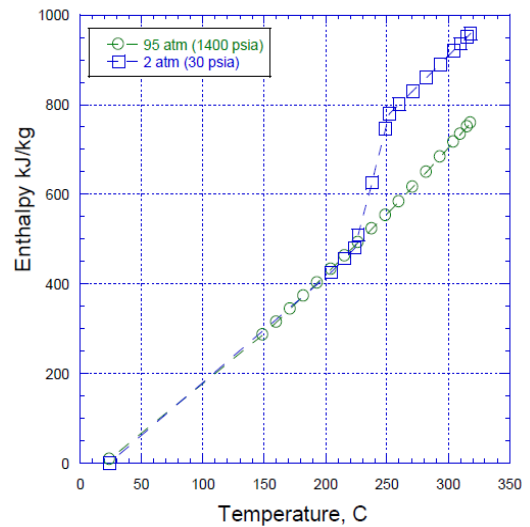


Figure 1.13 h-T curve

- surface tension-T: similarly to heat capacity, surface tension is also not a specification property. In this case, however, the current data do not match well with the SwRI (South west Research Institute) measurements (lower than data) or with the calculation (higher than data) (although the trends are the same, the discrepancies may again be due to density differences).
- vapor pressure-T: although vapor pressure is not a specification property, it is not independent from the other properties discussed. The CRC Handbook shows separate vapor pressure curves for JP-8, Jet A, Jet A-1 (flash point > 38 °C) and JP-5 (flash point > 60 °C).

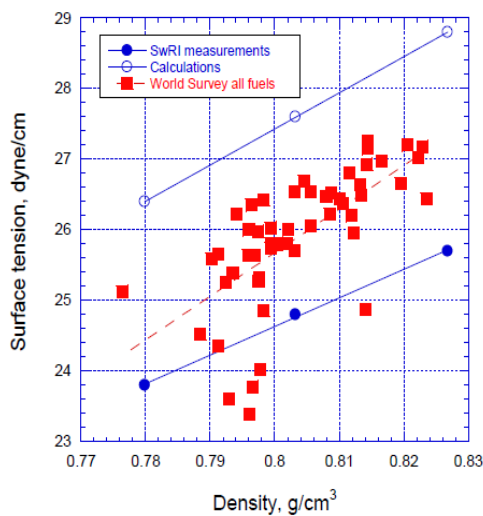


Figure 1.14 surface tension-T curve

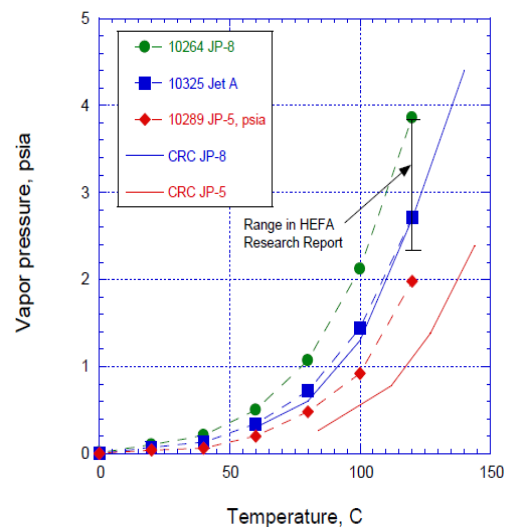


Figure 1.15 vapor pressure-T curve

1.1 Overview

Purpose

Summarizing what said so far, it is clear an urgent need to define proper mathematical tools for the modeling process of future jet fuels, which, in order to limit the harmful emissions of nitrogen oxides (NO_x) and of sulfur oxides (SO_x), are intended to be composed according to a proper blend of hydrocarbons, limiting the contribution of possible contaminants. In this context, it has been possible to develop this work of thesis, which is intended laying the computational foundations for the definition of the Input Formula of Surrogate (IFS), which should mimic the reference properties of the input fuel.

Rundown

In the following lines, the structure of the thesis is introduced, trying to summing up each section's main content:

1. the first chapter plays the role of the introduction of the thesis, trying to summing up the reasons of its draft. Furthermore, it submits the development's stages for new alternative fuels, according to the actual legislation
2. the second one shows the research's actual state of art and proposes a brief report about the fuel's historical usage in the civil and military field
3. in the third chapter, the chemical and physical properties of a fuel are summed up, endowing some mathematical tools for their evaluation
4. the fourth chapter deals with the "brute-force search" code. The code is characterized by a very simple basic theory but, in its simplicity, it allows the user to think that the solutions obtained refer to the input objective function's global minimum. The main problem of this kind of approach emerges in the huge computational cost required to the processor, that grows exponentially with the mesh refinement
5. the fifth one shows the directly optimized code, which exploits the PSO robust algorithm (Particle Swarm Optimization). This code proved to be computationally far lighter than the first option; however, because of calculation's stocastica nature, the users doesn't have the absolute certainty of succeeding in finding the global minimum but there is a remote possibility that the particle's swarm could be blockade in a local minimum
6. the results obtained from the two codes are compared in the sixth chapter of the thesis, trying to certify the work of thesis' goodness.
7. in the seventh and last chapter, some future developments are introduced, starting from eventual improvements on the previous codes arriving to the testing of next steps of the certification process proposed by the current legislation (see figure 1.6)

Chapter 2

Literature Overview

2.1 Jet Fuels

2.1.1 Alternative jet fuels

The main focus of this paragraph is to give a short introduction to the existent alternatives to conventional jet fuels. There are several types of fuels used in different engine applications. Nowadays, petroleum is the main used source to produce almost all jet fuels, but natural gas, shale oil and coal as other fossil fuel sources could also be used to produce jet fuels. In addition, there are several potential alternative aviation fuels such as bio-derived jet fuels, cryogenic fuels, Fischer-Tropsch (FT) synthetic fuels that are a main focus to investigate for scientific community, since they could guarantee a reliable solution too.

- **Bio-Derived Jet Fuels:** biomass is being increasingly considered as an alternative raw material of transportation fuels. Ethanol and biodiesel have been used in recent years as blend components for gasoline and diesel fuel and this use is likely to continue to expand as a result of government green mandates and a desire to diversify energy sources. The renewable jet fuels contain mostly normal/iso-paraffins and have nearly no aromatics or cycloalkanes. Due to the lack of these hydrocarbons families, in order to be allowed to be used as aviation fuels for commercial flights bio-jet fuels should need to be blended with petroleum based fuels [11]. In general, aviation biofuels have seen some use starting in 2008. The first demonstration flight, which was undertaken by Virgin Atlantic, used a blend of 20% biofuels in one of its engine. After many other tests, in October 2012, 100% biofuels was used by the National Research Council in Canada to power a Dassault Falcon 20 demonstration flight. However, given the more stringent limits, commercial flights have been using, at most, a 50%-50% blend. In order to make a 100% bio-jet fuel for commercial flight, a biosource must be found to be able to synthesize aromatics and cycloalkanes fuel compounds [12]. Theoretically these components can come from cellulosic biomass which would give a fully synthetical jet fuel [11]. Generally, production of kerosene from biomass can occur in several different ways; some possible paths are shown in the figure 2.1.

2.1. JET FUELS

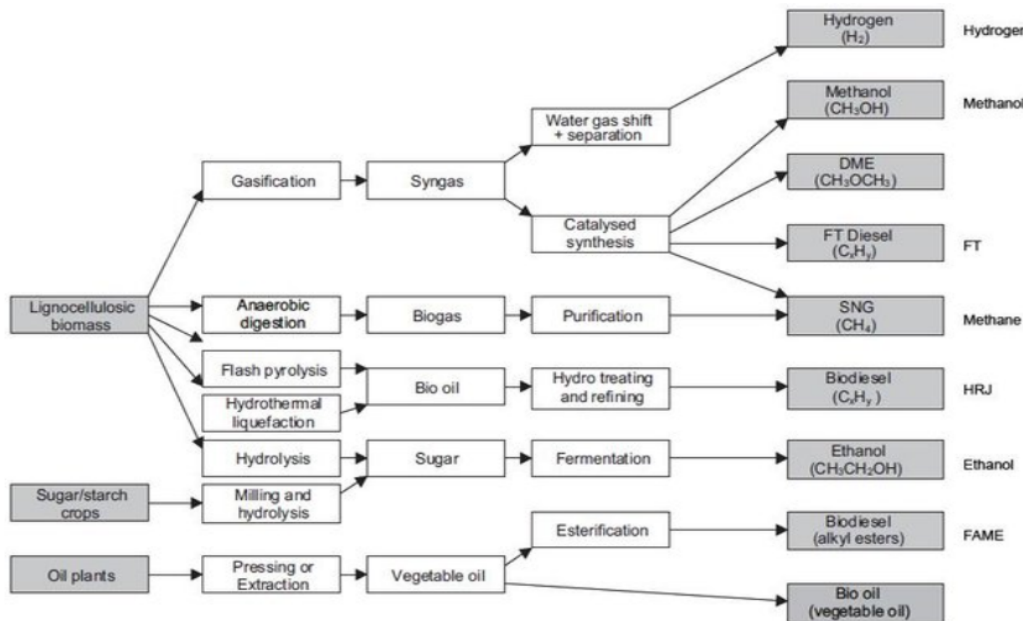


Figure 2.1 Different paths

- Cryogenic Fuels:** the term “cryogenic fuels” refers to materials that are gases at normal ambient conditions and that have been cooled to their boiling point and stored as low temperature liquids. Liquid hydrogen and liquid methane are examples of cryogenic fuels. These are fundamentally different from traditional jet fuels and would require new engines, airframes (since liquid CH_4 boils at $\simeq 120$ K, storage tanks need to be thermally insulated) and global airports infrastructure to supply and store cryogenic fuels. By the way, despite to the high costs, LNG (Liquefied Natural Gas) aircraft operations could offer a profitable investment due to the abundance of low cost feedstocks.

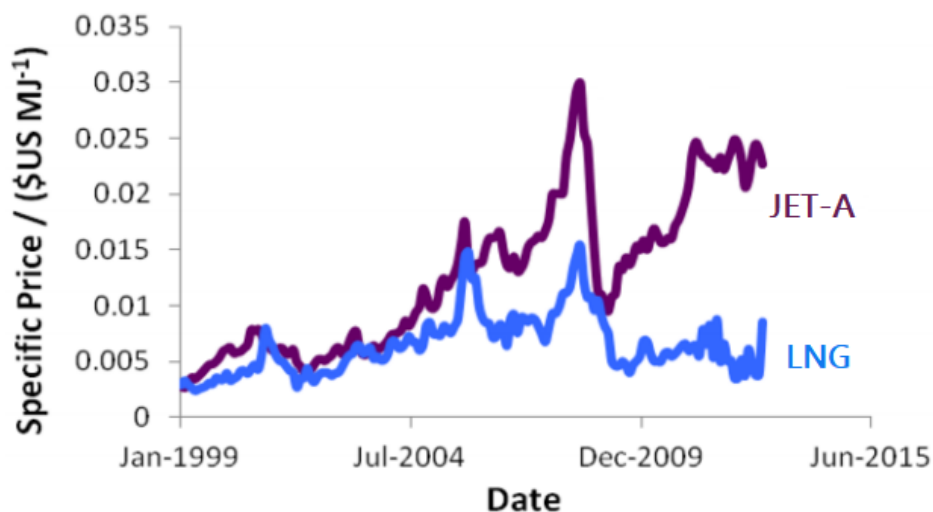


Figure 2.2 Evolution of cryogenic and Jet-A fuel cost

- Fischer-Tropsch (FT) Synthesis Fuels:** Fischer–Tropsch process (developed by the German researchers Franz Fischer and Hans Tropsch developed in 1922) is often regarded as the key technological component for converting synthesis gas to transportation fuels and other liquid products. FT fuels have several characteristics that make them attractive as a jet fuel. Their higher specific energy leads to a small reduction in the amount of energy required to fly a given distance with a given payload and could allow for increased payload capacity. Furthermore, they are clean burning without sulfur dioxide (SO_2) or sulfuric acid (H_2SO_4) aerosol emissions (property that leads to increased combustor and turbine life) and their improved thermal stability should reduce deposits on engine components and fuel lines. In addition, this aromatic-free fuel emits fewer particulates than conventional jet fuel. However, there are two disadvantages associated with no aromatics in the fuel. First, FT kerosene meets all other jet fuel specification properties with an exception of the minimum density requirement. Second, the absence of aromatic compounds can cause leaks in certain types of fuel system. Both of these issues may be resolved by blending the fuel with conventional jet fuel and with the appropriate use of fuel additives. There has been extensive evaluation of synthetic paraffinic kerosene (SPK) produced from a starting material of coal using the Fischer–Tropsch process. Since 1999, blends that are up to 50% FT liquids have been used by commercial airlines in South Africa. The FT-SPK fuels are composed of a combination of normal and iso-paraffins with a small percentage of cyclo-paraffins. The paraffins carbon number and type (iso-paraffins and n-paraffins) of the neat FT-SPK varies from C_9 to C_{15} which is a typical range found in conventional jet fuel. The whole FT process can be summed up in four main steps. The first step is the production of synthesis gas, which is a mixture of hydrogen H and carbon monoxide CO . The second main one removes undesired compounds such as CO_2 as well as impurities from the synthesis-gas stream. The third step is the FT synthesis, i.e. the process that makes mainly straight chain hydrocarbons. The product composition will vary depending on the hydrogen to carbon monoxide ratio, the catalyst and the process conditions. These raw products of FT synthesis are then further processed in the last step to make an acceptable fuel. The hydrocarbon product is upgraded to liquid fuels using well-established methods in common petroleum refineries. This processing includes cracking the long chains into smaller units and rearranging some of the atoms (isomerizing) to provide the desired properties (see figure 2.3).

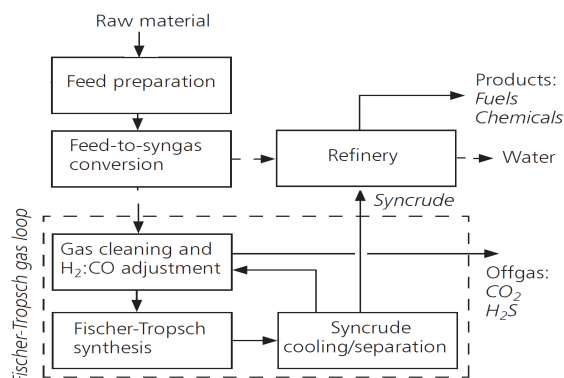
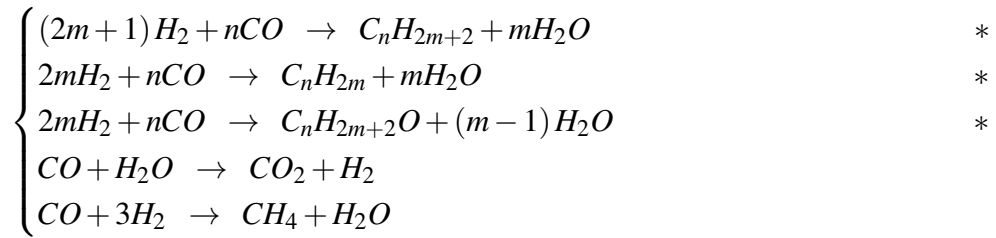


Figure 2.3 FT process

The kinetic process can be expressed by the following equations, where n is the average carbon number and m is the average number of hydrogen atoms of the hydrocarbon products (the marked reactions [*] are the main ones for the generation of straight-chain alkanes and olefins):



The FT process produces a mixture of hydrocarbons with carbon chains corresponding to gases (range from C_1 to C_4), liquids (from C_5 to C_{20}) and even waxes ($> C_{20}$). The main products of this process are olefins, alcohols, acids, oxygenate and paraffins of different length depending on a reactor and catalyst type. The FT approach provides a series of production of liquid fuels (including jet fuel) from various carbonaceous feedstocks, of which the most relevant are coal, natural gas and biomass.

- **Gas-To-Liquid (GTL) Process Fuels:** GTL process is a process to convert natural gas or other gaseous hydrocarbons (e.g. methane-rich gases) into longer-chain hydrocarbons such as gasoline or diesel fuel. This conversion process is achieved either via direct conversion or via syngas as an intermediate, e.g. using the Fischer-Tropsch processes. The GTL process begins with partial oxidation of methane (CH_4) to carbon dioxide (CO_2), carbon monoxide (CO), hydrogen (H_2) and water (H_2O). The ratio of carbon monoxide to hydrogen is adjusted by using the water gas shift reaction and the excess carbon dioxide by aqueous solutions of physical solvents. The water is then removed yielding synthesis gas that is chemically reacted over an iron or cobalt catalyst to produce liquid hydrocarbons and other byproducts.

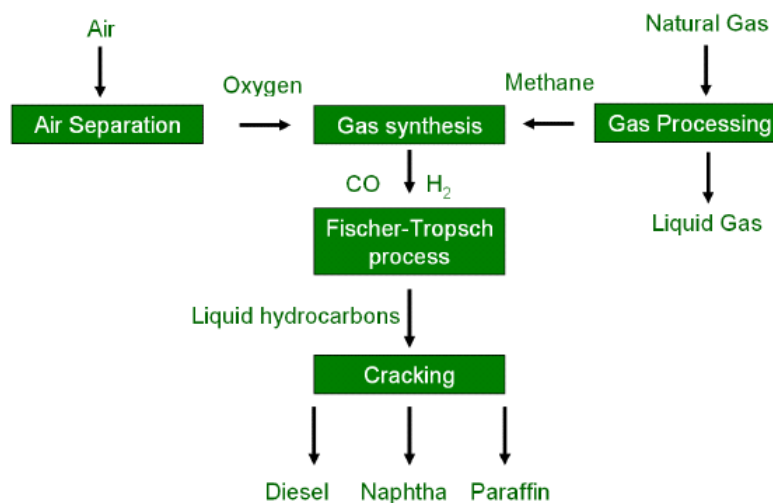


Figure 2.4 GTL process using the FT method

- Biomass-To-Liquid (BTL) Process Fuels:** the term BTL is applied to synthetic fuels made from biomass through a thermochemical route. The objective is to produce fuel components that are similar to those of current diesel fuels and fossil-derived gasolines and hence can be used in existing fuel distribution systems and with standard engines. The advantage of the BTL route to liquid transport fuels lies in the ability to use almost any type of biomass, with little pre-treatment other than moisture control. This is because the feedstock is gasified in the first stage of the process and then further treated to clean it, to remove tars, particulates and gaseous contaminants and to adjust the ratio of the required gases. Gasification is a thermochemical process at 800-1300 °C run at under-stoichiometric conditions (typically $\lambda^1 = 0.2-0.5$). Under these conditions the biomass is fragmented into raw gas consisting of rather simple molecules such as hydrogen, carbon and their combinations. Solid by-products are char, ashes and impurities. After size reduction of the raw material, it is moved into the gasifier. Typical gasification agents are oxygen and water/steam. The choice of the gasification agents depends on the desired raw gas composition. A higher process temperature or using steam as gasification agent leads to increased H_2 content. High pressure, contrarily, decreases the H_2 and CO . Impurities of the raw gas depend on the gasification conditions and used biomass and can cause corrosion, erosion, deposits and poisoning of catalysts (therefore it could be necessary to clean the raw gas). Technology-dependent impurities such as dust, ashes, bed material, tars and alkali compounds are removed through various cleaning steps. Components having mainly poisonous effects are sulphur compounds, nitrogen and chloride. The cleaned raw gas will then be upgraded to clean syngas. In the Fischer-Tropsch (FT) process, the clean syngas is transformed into alkanes using mostly iron and cobalt as catalysts. The raw product can not be directly used as fuel. It needs to be upgraded via distillation to split it into fractions. It could happen via hydration and isomerization of the C_5-C_6 fraction and via reforming of the C_7-C_{10} fraction in order to increase the octane number for gasoline use or via cracking by application of hydrogen under high pressure in order to convert long-chain fractions into gasoline and diesel fraction.

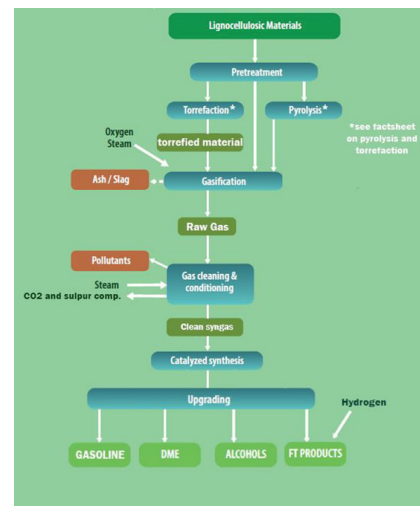
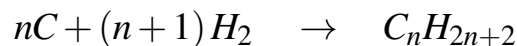


Figure 2.5 BTL process

¹ λ is the air-to-fuel equivalence ratio. It can be calculated as the mathematical ratio between the AFR (air-fuel ratio) under consideration and the stoichiometric one (distinguished by subscript "s"). $\lambda = 1.0$ is at stoichiometry, $\lambda < 1.0$ refers to rich mixtures and $\lambda > 1.0$ to lean ones.

$$\lambda = \frac{AFR}{AFR_s} = \frac{m_a}{m_f} \cdot \left(\frac{m_f}{m_a} \right)_s$$

- **Coal-to-Liquid (CTL) Process Fuels:** coal liquefaction is a process of converting coal into liquid fuels which was originally developed at the beginning of the 20th century. Specific liquefaction technologies generally fall into two categories: direct (DCL) and indirect liquefaction (ICL) processes.
 - Direct processes are based on approaches such as carbonization, pyrolysis and hydrogenation:
 - i. pyrolysis and carbonization processes: The carbonization conversion typically occurs through pyrolysis or destructive distillation. It produces condensable coal tar, oil and water vapor, non-condensable synthetic gas and a solid residue char. One typical example of carbonization is the Karrick process, a low-temperature carbonization process where coal is heated from 360 °C to 750 °C in the absence of air. These temperatures optimize the production of coal tars richer in lighter hydrocarbons than normal coal tar. Karrick process is generally too low for practical use for synthetic liquid fuel production. Furthermore, the resulting liquids are generally of low quality and require further treatment before they can be usable as motor fuels. Resulting coal tars and oils from pyrolysis are then further processed by hydrotreating to remove sulfur and nitrogen species, after which they are finally processed into liquid fuels.
 - ii. hydrogenation processes: One of the main methods of direct conversion of coal to liquids by hydrogenation process is the Bergius process, developed by Friedrich Bergius in 1913. In this process, dry coal is mixed with heavy oil recycled from the process. A catalyst is typically added to the mixture. The reaction occurs at 400-500 °C and 20-70 MPa hydrogen pressure. The reaction can be summarized as follows:



- Indirect coal liquefaction (ICL) processes operate in two stages. In the first stage, coal is converted into syngas (a purified mixture of CO and H₂ gas). In the second stage, the syngas is converted into light hydrocarbons using one of three main processes: Fischer–Tropsch synthesis (the oldest ICL processes), methanol synthesis with subsequent conversion to gasoline or petrochemicals and methanation. In methanol synthesis processes syngas is converted to methanol, which is subsequently polymerized into alkanes over a zeolite catalyst. This process was developed in the early 1970s. Methanation reaction converts syngas to substitute natural gas.

In contrast, direct liquefaction processes convert coal into liquids directly without having to rely on intermediate steps by breaking down the organic structure of coal with application of solvents or catalysts in a high pressure and temperature environment.

2.1.2 General compositions of jet fuels

Jet fuels consist mostly of hydrocarbon compounds (paraffins, cycloalkanes or naphthenes, aromatics and olefins) and are mostly derived from fossil fuels. In addition to hydrocarbons, they could also contain small fraction of non-hydrocarbons compounds as well as additives.

- **Paraffins:** paraffins, also known as alkanes, are saturated hydrocarbons and are the major component of the jet fuels. Paraffins consist of only hydrogen and carbon atoms and they are bounded exclusively by single bonds without any cycles with the general formula of C_nH_{2n+2} . Paraffins have a high hydrogen-to-carbon ratio, with a high heat release per unit of weight. Alkanes with more than three carbon atoms can be arranged in various different ways, forming structural isomers. The simplest isomer of an alkane is the one in which the carbon atoms are arranged in a single chain with no branches. However the chain of carbon atoms may also be branched at one or more points. The number of possible isomers increases rapidly with the number of carbon atoms. Even with the same molecular formula different isomers have different shapes. It is then possible to divide the family in two categories, the n-paraffins and the i-paraffins, whose structures are shown respectively in figure 2.6 and in figure 2.7:

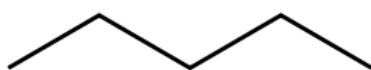


Figure 2.6 n-pentane

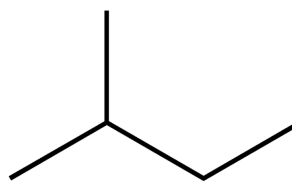


Figure 2.7 i-pentane

The two categories differ even for their cetane number CN. In fact, with the same amount of carbon's atom, the n-paraffins show a higher CN value than the i-paraffins (see figure 3.6). This difference should be due to the healthy effect of the carbon chain length, since the cetane number increases as the chain length increases. Another important difference concerns the boiling point of the two families. In fact, on equal number of carbon atoms, the n-paraffins shows a higher boiling point than the iso-paraffins. This feature is thought to be due to the molecular interactions and to the dispersion forces of the two structures.

- **Olefins:** olefins are similar to the paraffins but are unsaturated with chemical compound containing at least one carbon-to-carbon double bond with the general formula of C_nH_{2n} . Because of their high reactivity and availability and their low cost, olefins are widely used in petrochemical synthesis, in the manufacture of plastics and in the preparation of certain types of synthetic rubber, chemical fibers and other commercially valuable products. Furthermore, they show a lower cetane number than n-paraffins, but higher than the i-paraffins one (see figure 3.6).

- **Cycloalkanes:** cycloalkanes, also called naphthenes, are another essential hydrocarbon compounds found in jet fuels. Cycloalkanes are types of alkanes which have one or more rings of carbon atoms in the chemical structure of their molecules. Cycloalkanes consist of only carbon and hydrogen atoms and are saturated because there are no multiple C-C bonds to hydrogenate. A general chemical formula for cycloalkanes is $C_nH_{2(n+1-g)}$ (where n represents the number of carbon atoms and g is the rings number in the molecule). Adopting a more general notation, larger cycloalkanes are typically called cycloparaffins. Due to their ring structure, cycloalkanes are much more stable than the corresponding paraffins. Cycloalkanes have a lower hydrogen-to-carbon ratio, which results in less heat release per unit of weight but increases the fuel's density. Paraffins and cycloalkanes components have also the ability to reduce the freezing point of the fuel. In addition to the simplest cycloalkanes, substituted cycloalkanes are also present in the fuel mixture. They show an additional methyl group, which replaces a hydrogen atom. Its presence causes additional RO_2 isomerization pathways available (and these substantially increase the fuel reactivity). A typical structural difference between a standard cycloalkane and its substituted is shown in the next figure, which displays the two different possible cyclohexane's structures:

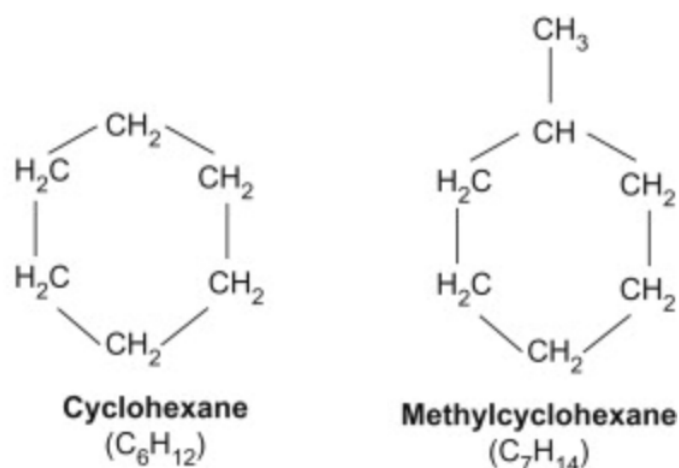


Figure 2.8 Cyclohexane structures

- **Aromatic hydrocarbons:** aromatic hydrocarbons are hydrocarbons that have at least one aromatic ring and are a good energy source in the fuel. The configuration of six carbon atoms in aromatic compounds is known as benzene ring. Aromatic hydrocarbons can be monocyclic (MAHs) or polycyclic (PAHs). Monocyclic aromatic hydrocarbons (MAHs) are an important fraction of volatile organic compounds and are toxic or even carcinogenic. Polycyclic aromatic hydrocarbons (PAHs) are some of the worst atmospheric pollutants and they could lead to soot formation. Aromatic hydrocarbons can be generally summed up in two categories, the unsubstituted PAHs (see figure 2.9) and the substituted PAHs (see figure 2.10).

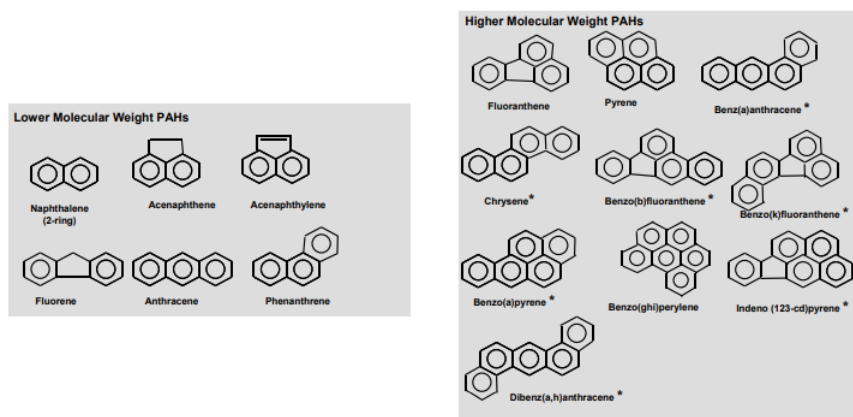


Figure 2.9 Unsubstituted PAHs

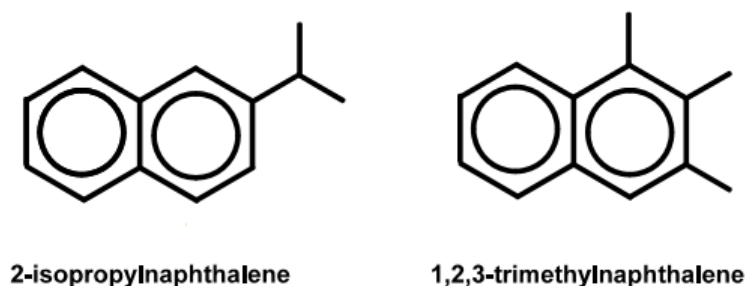


Figure 2.10 Substituted PAHs

- Unsubstituted PAHs: PAHs could be divided into two classes: low molecular weight PAHs (LPAHs) and high molecular weight PAHs (HPAHs). LPAHs (e.g. naphthalene, acenaphthene, acenaphthylene, fluorene, anthracene, phenanthrene) tend to have a core structure of two to three benzenoid rings (six-sided aromatic rings of carbon). HPAHs tend to have molecular structures of four or more benzenoid rings and include fluoranthene, pyrene, benzopyrene and benzofluoranthenes. LPAHs used to be more acutely toxic to aquatic organisms than HPAH since they are more watersoluble [14]. The toxicity and environmental cycling of PAHs may be further modified by the presence of various molecular side groups around the central ring (this derivation focuses primarily on the higher-molecular weight).
- Substituted PAHs: alkylated PAHs, having attached carbon-hydrogen chains (especially methyl groups), have been frequently identified in environmental samples. Basic research on alkylated and halogenated PAHs in the environment has been very limited up to the last five to ten years; therefore, knowledge of environmental cycling or toxicity is very limited. The location of alkyl groups around the ring structure strongly influence carcinogenicity and other toxic effects.

Furthermore, all aromatic hydrocarbons have a special importance in the investigation of soot or in efforts for soot reduction in jet fuels. Therefore, in comparison to cycloalkanes and paraffins, aromatic hydrocarbons occur in smaller quantities in jet fuels and their maximum levels are restricted. The generic process of soot formation is shown in the following figure:

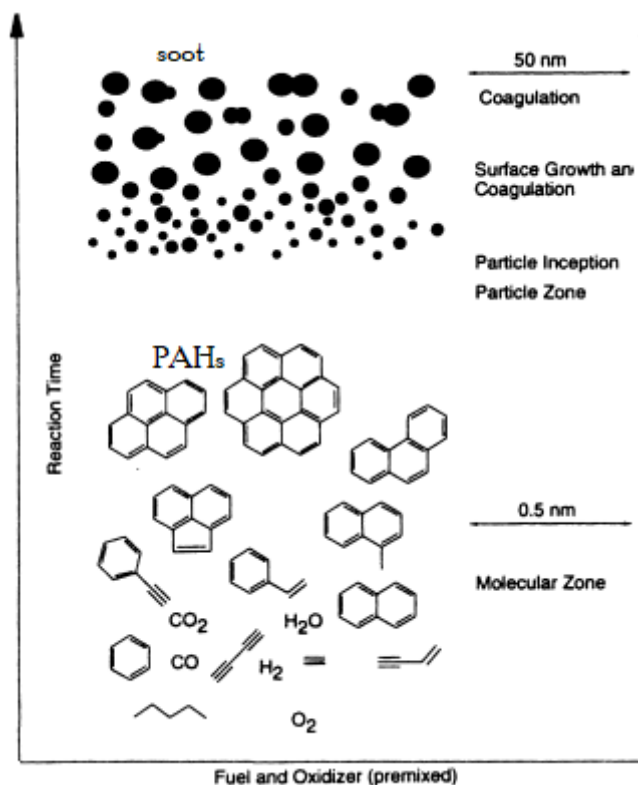


Figure 2.11 Soot formation

- **Non-hydrocarbon compounds:** non-hydrocarbon compounds, such as sulfur and its derivatives, are also found in jet fuels. Besides them, it's important to remind additives, present in limited quantities (they are often only measurable in parts per million) in order to improve the combustion performance (generally by eliminating undesirable effects) or to meet specific requirements of certain aircraft or airline operators. They divide in:
 - Antioxidants: olefinic components are often used in refineries to maximise gasoline volumes, despite being fundamentally unstable to oxidation, principally via free-radical propagation. Fuels containing these components can be prone to gum formation, color degradation and shortened induction periods. Furthermore, the presence of significant levels of hydroprocessed components in jet fuels are prone to forming peroxides, which can attack fuel-system elastomers. These additives extend the induction period and eliminate radical chain reactions involved in hydrocarbons oxidation, holding the side effects.
 - Antiknock agent: an antiknock agent is a gasoline additive used to reduce engine knocking and to increase the fuel's octane rating by raising the temperature and pressure at which autoignition occurs.

- Metal deactivators: they are fuel and oil additives used to stabilize fluids by deactivating (usually by sequestering) metal ions, mostly introduced by the action of naturally occurring acids in the fuel and acids generated in lubricants by oxidative processes with the metallic parts of the systems (e.g. copper or iron). Metal deactivators inhibit the catalytic effects of such ions, retarding the formation of gummy residues and sediment formation.
- Metal passivation: metal passivation additives are designed for being used in fuels containing elemental sulfur, hydrogen sulfide (H_2S) or mercaptans. The additives bond to the surface of copper, copper alloy or silver components to protect them from degradation.
- Fuel system icing inhibitors: it is an additive to aviation fuels that prevents the formation of ice in fuel lines. As an aircraft gains altitude, the temperature drops and jet fuel's capacity to hold water is diminished. Dissolved water can separate out and could become a serious problem if it freezes in fuel lines or filters, blocking the flow of fuel and shutting down an engine.
- Corrosion inhibitors: it is a chemical compound that, when added to a liquid or gas, decreases the corrosion rate of a material, typically a metal or an alloy. A common mechanism for inhibiting corrosion involves formation of a coating, in general a passivation layer, which prevents access of the corrosive substance to the metal.
- Static dissipator: hydrocarbon liquids, such as jet fuels and aviation gasolines, can generate sufficient electrostatic charge when flowing through the pipes and filters of a modern fuel handling system to produce electrical discharges when the liquids are loaded into receiving tanks. One way of reducing the danger of electrostatic discharges during fuel handling is the use of a static dissipator additive to raise the conductivity of the fuel and thereby promote the rapid dissipation of the charge.

Table 3.5 depicts the hydrocarbons related to respective families. These hydrocarbons are mainly chosen according to composition of target fuel. The physical properties of each compound in table 3.5 were calculated through their specific numerical models or taken through the literature review. Formation enthalpy Δh_f^0 and combustion enthalpy $\Delta_c H^0$ were calculated at 298 K using Benson's Method [15] [16]. Threshold Sooting Index (TSI) values, boiling temperature T_{boil} , critical temperature T_{crit} , critical pressure p_{crit} , liquid density ρ and standard normal entropy s^0 were taken from bibliography [17], [15] and [18]. Dynamic viscosity η of individual compounds were calculated at 20 °C using Morrio's Method [15], [19]. Kinematic viscosity ν and reduced temperature T_r were calculated using the following equations:

$$\left\{ \begin{array}{l} T_r = \frac{T}{T_{crit}} = \frac{273.15 + T_g}{T_{crit}} \\ \nu = \frac{\eta}{\rho} \end{array} \right. \quad \text{where} \quad \left\{ \begin{array}{l} T_g \text{ is the given temperature} \\ \rho \text{ is the compounds liquid density} \end{array} \right.$$

2.2 Kerosene

This master thesis is mainly focused on the development of a surrogate model for kerosene. The general principle to design a surrogate model is that the model must have similar physical and chemical characteristics of the target fuel. Therefore, this chapter is mainly concentrated to define the composition and to identify the most important physical and chemical properties of kerosene, trying at the same time to introduce some historical information about the fuel's utilization.

2.2.1 Kerosene types

Kerosene mixtures are thin, colorless and have low-volatile components of crude oil with a boiling range of about 150–300°C and density of 0.780–0.810 $\frac{\text{kg}}{\text{dm}^3}$. Previously, kerosene was only obtained by fractional distillation of petroleum (also known as straight run distillation), which consists of the separation of crude into several fractions, each with its boiling point. Technically, this is achieved by heating the crude oil, then separating and condensing the vapors. The results are fuel distillates and the remaining heavy residue. Straight distillation is performed in continuous systems, which allow to evaporate and to fraction the distillates in a single process loop. Nowadays, kerosene is mostly mixtures of such straight run distillates with converted components which were generated by catalytic crack-processes in hot hydrogen rich atmosphere or at moderate temperatures and pressure in hydrogen atmosphere. Kerosene, in general, can be thought as the starting point for the development of jet fuels, which are a mixture of a large number of different hydrocarbons. Because the exact composition of jet fuel varies widely based on petroleum source, it is impossible to define jet fuel as a ratio of specific hydrocarbons. Jet fuel is therefore defined as a performance specification rather than a chemical compound. Furthermore, the range of molecular mass between hydrocarbons (or different carbon numbers) is defined by the requirements for the product, such as the freezing point or smoke point. Kerosene-type jet fuel (including Jet A and Jet A-1) usually has a carbon number distribution between about 8 and 16 (carbon atoms per molecule) and shows the following percentage of hydrocarbons (figure 2.12).

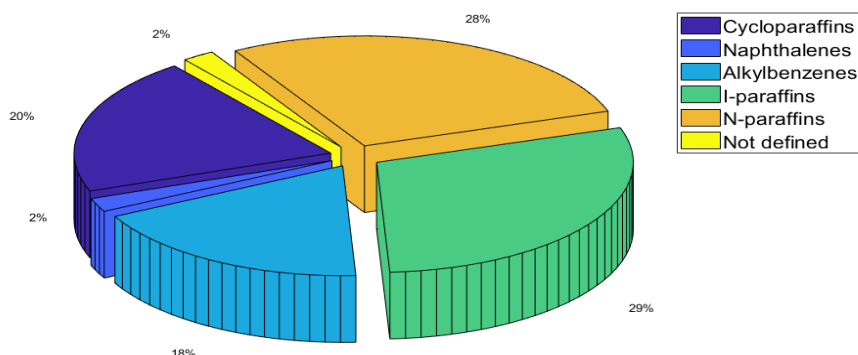


Figure 2.12 Typical hydrocarbon distribution for kerosene-type jet fuel

Typical physical properties for JP–4, JP–5, JP–7, JP–8, Jet A–1, Jet A and RP–1 are specified in the table 2.1 [20], [21].

2.2. KEROSENE

Property	JP-4	JP-5	JP-7	JP-8	Jet A-1	Jet A	RP-1
Approximate formula	$C_{8.5}H_{17}$	$C_{12}H_{22}$	$C_{12}H_{25}$	$C_{11}H_{21}$	$C_{11}H_{21}$	$C_{11}H_{21}$	$C_{12}H_{24}$
HC ratio [-]	1.99	1.87	2.02	1.91	1.91	1.91	1.98
Boiling range [°C]	160–238	182–257	188–249	166–266	166–266	166–266	177–289
Freezing point [°C]	–62	–49	–44	–51	–46	–51	–48
Flash point [°C]	–48	64	60	53	53	53	57
Net heating value $\left[\frac{BTU}{lb}\right]$	18.7	18.53	18.7	18.58	18.58	18.58	18.65
Specific gravity at 16 °C $\left[\frac{kg}{m^3}\right]$	760	810	790	810	810	810	810
T_{crit} [°F]	327	399	399	410	410	410	410
P_{crit} [psia]	450	290	305	340	340	340	315
Average composition							
Aromatics [%vol]	10	19	3	18	18	18	3
Naphtenes [%vol]	29	34	32	20	20	20	58
Paraffines [%vol]	59	45	65	60	60	60	39
Olefines [%vol]	2	2	-	2	2	2	-
Sulfures [ppm]	370	470	60	490	490	490	20

Table 2.1 Fuel characteristics for different aviation fuels

The main properties of these fuels (and many others) are presented in the following pages. It's important to remind that the first three fuel jets proposed have limited consumption, since they are used only in Russia and in the Commonwealth of Independent States nations, and that the fuel properties could change up to the origin of the feedstocks and the production method.

- **T-1:** T-1 is a product of distillation of low sulfur content naphthene based oil with boiling range of 130-280 °C. It contains a large volume of naphthenic acids and therefore has a high acidity level. It is leached and washed with water after fractionation. Heterotopic naphthenic compounds in the fuel provide good wear-reducing properties and chemical stability. On the other hand, the fuel has very low thermal oxidative stability. Continuous tests have demonstrated that when fuel is used in Tu-154 engines, this leads to increased resin deposits and reduced life term of the engine. Only premium fuel grades are currently produced, but with limited volumes.
- **T-2:** T-2 is a product of distillation oil of wide fractional composition (60-280 °C). It contains up to 40% gasoline cuts which leads to high pressure of saturated vapours, low viscosity and density. The maximized pressure of saturated vapours will lead to potential formation of vapour locks in the fuel system of the aircraft which limits its flight altitude.
- **TS-1:** TS-1 is produced by straight atmospheric distillation from a high sulfur crude, half of which is hydrotreated and the other half a straight-run product which may have had mild caustic treatment. It is a kerosene-type fuel with slightly higher volatility (flash point is 28°C minimum) and lower freeze point (< –50°C) compared with Jet A-1. It is supplied against the GOST 10227 specification and it is the main jet fuel grade available in Russia and the C.I.S..

2.2. KEROSENE

The main properties of these fuels are reported in the following table [22]:

Charateristic	T-1	TS-1	T-2
Density $\left[\frac{kg}{m^3}\right]$	800-850	> 775	> 775
Initial boiling point $[^{\circ}C]$	150	150	> 60
Kinematic viscosity $\left[\frac{m^2}{s}\right]$	1.50	1.25	1.05
Flash point $[^{\circ}C]$	30	20	-
Crystallization point $[^{\circ}C]$	-60	-60	-60
Aromatic hydrocarbon content $\left[\frac{mg}{100\text{ ml}}\right]$	25	22	22
Sulphur content [%]	0.10	0.25	0.25
Net calorific value $\left[\frac{MJ}{kg}\right]$	42.915	42.915	42.915
Soot [%]	0.005	0.005	0.005

Table 2.2 Main properties of T-family jet fuels

- **JP-1:** JP-1, also known as avtur, was the first U.S. military standard jet fuel (hence the 1 in the designation), with its specifications issued in 1944; it was an extremely narrow-cut, high-alkane kerosene, not far from what would later become RP-1. As a result, it had both a very low freezing point ($-60^{\circ}C$ maximum) and a very high flash point ($\simeq 40^{\circ}C$). Its only drawback was that it was hard to produce and therefore expensive and in chronically short supply, which prompted the development of wide-cut fuels (first the extremely-wide-cut JP-3, followed by the somewhat saner JP-4) and the gradual disappearance of JP-1 (although, judging by mentions in various aircraft accident reports, it was still being produced into the 1970s).
- **JP-2:** in order to overcome the production problems of JP-1, a wide-cut distillate fuel, JP-2 (specification AN-F-34) was developed in the last years of World War II. However, the use of JP-2 was limited to experimental testing and experimental service use and was found to have unsuitable viscosity and flammability (even if it shows a higher freezing point than JP-1). Then, nowadays, this fuel is considered rather obsolete.
- **JP-3:** JP-3, specified in 1947, was a mixture of 65% gasoline and 35% kerosene. Because of its gasoline high percentage, its characteristics were quite similar to. This included low flash point ($4^{\circ}C$), easy cold weather starting and poor lubricating qualities. There was also a high fuel loss due to evaporation (its vapor pressure of 7 psi ($\simeq 48300$ Pa) let a maximum cruising altitude of $\simeq 6000$ m)², a high tendency to vapor lock and it was even more volatile than JP-2.

² Pressure on Earth varies with the altitude; as it increases, atmospheric pressure decreases. The following equation (also known as barometric) relates atmospheric pressure p to altitude h :

$$p = p_0 e^{-\frac{ghMW}{T_0 R}}$$

where g is the gravitational acceleration, p_0 is the standard atmospheric pressure, MW is the molar mass of the air, T_0 is the standard temperature and R the universal gas constant

2.2. KEROSENE

- **JP-4:** JP-4, also known as avtag or as F-40 (NATO), is an aviation 50% gasoline and 50% kerosene blend used by the U.S. Air Force (USAF) from 1951 until the 1980s. The JP-4 fuel, covered by the MIL-DTL-5624U specification, was intended for use in aircraft turbine engines. JP-4 is called a wide-cut fuel because it is produced from a stock comprising products from direct distillation, products of thermal and catalytic cracking and contains a wide array of carbon chain-lengths, from 4 to 16 carbons long. It was initially developed for broad availability in times of need and to overcome the JP-3 critical pressure problems. In fact, JP-4 vapor pressure is restricted to 2-3 psi (≈ 13800 - 20700 Pa), guaranteeing adequate low temperature starting and high-altitude relight performance. The composition of JP-4 is approximately 13.0% (by volume) aromatics, 1.0% olefins and 86.0% saturated hydrocarbons. It has a distillation temperature range of 60-270 °C. The maximum levels of aromatics are limited to 20-25% by volume. Olefins, the most reactive hydrocarbons, are permitted at only 5% by volume. Benzene is a contaminant usually present below 0.5% by volume.
- **JP-5:** JP-5, also known as avcat or as F-44 (NATO), is one of the most important and commonly used kerosene. JP-5, covered by the MIL-DTL-5624U specification, was developed for the U.S. Navy in 1952 for use in aircraft stationed aboard aircraft carriers and was intended for use in aircraft turbine engines. The fuel is refined by a straight distillation of crude or shale oil or by a distillation of crude oil in the presence of a catalyst. It is mainly composed by primarily aliphatic and aromatic hydrocarbons and could further include some additives, in order to improve the chemical and physical features of the blend. These additives are used in specified amounts only, as governed by commercial and military specifications. However, JP-5 usually consists of $\approx 23\%$ by volume of alkanes, $\approx 53\%$ of cycloalkanes, $\approx 25\%$ of aromatics and $\approx 2\%$ of olefins. JP-5's flash point temperature is 60 °C, value that affords an additional degree of safety in handling fuel on aircraft carriers, and a maximum freezing point of -46 °C.

Characteristic	JP-1	JP-2	JP-3	JP-4	JP-5
Density $\left[\frac{kg}{m^3}\right]$	814	764	792	764	830
Vapor pressure at 38 °C [mmHg]	-	315	368	134-160	55
Initial boiling point [°C]	-	65.5	70	65	210
Kinematic viscosity at -40°C $\left[\frac{m^2}{s}\right]$	10	10	10	-	-
Flash point [°C]	43	-	-23	-13.8	38
Freezing point [°C]	-60	-60	-60	-60	-40
Aromatic content $\left[\frac{mg}{100ml}\right]$	14.3	11.3	25	13	20
Sulphur content [%]	0.20	0.20	0.50	0.40	0.40
Net calorific value $\left[\frac{kJ}{kg}\right]$	42550	42760	42727	42760	42510

Table 2.3 Properties of the previous jet fuel

- **JP-6:** JP-6 was a kerosene fuel developed in 1956 for the General Electric YJ93 jet engine of the XB-70 Valkyrie supersonic aircraft. Although the XB-70 was also designed to burn an exotic, boron-based fuel to give increased range, the relative program was later cancelled because of costs and the marginal range increase obtained. JP-6 was similar to JP-5 but with lower freeze point and improved thermal oxidative stability.
- **JP-7:** JP-7 is a special kerosene fuel used for the Lockheed SR-71 Blackbird, an advanced, long-range, strategic reconnaissance aircraft, and used by the U.S. Air Force from 1964 to 1998. It was developed to obtain a new fuel having a low vapor pressure and excellent thermal oxidative stability (the flash point is $\simeq 60\text{ }^{\circ}\text{C}$), because of the very high altitude and Mach 3+ cruising speed of the SR-71. To insure adequate combustor life, the fuel was also required to have excellent combustion characteristics, initially specified in terms of hydrogen content. A high net heat of combustion was also specified. These requirements essentially have the effect of limiting the composition of JP-7 in paraffins' and cycloparaffins' percentages. The aromatic content is typically below 5.0% by volume. JP-7 usually consists of $\simeq 60.0\%$ by volume of alkanes, $\simeq 30.0\%$ of cycloalkanes and $\simeq 5.0\%$ of aromatics. This fuel composition results in a fuel with a relatively high freezing point (-43.5°C), but the SR-71 spends little time at subsonic speeds at high altitude. JP-7 is not a distillate fuel as are most other jet fuels but is composed of special blending stocks that have been subjected to special processes to remove aromatics. This special processing results in a very clean hydrocarbon mixture that is very low in the sulfur, nitrogen and oxygen impurities typically found in distillate fuels, giving a fuel with excellent thermal oxidative stability but very poor lubricating properties.



Figure 2.13 A Pratt&Whitney J58 burning off JP-7 fuel

- **JP-8:** JP-8 was developed as a result of the dire combat experience obtained during the South-East Asian Conflict, which revealed that USAF aircrafts using highly volatile JP-4 had higher losses than US aircrafts using low volatility JP-5. Furthermore, crash data indicated that the probability of a postcrash is almost 100% when using JP-4 fuel, much higher than with a kerosene fuel such as JP-5. The increased safety of kerosene fuels, as compared to wide-cut fuels as JP-4, was also evident in the number and severity of ground handling accidents. Therefore, JP-8 was developed to give the Air Force a safer, kerosene-based jet fuel that would still have adequate availability and an acceptable freeze point. The properties of JP-8 were selected to be identical to those of commercial Jet A-1, which had a freezing point of -50°C (this was done to simplify the production of JP-8). Subsequently the freezing point of Jet A-1 was raised to -47°C , forcing the freezing point of JP-8 to increase accordingly (for some polar locations the ground temperatures can be as low as -50° for up to 24 hours, but a maximum allowable freeze point of -47°C is believed adequate for European theater flight and ground operations). JP-8, also known as F-34 (NATO), usually consists of $\simeq 13.0\%$ by volume of alkanes, $\simeq 27.0\%$ of cycloalkanes, $\simeq 20.0\%$ of aromatics (included benzene, alkyl benzenes, toluene, xylene, indenenes naphthalenes) and $\simeq 40.0\%$ of olefins. Its minimum flash point temperature is 38°C and it has a volumetric energy content of about $42800 \frac{\text{kJ}}{\text{m}^3}$. When thermal stability additive is in JP-8, the fuel is called JP-8+100. Furthermore, it's important to remind JP-8+100LT, which is a variant of JP-8+100, with additives to facilitate low-temperature performance. Because JP-8 is a kerosene-based fuel with relatively low volatility, ground starting and altitude relight performance of jet aircraft are affected. US Army helicopters have experienced significantly degraded starting performance when using JP-8. Although the technology is available to provide adequate solutions, modification of existing aircraft engines are required.



Figure 2.14 JP-8 strip

- **JP-9 and JP-10:** JP-9 and JP-10 are specialty fuels that have been developed for demanding applications, such as aircraft-launched missiles [23]. The required properties are: maximum volumetric energy content, clean burning and good low-temperature performance. To achieve these properties, the fuels are formulated with high-density naphthenes in nearly pure form. These fuels only are used in limited volumes and in situations where price is a minor consideration. JP-9 is mainly a blend of three hydrocarbons: methylcyclohexane, perhydronorbornadiene (a norbornadiene dimer) and exo-tetrahydrodicyclopentadiene. JP-9 has a minimum volumetric heat content of $39573 \frac{\text{kJ}}{\text{m}^3}$. JP-10 could be essentially composed by a single-hydrocarbon exo-tetrahydrodicyclopentadiene and it superseded JP-9 fuel, achieving a lower low-temperature service limit of -54°C . It has a minimum volumetric heat content of $39434 \frac{\text{kJ}}{\text{m}^3}$.

2.2. KEROSENE

A sum up of the main properties of the previous fuels is shown in the next table:

Specification Requirements	JP-1	JP-2	JP-3	JP-4	JP-4	JP-5	JP-6	JP-7	JP-8
Specification Number	AN-F-32	AN-F-3	AN-F-58	MIL-F-5624A	MIL-T-5624M	MIL-T-5624M	MIL-25656B	MIL-T-38219B	MIL-T-83133B
Distillation Temperature °C									
Initial Boiling Point, min	-	66	-	-	R	R	138	182	-
10 percent recovered, max	210	-	-	121	R	205	177	196 min	205
20 percent recovered, max	-	-	-	-	145	R	-	206 min	R
50 percent recovered, max	-	-	-	-	190	R	218	R	R
90 percent recovered, max	254	-	204	-	245	R	260	260	R
End Point, max	300	260	316	288	270	290	-	288	300
Reid Vapor Pressure, $\left[\frac{lb_f}{in^2}\right]$ at 38 °C	-	2 max	5-7	2-3	2-3	-	-	-	-
Flash Point, °C, min	43	-	-	-	-	60	-	60	38
Viscosity, $[cSt]$, max at temperature °C	10	10	-	-	-	8.5	7	8	8
Freezing Point, °C, min	-40	-40	-	-	-	-20	-40	-20	-20
Density, $\left[\frac{kg}{l}\right]$ at 15°	-60	-60	-60	-60	-58	-46	-54	-43.3	-47
minimum	-	-	-	-	-	-	-	-	-
maximum	0.850	0.850	0.728	0.747	0.751	0.788	0.780	0.779	0.775
Aromatics, vol percent, max	20	20	0.802	0.825	0.802	0.845	0.840	0.806	0.806
Olefins, vol percent, max	-	-	25	25	25	25	25	25	25
Bromine Number, max	3	3	30	30	5	5	5	-	5
Sulfur, wt percent, max	0.20	0.20	0.40	0.40	0.40	0.40	0.40	0.10	0.30
Mercaptan Sulfur, weight percent, max	-	-	0.005	0.005	0.002	0.002	0.001	0.001	0.002
Existent Gum, $\left[\frac{mg}{100ml}\right]$, max	5	5	10	10	7	7	5	5	7
Accl. Gum, $\left[\frac{mg}{100ml}\right]$, max	8	8	20	20	-	-	10	-	-
test length, hours	16	7	16	16	-	-	16	-	-
Corrosion, copper strip, max	-	-	-	-	1b	1b	1b	1b	1b
Total acid, $\left[\frac{mgKOH}{g}\right]$, max	-	-	-	-	0.015	0.015	-	-	0.015
Heating Value, $\left[\frac{BTU}{lb}\right]$, min	-	-	18400	18400	18400	18300	18400	18700	18400
Smoke Point, mm, min, or	-	-	-	-	20	19	20	-	19
Hydrogen Content, wt %, min	-	-	-	-	13.6	13.4	-	14.4	13.4
Thermal oxidative stability	-	-	-	-	-	-	-	-	-
JFTOT test temp, °C	-	-	-	-	260	260	-	355	260
Test length, hours	-	-	-	-	2.5	2.5	-	5.0	2.5

Table 2.4 Sum up of JPs properties

- **Jet A-1 and Jet A:** the Check List for Jet A-1 forms the basis of international supply of virtually all commercial aviation world-wide outside of North America, Former Soviet Union, some East European countries and the People's Republic of China. Jet A-1, also known as avtur or as F-35 (NATO), embodies the most stringent requirements of the following specifications: British Def Stan 91-91, ASTM D1655 Kerosine Type Jet A-1 and IATA Guidance Material-Kerosine Type. In the USA and parts of Canada, Jet A is the fuel supplied at civil airports. Jet A-1 and Jet-A are almost the same, but the first one has lower freezing point (-47 °C vs. -40 °C). The lower freezing point makes Jet A-1 more suitable for long international flights, especially on polar routes during the winter. International Jet A-1 requires the use of an additive to increase the electrical conductivity of the fuel. Furthermore, it contains a static dissipator additive and may also have an antioxidant. The aromatic content of Jet A-1 is limited to 25% by volume. Indeed, Jet A fuel must reach ASTM specification D1655. The choice of Jet A for its use in the United States is driven by concerns about fuel price and availability (many years of experience have shown that Jet A is suitable for use in the United States, especially for domestic flights). Both of them are a petroleum distillate blended from kerosene fractions.
- **Jet B:** Jet B is a blend of approximately 30% kerosene and 70% gasoline, that is used for its enhanced cold-weather performance in the coldest regions of the world, as Canada or Alaska. However, Jet B's lighter composition makes it more than little dangerous to handle. It has a very low freezing point of -55 °C and a low flash point, as well.

Properties	Jet A	Jet A-1	Jet B
Aromatics [%] vol	23.4	19.5	20
Sulphur [%] mass	0.07	0.02	0.3
Final boiling point [°C]	280	258	-
Density at 15° $\frac{kg}{m^3}$	775-840	751-802	751-802
Freezing point [°C]	-40	-47	-55
Viscosity at -20°C $\frac{mm^2}{s}$	5.2	3.5	-
Specific energy, net, $\frac{kJ}{kg}$	43020	43150	42800
Energy density $\frac{kJ}{m^3}$	35300	34700	33230
Flash point [°C]	38		-
Autoignition temperature [°C]	210		-
Smoke point [mm]	19.5	25	20
Naphthalenes [%] vol	2.9	1.5	-

Table 2.5 Comparison between Jet A-1, Jet A and Jet B properties

2.2. KEROSENE

- **RP-1:** RP-1 is a highly refined form of kerosene outwardly similar to jet fuel, used as the standard U.S. rocket fuel. RP-1 has a lower specific impulse than liquid hydrogen (lH_2), but is cheaper, stable at room temperature (far less than an explosion hazard) and far denser. RP-1 is significantly more powerful than lH_2 by volume. RP-1 also has a fraction of the toxicity and carcinogenic hazards of hydrazine, another room-temperature liquid fuel. In RP-1 olefin content is not supposed and the percentage of aromatics is strictly limited. Referring to the figure 2.15, it is possible to notice that the use of the RP-1 for the Saturn V is limited to the first stage, since RP-1 doesn't provide as much energy per unit mass as lH_2 but it is twice the density, so, the only way they could get the necessary total impulse from the first stage, was to use the denser fuel.

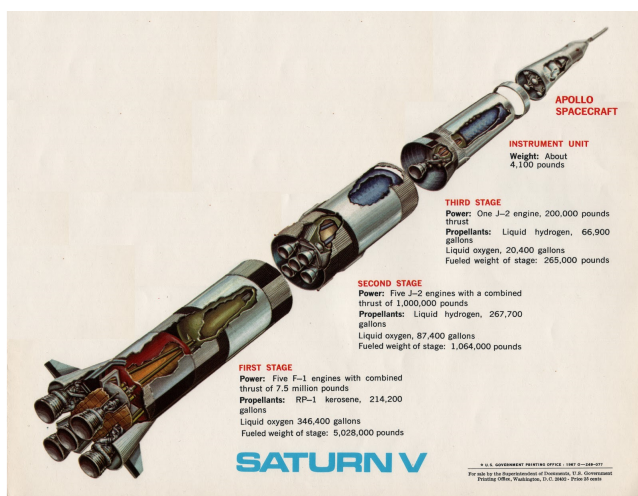


Figure 2.15 Saturn V

- **RJ-1:** distributed under the specification NIL-F-25558, RJ-1 was first released in April 1956. According to the available records, RJ-1 was intended to be a high boiling range kerosene distillate fuel and it was designed for the Navaho missile, a long-range cruise missile that never became operational. Then, since no existing or planned system would have used the fuel, the RJ-1 specification was cancelled in March 1983.
- **RJ-2 and RJ-3:** no information has been found on these fuels. It stands to reason that these fuels never progressed past the development stage.
- **RJ-4:** TH dimer (see figure 2.16), grade RJ-4, describes the first high density synthetic hydrocarbon missile fuel. Developed by the US Navy, RJ-4 was used in the mid-1960s in the ramjet-powered Tales missile. The freezing point of RJ-4 is -46°C , too high for use in air launched missiles. However, RJ-4 is the primary fuel for the Ground Launched Cruise Missile.

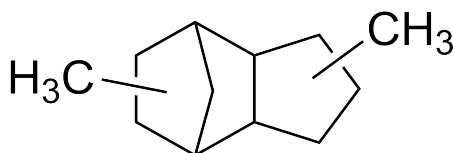


Figure 2.16 TH-dimer

2.2. KEROSENE

- **RJ-5:** RJ-5, a proposed fuel that is a mixture of hydrogenated dimers of norbornadiene, is based on Shelldyne H technology developed by the Shell Oil Company in the 1960s. It is unusual in being a liquid hydrocarbon with a density greater than that of water. Its high freezing point, high viscosity and high cost have deterred its use in Air Force systems.
- **RJ-6:** RJ-6 is a proposed fuel consisting of a mixture of RJ-5 and JP-10. This mixture eliminates the freezing point problem and reduces the high costs and high viscosity of RJ-5, while retaining much of its high volumetric energy density. Its proposed composition is 60% RJ-5 and 40% JP-10.

The chemical and physical properties of the last three fuels are summed up in the following table:

Typical Properties of Liquid Hydrocarbon Missile Fuels			
	RJ-4	RJ-5	RJ-6
Specification	MIL-F-82522	DRAFT	DRAFT
Molecular Formula	$C_{12}H_{20}$	$C_{14}H_{18}$	$C_{12}H_{17}$
Molecular Weight	164	186	161
Density \@ -40°C $\left[\frac{kg}{dm^3}\right]$	0.93	1.08	1.024
Boiling Range °C			
minimum	207	260	182
maximum	221	285	285
Flash Point °C	71	104	61
Freeze Point °C	-46	-29	-54
Viscosity \@ -40°C $[cSt]$	60	2000	140
Net heat of combustion	39600	44900	42400
$\left[\frac{MJ}{m^3}\right], \left[\frac{BTU}{gsl}\right], \left[\frac{BTU}{lb}\right]$	142000 18300	161000 17900	152000 18000

Table 2.6 Comparison between some missiles fuels properties

Comparing the fuel compositions represented in the previous pages, it can be concluded that defining fuel's chemistry is a very complex task, since it could greatly vary up to many factors (starting from the chemical development's processes arriving even to the geographical location of the feedstocks). These diverse compositions also complicate both experimentally and numerically the simulations of its components because of all the possible interactions between the compounds. As a result, the idea of finding numerical models which could lead to the development of alternative fuels is likely to become extremely complicated, but it has never been so urgent.

2.2.2 Kerosene modelling

Surrogate models are defined as having the same physical and chemical properties of the target practical fuels. These models, since characterized by a computationally lighter weight, are desirable for experimental compliance and could be used to simulate the reference fuel characteristics, such as density, heat capacity, viscosity, surface tension, volatility, etc. On the other hand, a chemical surrogate could be used to forecast chemical properties such as pre-oxidation stability, ignition behavior, flame speed, emission behavior, etc. Accounting these advantages, a significant progress in the development of surrogate mixtures for aviation fuels has recently occurred. The investigations are mostly concentrated to create surrogate mixtures which, in theory, could mimic the target kerosene. The proposed surrogate models differ in complexity and are valid for different applications. Eddings & coll. [24] developed two different surrogates, named Hex-11 and Hex-12, which are based on specific criteria for surrogate development and are composed of six compounds (see table 2.7). The surrogate models are formulated to match sooting tendency and volatility of Jet A. The results indicate that the two proposed surrogates are similar to Jet A in terms of volatility, which is reflected by the flash point and average boiling point. The SP of the surrogate Hex-12 seems to be close to that of Jet-A, whereas the SP of Hex-11 was off by 4 mm (table 2.8). Furthermore, the two surrogate mixtures matched the distillation curve of Jet A (figure 2.17).

Hex-11		Hex-12		Jet A	
	mol %		mol %		mol %
				n-paraffins	≈ 28
n-C ₈ H ₁₈	3.5	n-C ₈ H ₁₈	3		
n-C ₁₂ H ₂₆	40	n-C ₁₂ H ₂₆	30		
n-C ₁₆ H ₃₄	5	n-C ₁₆ H ₃₄	12		
				branched paraffins	≈ 29
Xylenes	8.5	Xylenes	15.0	mono-aromatics	≈ 18
Tetralin	8.0	Tetralin	13.0	diaromatics	≈ 2
Decalin	35.0	Decalin	27.0	cycloparaffins	≈ 20
				non-determined	≈ 3

Table 2.7 Composition of tested surrogate blends

Properties	Jet-A	Hex-11	Hex-12
Smoke point [mm]	24.5	28.7	23.1
TSI [-]	26.7	17.6	22.1
MW [$\frac{g}{mol}$]	173.5	151.5	152.2
VABP ^a [°C]	220.2	211.1	215.7
Flash point [°C]	40.9	40.3	41.3
Latent heat ^b [$\frac{kJ}{kg}$]	254.6	280.4	281.8
Combustion heat [$\frac{kJ}{kg}$]	44900	44500	44600

Table 2.8 Surrogates properties. ^a VABP means volumetric average boiling point; it is the mean of 10, 30, 50, 70, 90 % recovery temperature determined in ASTM D86. ^b Latent heat is estimated at VABP.

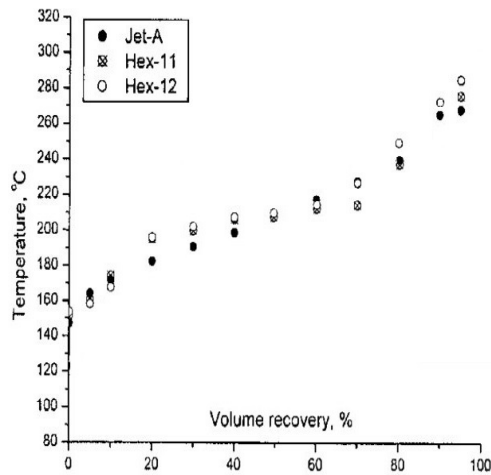


Figure 2.17 Distillation curve

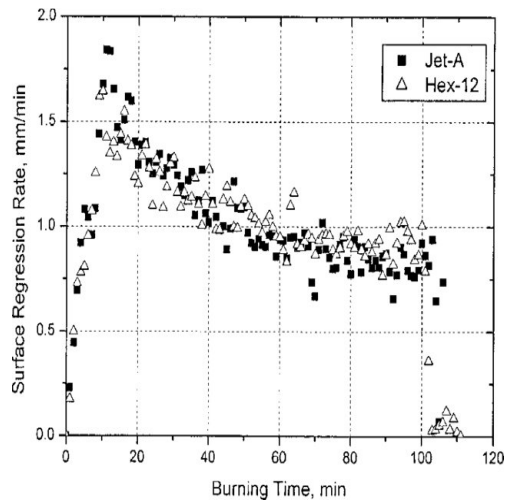


Figure 2.18 Surface regression rate

Since the most promising surrogate turned out to be Hex-12, some of its properties are shown in figure 2.18 and in figure 2.19:

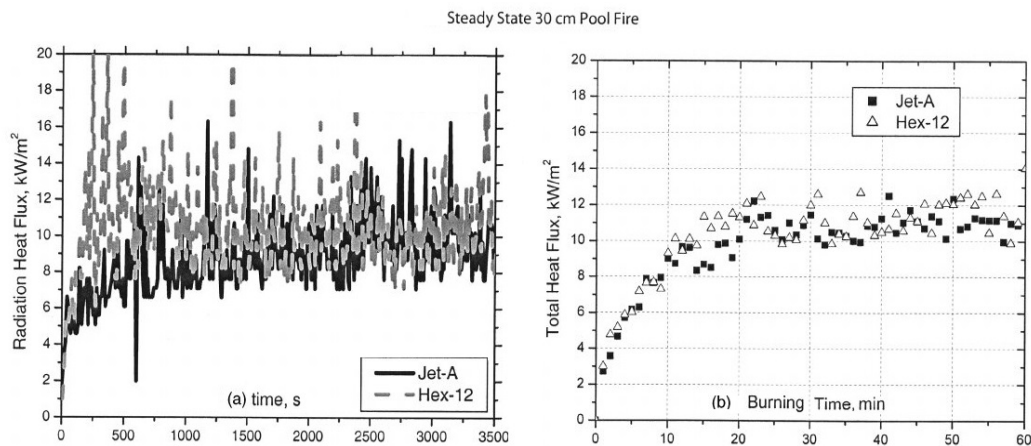


Figure 2.19 Hex-12 heat flux

Mati & coll. [25] compared computed results of a five component mixture model with experimental measurements using blended synthetic diesel fuel in a jet stirred reactor (JSR). A detailed kinetic reaction mechanism consists of 377 species and 2755 reversible reactions. The chemical kinetic model was formulated to match the amount of the various classes in the synthetic diesel fuel and was composed of 23.5% n-hexadecane, 19.0% iso-octane, 26.9% n-propyl-cyclohexane, 22.9% n-propyl-benzene and 7.7% 1-methyl-naphthalene. These represent respectively n-paraffins, cycloalkanes, mono-aromatic hydrocarbons, isoparaffins and polyaromatic hydrocarbons. The fuel density was $835 \frac{\text{kg}}{\text{m}^3}$, it had a cetane number of 50.4 and a 50% ASTM distillation temperature of 267°C . The global formula for this diesel fuel was determined to be $\text{C}_{15.5}\text{H}_{30}$. Overall, using the relative path analyses to delineate the most important reactions, the modelling showed a good consistency with the experimental data (figure 2.20).

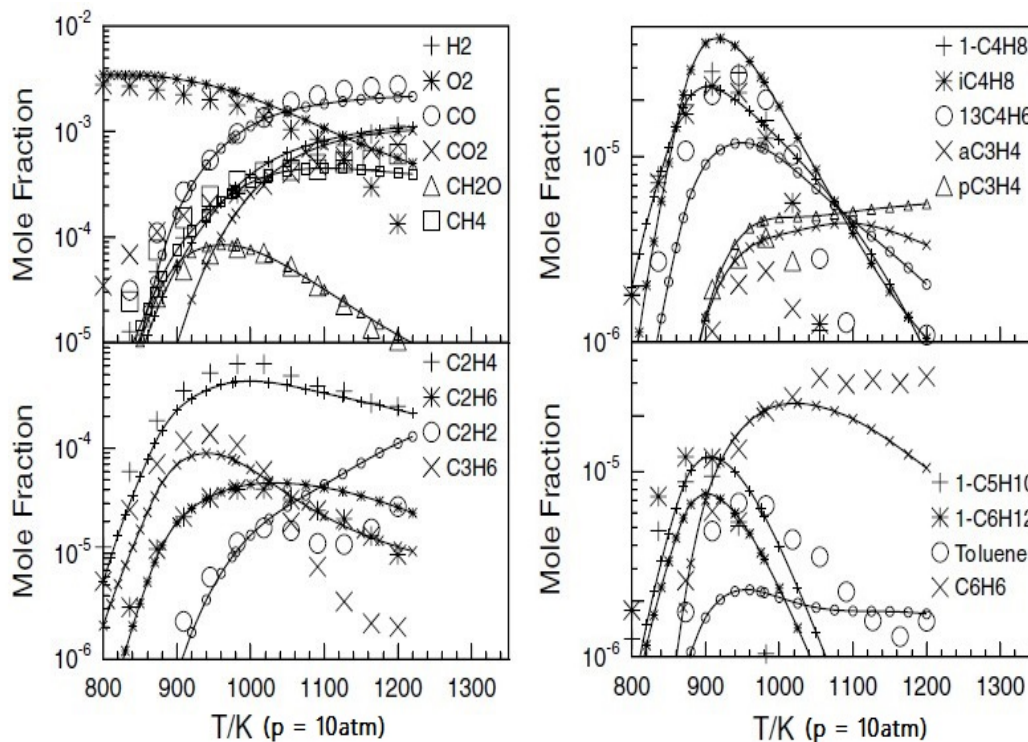


Figure 2.20 Predicted and measured intermediate species profiles

Dryer & coll. [31] presented a method for specifying a surrogate fuel composition for two jet fuels, Jet A and JP-8. In order to formulate mixtures for these gas turbine fuels, they chose to use the following hydrocarbons: n-alkanes (n-heptane, n-decane, n-dodecane), alkane isomers (iso-octane, iso-cenaten), cycloalkanes (n-methyl-cyclohexane) and alkylated aromatics (toluene, n-propylbenzene, 1,3,5-tri-methyl-benzene, 1-methyl-naphthalene). Two different sets of low temperature reactions for n-decane oxidation were tested, one from the studies of Gokulakrishnan & coll. [26] and the other one from the work of Westbrook & coll. [27]. The two formulated models for the surrogates oxidation's description consisted of 614/1615 and 830/2273 species/reversible reactions, respectively. C/H ratio, TSI and CN succeeded in matching properties in both surrogate and the target jet fuel. They stated that it is important to equal the C/H ratio, because it affects properties such as heat of reaction, flame temperature and flame speed. CN was suggested to match the ignition property of the surrogate and jet fuel. Figure 2.21 compares available jet fuel ignition delay data [28], [29], [30] against modeling predictions using the two models described above. Given the lack of optimization of the a priori assembled models, the agreement is excellent. At high temperatures, both models yield similar results, whereas discrepancies become more evident at lower to intermediate temperatures (i.e. $T \leq 950\text{K}$). This is an indication of the different developmental approaches to n-decane low-temperature chemistry in the studies of Gokulakrishnan and Westbrook. Generally, from these researches it's clear the need for additional validation data in the low-temperature regime.

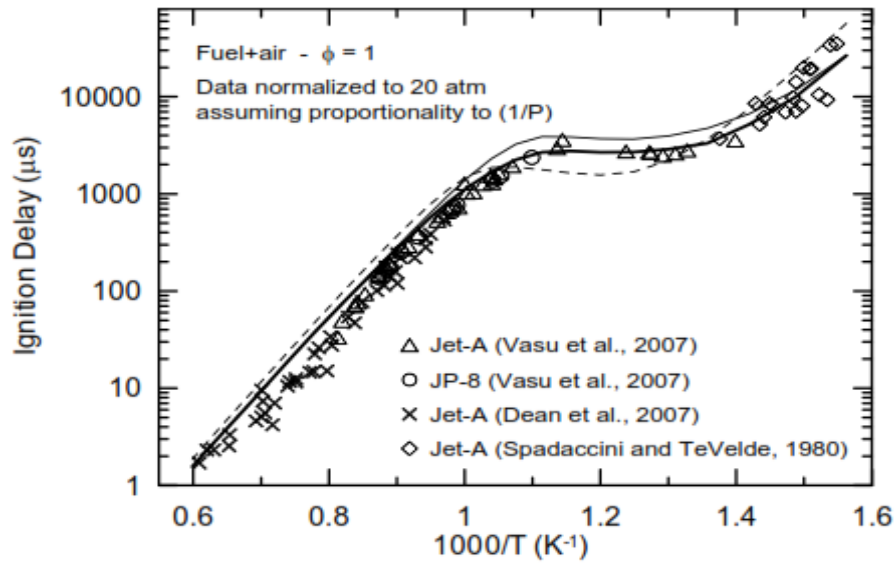


Figure 2.21 Experimental and model data for ignition delay

In the previous image, while solid lines are predictions using the n-decane low temperature kinetic subset of Gokulakrishnan & coll., dashed lines use the subset of Westbrook & coll. If the bold line denotes computations assuming a linear pressure rise of $10 \frac{\%}{\text{ms}}$ prior to ignition, the other curves were numerically modeled for stoichiometric fuel/air mixtures at an initial pressure of 20 atm assuming homogeneous, adiabatic and isochoric conditions (i.e. constant volume and internal energy). Honnet [32], in order to represent jet fuel JP-8, investigated the Aachen Surrogate with the composition of 80% n-decane and 20% 1,2,4-trimethylbenzene. Experiments made in a laminar counter flow diffusion flame (fig. 2.22) showed similar soot concentrations and ignition/extinction characteristics compared to the JP-8 ones. In general, their process of description of the Aachen surrogate is focused on a detailed kinetic model (based on n-decane chemical behaviour) and on the surrogate's properties validation over a wide range of conditions (from fig. 2.23 to fig. 2.26).

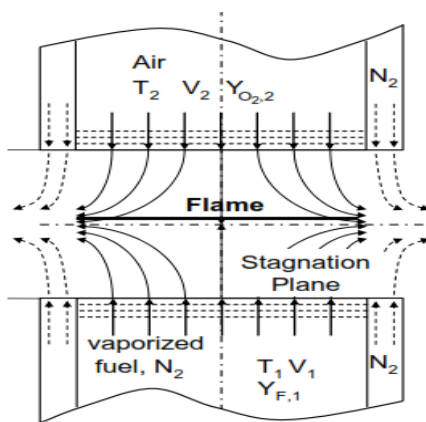


Figure 2.22 Counterflow

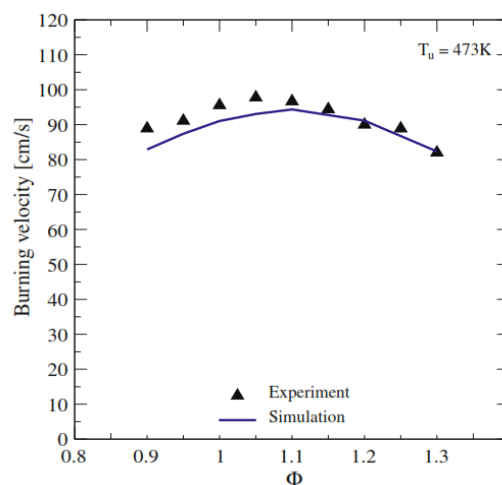


Figure 2.23 Surrogate burning velocity

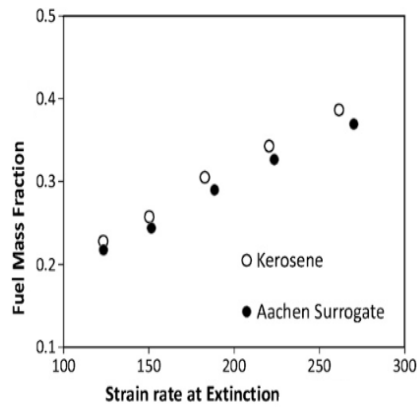


Figure 2.24 Fuel mass fraction

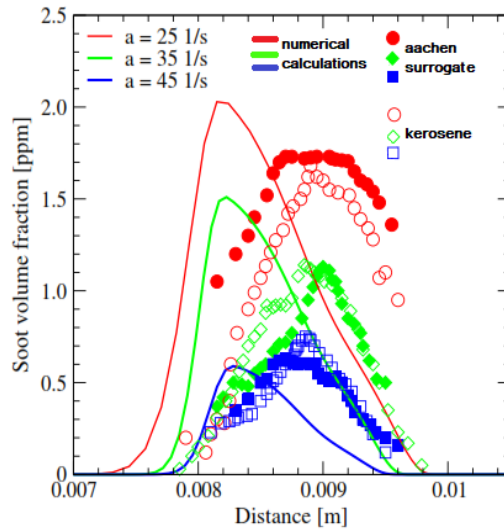


Figure 2.25 TSI

Furthermore, the improved n-decane mechanism showed promising results on the surrogate's ignition delay times, which are summed up in the following images. In fig. 2.26, the lines represent results obtained using the upgraded n-decane model, the dotted ones represent calculations performed using the mechanism shown in [33] and the symbols display the experiments described in [34].

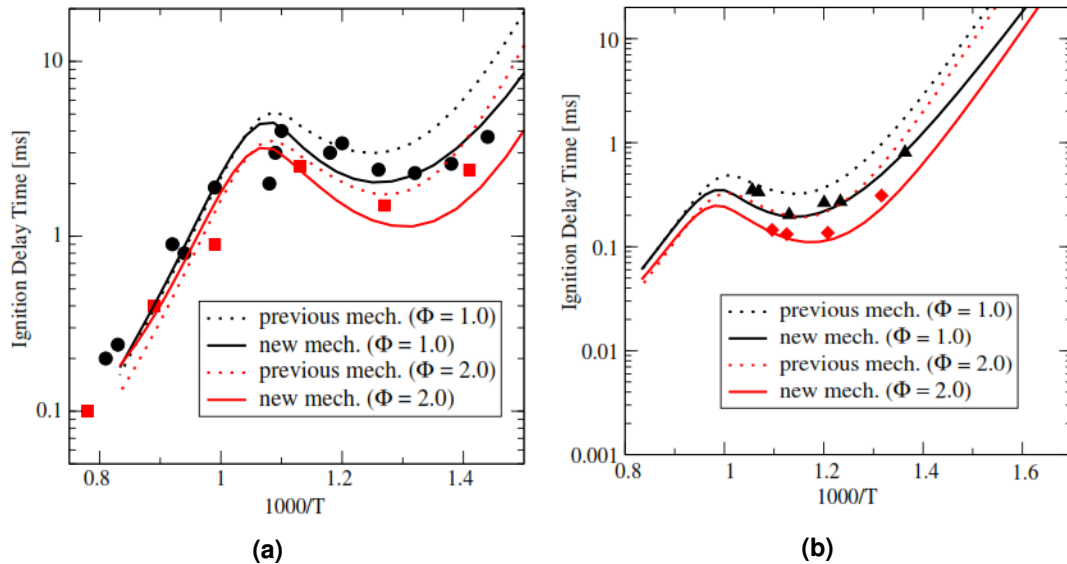


Figure 2.26 n-decane's ignition delay times

The n-decane's model was recovered from many studies, starting from the one of Lindstedt & Maurice [42], who reported a n-decane mechanism that satisfactorily reproduces several species profiles from the experiments of Vovelle [43].

Zeppieri [44] and Bikas & Peters [45] have developed n-decane mechanisms based on experimental measurements on shock-tube ignition, flow reactor and jet-stirred reactor experiments. Zeppieri's method includes detailed chemistry of n-decane and five n-decyl radicals and incorporates both internal hydrogen isomerization reactions and β -scission pathways for the various system radicals. To include this additional detailed reaction and simultaneously minimize the number of species present in the model, researchers made an important assumption regarding the distribution of radical isomers. It was assumed that the different isomers of a given alkyl radical are in equilibrium at each carbon number above the C_4 level, thereby allowing the inclusion of the reaction channels associated with each isomer, without imposing the computational penalty associated with including each isomer as a separate species in the mechanism. As a result, only a single radical is needed to represent all the isomers associated with it. Then, the high temperature model has been further revised and compared against a much wider set of experimental parameters, including high-temperature pyrolysis and oxidation data at atmospheric pressure. Turning to Bikas & Peters' mechanism, the model validation has been performed by using experimental measurements on a premixed flame of n-decane, O_2 and N_2 , stabilized at 1 atm. The reaction mechanism is characterized by 600 reactions and 67 species. Furthermore, special attention was directed towards an accurate description of species relevant to pollutant formation. Some years ago, Zhao & Zeppieri [41] made additional model/experimental comparisons to laminar burning rate measurements in a jet-wall stagnation flame configuration, burner-stabilized species profiles and stirred reactor data. While computed data, derived thanks to the previous partially reduced skeletal mechanism for n-decane pyrolysis and oxidation [44], were found to be in poor agreement, the analyses of experimental data based on the revised model, obtained updating the hydrogen/oxygen monoxide oxidation and small carbon number C_1 - C_3 sub mechanisms, thermochemistry and elementary rates, results in acceptable prediction of the experimental results. Predictions using the revised model were found to reproduce data used in validating the original model in including high temperature, atmospheric pressure flow reactor pyrolysis and oxidation, high pressure shock tube ignition delay and stirred reactor species measurements. The revised model predictions also agree well with atmospheric pressure, burner stabilized flame data and recently published shock tube ignition delay measurements at both low and high pressure (figure 2.27). While this mechanism is developed for high temperature applications, authors' recent work is intended to the addition of low and intermediate temperature submechanisms to the present one.

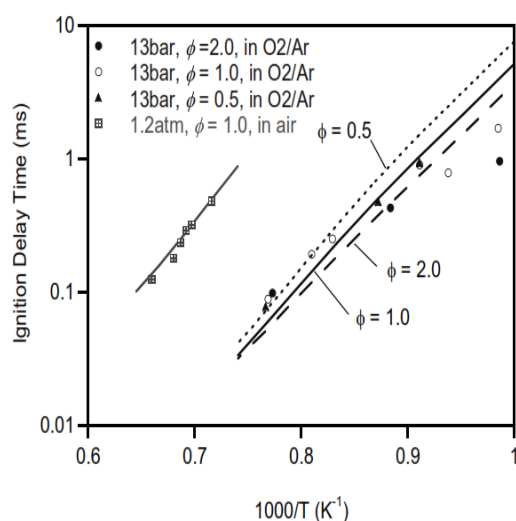


Figure 2.27 Ignition delay times

2.2. KEROSENE

Naik & coll. [35] proposed three components of FT fuel surrogate blends containing of n-dodecane, n-decane and iso-octane and optimized their composition to represent various properties of two different FT fuel sources, namely Syntroleum S-8 and Shell GTL. Both FT fuels were produced from natural gas using low temperature hydrocracking and isomerization process using cobalt. To generate optimal composition of the surrogate blend consisting of the three hydrocarbons, they used certain measured properties as targets (mainly CN, H/C molar ratio, lower heating value, ASTM D-86 T50 distillation point and density). The surrogate blend composition for the Shell GTL and the Syntroleum S-8 fuels and associated properties are given in table 2.9.

Property		Measured		Surrogate	
		Shell GTL	S-8	Shell GTL	S-8
iso-octane	%mol			28	32
n-decane				61	25
n-dodecane				11	61
CN [-]		61	60	61	61
H/C [-]		2.17	2.17	2.21	2.20
lower heating value $\frac{MJ}{kg}$		44.2	44.1	44.55	44.45
distillation point [K]		445	474	404	447
density $\frac{kg}{m^3}$		0.736	0.755	0.723	0.729

Table 2.9 Fuels' properties

An improved chemical kinetic mechanism for modeling the surrogate components' combustion and emissions behavior has been assembled and developed to accurately predict fundamental properties. Containing 753 species and 4668 reactions in CHEMKIN-compatible format, the mechanism has been validated against a variety of fundamental experimental data for individual components over a broad range of conditions, including autoignition time, autoignition temperature, laminar flame speeds, NO_x emissions and soot formation (for the record, researchers developed a smaller version of the improved FT surrogate mechanism excluding the PAH chemistry containing 597 species and 3854 reactions).

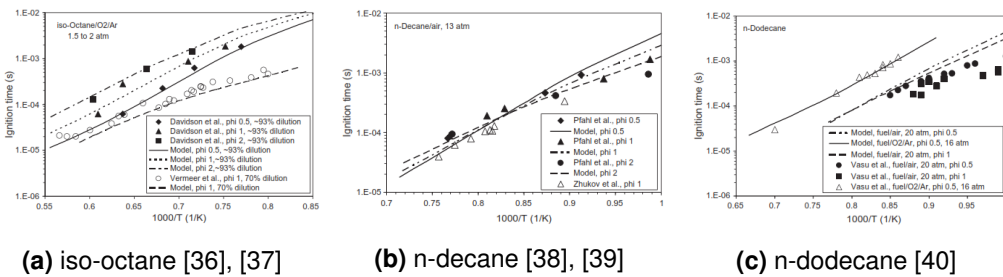


Figure 2.28 Effect of Φ and dilution on ignition-delay times

2.2. KEROSENE

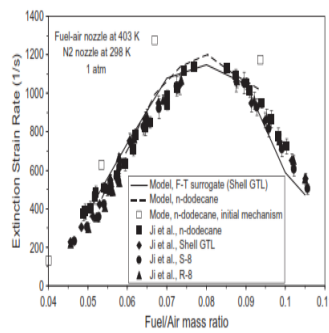


Figure 2.29 Extinction strain rate

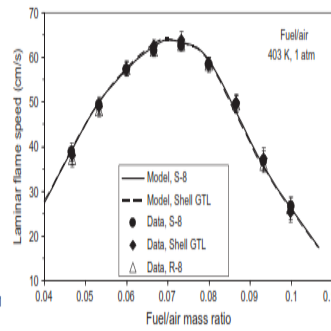


Figure 2.30 Laminar flame speed

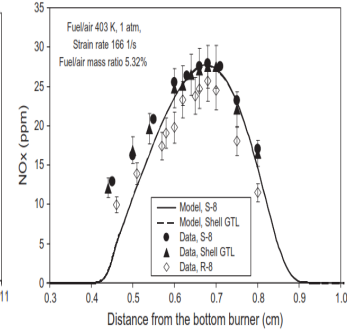


Figure 2.31 NO_x ppm

Dooley & coll [46],[47] formulated two different surrogates for POSF 4658 Jet-A fuel. While the first one is a three component surrogate formulated by constraining a mixture of n-decane, iso-octane and toluene, the second one is a mixture of n-dodecane, iso-octane, 1,3,5-tri-methyl-benzene and n-propyl-benzene in a predictive manner to mimic the same gas phase combustion phenomena of the reference fuel. As the target properties, they specified average molecular weight, H/C ratio and TSI. The experiments made for the first surrogate showed that the POSF 4658 surrogate closely emulates the chemical behavior of POSF 4658, supporting considerable optimism that surrogates composed of somewhat larger molecular weight alkanes and alkyl-aromatics can lead to further improvements in surrogate performance. Indeed, although the tested surrogate emulates overall ignition times (fig. 2.32), it fails to emulate the two-stage ignition behavior exhibited by POSF 4658 in the RCM study (however, this is not surprising as the surrogate was not formulated to do so).

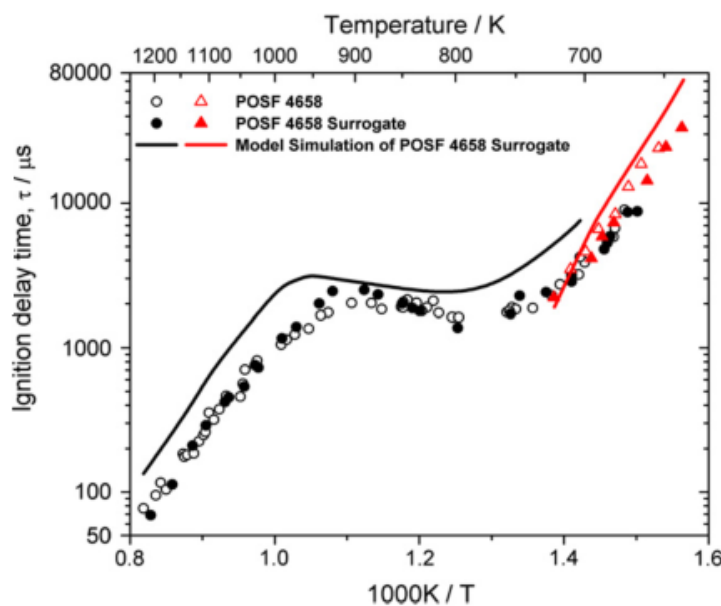


Figure 2.32 Ignition delay times

2.2. KEROSENE

The appropriateness of the second surrogate's formulation technique is tested by the experimental measurement of a series of practically important and fundamentally significant gas phase combustion kinetic phenomena. Overall, this surrogate is observed to exhibit combustion properties similar to those of the target real fuel, indicating the validity of the methodology employed. The experimental comparisons point out that the suggested surrogate fuel is an appropriate candidate for the dedicated development of combustion kinetic models for the prediction of the gas phase combustion behavior of Jet-A fuels. The combustion kinetic behavior of the n-dodecane, iso-octane, 1,3,5-trimethylbenzene and n-propylbenzene surrogate fuel is shown to be very similar to that previously reported for an n-decane, iso-octane and toluene surrogate fuel.

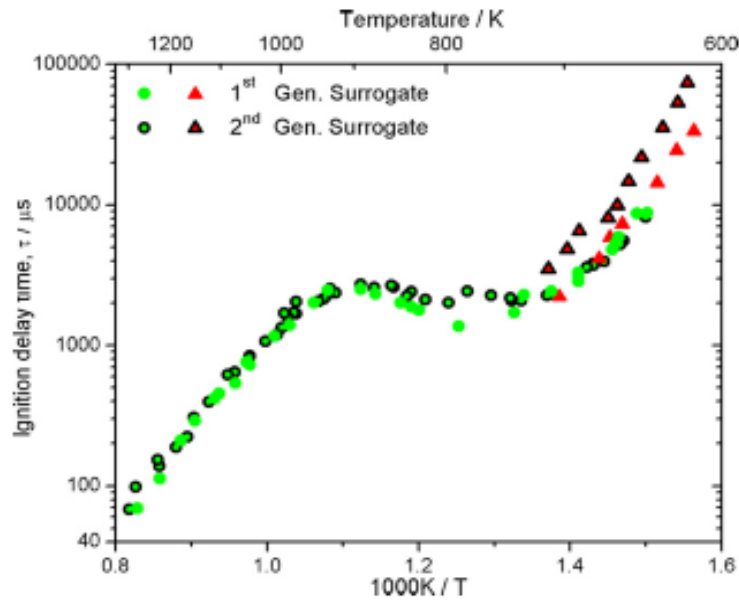


Figure 2.33 Ignition delay times

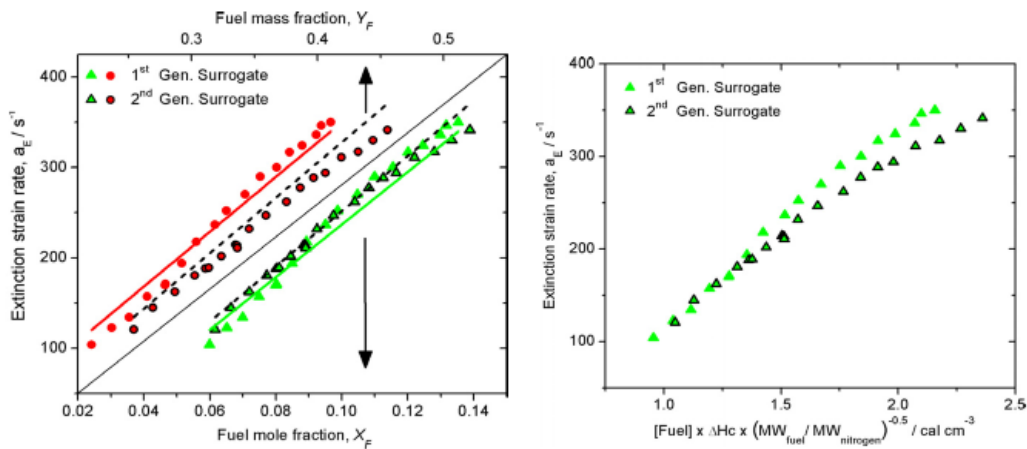


Figure 2.34 Strain rates of extinction for counter flow diffusion flames

2.2. KEROSENE

However, these two surrogates show huge differences on the physical properties branch. Huber & coll. [49] have measured the liquid density and viscosity of Jet-A POSF 4658. Indeed, the liquid density and viscosity behaviors of the first and second generation surrogate fuels are calculated from the equation of state methods implemented in the REFROP code and compared to the measured values of Jet-A POSF 4658 in fig. 2.35 and fig. 2.36 respectively. Thus, the second generation surrogate is of higher density and viscosity than the lighter first generation surrogate. The density of the second generation surrogate is estimated to be 5-6% lower than the measurements of Huber & coll. However, the deviation from the measured Jet-A POSF 4658 viscosity is larger, ranging from 50-30% from 273-373 K but is likely to deviate only minimally at the operating temperatures of gas turbine atomizers.

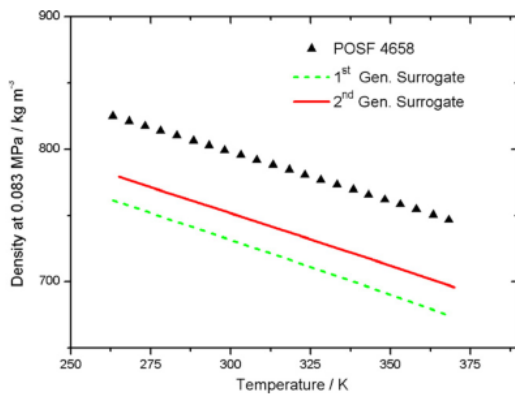


Figure 2.35 Surrogates density

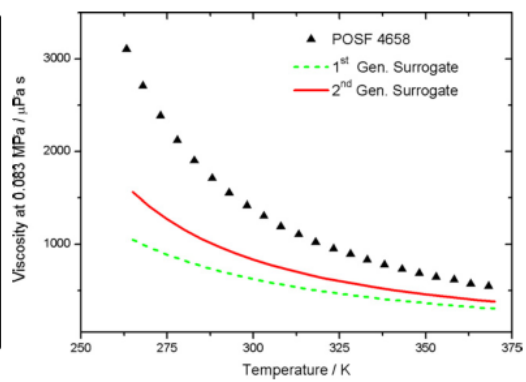


Figure 2.36 Surrogates viscosity

A brief sum up of fuels' main characteristics are shown in the following table:

Fuel	CN [-]	H/C [-]	MW $\left[\frac{\text{kg}}{\text{kmol}}\right]$	TSI [-]
n-dodecane	$\simeq 78$	2.16	170.3	7
iso-octane	$\simeq 17$	2.25	114.2	6.8
1,3,5-trimethylbenzene	21.8	1.33	120.2	62
n-propylbenzene	28.2	1.33	120.2	53
Kerosene fuel range	30-60	1.84-2.07	-	15-26
Jet-A POSF 4658	47.1	1.96	142 ± 20	21.4
1 st Generation Surrogate	47.4	2.01	120.7	14.1
2 nd Generation Surrogate	48.5	1.95	138.7	20.4

Table 2.10 Fuels' properties

Lemaire & coll. [50] have investigated the IDEA (Integrated Diesel European Action) surrogate diesel fuel [51] which consists of 70% n-decane and 30% 1-methyl-naphthalene (1-MN) and have compared it to a low-sulfur diesel that contained 8% by volume esters. They investigated these fuels in an atmospheric pressure, flat flame burner with an injector tube that nebulizes the liquid fuel and produces an aerosol. The flat flame burner is supplied with methane-air mixture.

2.2. KEROSENE

Based on laser induced incandescence (LII) of the soot and laser induced fluorescence of the PAHs, they found that the IDEA fuel produced more soot and PAHs compared to the low sulfur diesel fuel. Therefore, they reduced the amount of 1-MN in the surrogate fuel. To determine the amount of 1-MN, they used the threshold soot index and matched the TSI of the surrogate with the diesel fuel's one, finding the optimized surrogate with 20% 1-MN. This new surrogate also matched the diesel's measured LII and PAH levels quite well (see fig. 2.38). This work supports the use of TSI to match the sooting behavior of the surrogate with the target real fuel [52], [53], [54]. When the researchers examined the PAHs absorbed on the soot, they found out that the molecular weight distribution of the measured PAHs from the surrogate was narrower compared to that from the diesel. They also noted that the oxygenate content of the ester components in the low sulfur fuel likely reduced the level of soot and PAHs below that of produced by a conventional diesel. This means that, although the new surrogate works better compared to this diesel containing esters, the standard IDEA surrogate with 30% 1-MN may still work best in comparison to conventional diesel fuel. However, the findings of this work about how to match a surrogate to a target real fuel are still of great significance.

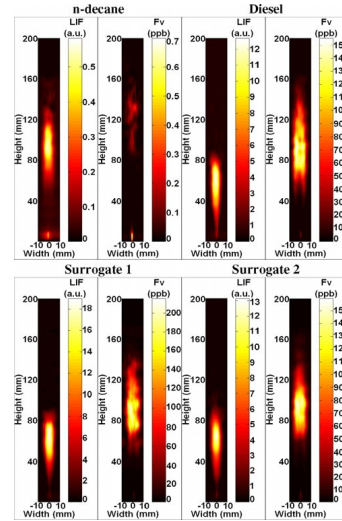


Figure 2.37 Flames reconstituted 2D-images

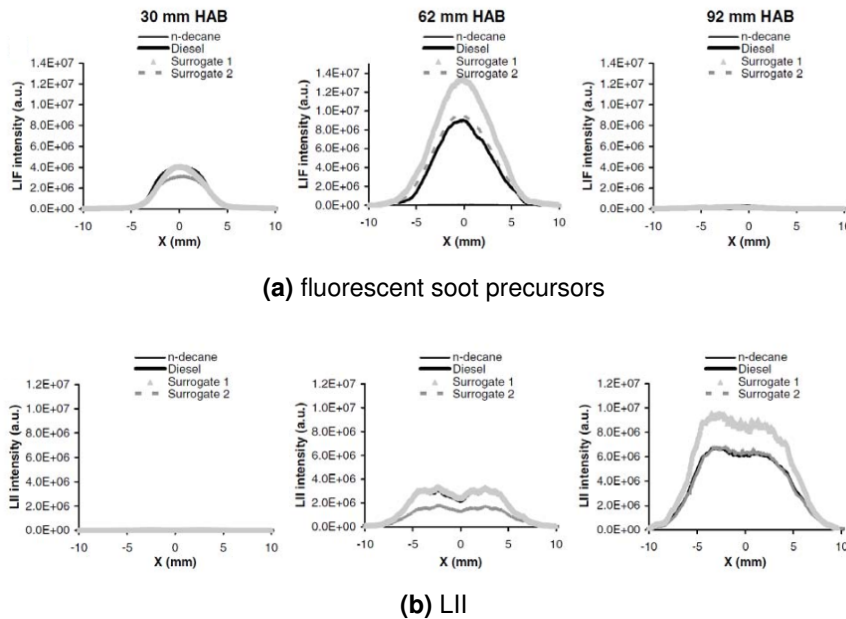


Figure 2.38 Radial profiles at different HAB

Kook and Pickett [55] investigated a surrogate of 23% m-xylene and 77% n-dodecane and compared it to a conventional jet fuel in a high-pressure and high-temperature combustion vessel used to simulate conditions in a diesel engine. Using planar laser-induced incandescence, they showed that the surrogate fuel sooted more than the conventional jet fuel in the diesel engine. They attributed this behavior to the surrogate fuel having a higher aromatic content than conventional fuel jet. Natelson & coll. [56] tested the reactivity of a [2:1:1] surrogate containing 50% n-decane, 25% n-butylbenzene and 25% n-butylcyclohexane in a pressurized flow reactor at 8 bar and they found almost the same reactivity properties of another [1:1:1] surrogate containing, on the contrary, 33% n-decane, 33% n-butylbenzene and 33% n-butylcyclohexane which was proposed to match diesel fuel properties. They used the amount of CO formation in the flow reactor as a measure of reactivity of the surrogate and the target fuels. They found these surrogates to be more reactive than the jet and diesel fuels they were designed to match (fig. 2.39).

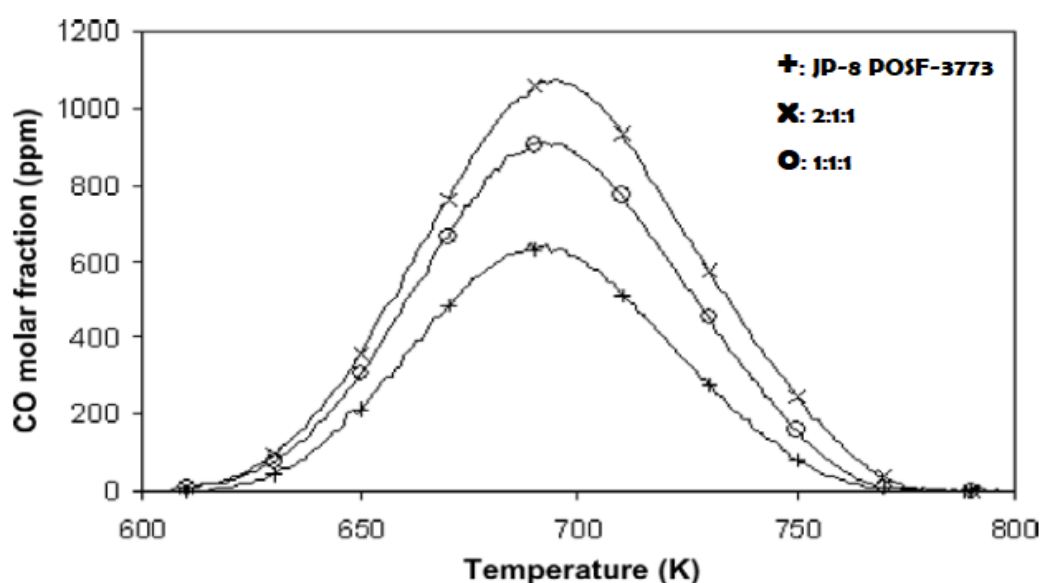


Figure 2.39 Reactivity map

Steil & coll. [57] made measurements on the ignition delay time of a kerosene sample. These experiments were performed by applying the shock tube technique, in the temperature range of about 1250 to 1700 K at pressures around 6 bar, for up to three equivalence ratios. A fuel (a mixture of 70% n-decane and 30% propylbenzene) was investigated also, under similar conditions, as a representative of a surrogate model for kerosene. The two sets of experiments consisting of almost 200 shocks are analyzed, statistically evaluated and compared to ignition delay times predicted by using two detailed reaction models. The predictions obtained with the binary surrogate fuel turned out to be not a good choice for representing autoignition behavior of kerosene, according to the findings of the present investigation. Myong & coll. [58] found that evaporation of the surrogate fuel is promoted by addition of a low boiling point component because the saturated-vapor pressure line of the high boiling point component shifts to a lower temperature in the two-phase region.

Chapter 3

Fuel Properties

According to the previous chapter, numerical models must be developed for calculating chemical and physical properties of the surrogate mixtures to obtain the optimal composition of the surrogate's formulae. The numerical models include:

- | | | |
|---|---|---------------------|
| <ul style="list-style-type: none">• average molecular weight (MW)• liquid density (ρ)• viscosity ($\eta - \nu$)• formation enthalpy• combustion enthalpy• specific energy* distillation curve and phase diagram* boiling temperature | } | Physical properties |
| <ul style="list-style-type: none">• cetane number (CN)• iso-to-normal paraffin ratio• TSI• C/H ratio* flame speed* IDT (ignition delay time)* concentration profiles* flash/freeze/smoke point | } | Chemical properties |

For the record, the [*] marked properties are not under further investigation in this work of thesis.

3.1 Physical properties

- **Average Molecular Weight (MW_{mix})**

Fuel diffusive properties correlate strongly with its molecular weight. The higher the molecular formula, the greater the proportion of large aromatics which leads mainly to soot formation. Therefore, in order to emulate the diffusive properties of the real jet fuel in flame environments, a surrogate model must have a similar average molecular weight [48]. The average molecular weight of the surrogate can be calculated from the mole fractions χ_i of the components and their molecular weight MW_i :

$$MW_{mix} = \sum_{i=1}^I \chi_i \cdot MW_i \quad \left[\frac{kg}{kmol} \right]$$

where:

- χ_i is the mole fractions of each component involved
- MW_i is the molecular weight of each species involved

- **Liquid Density (ρ_{mix})**

The liquid density of the surrogate can be calculated from the mole fractions χ_i of the components and their respective liquid density ρ_i :

$$\rho_{mix} = \sum_{i=1}^I \chi_i \cdot \rho_i \quad \left[\frac{kg}{m^3} \right]$$

where:

- χ_i is the mole fractions of each component in the surrogate mixture
- ρ_i is the liquid density of each compound in the mixture

- **Viscosity (η_{mix} - ν_{mix})**

A huge number of papers have been published to suggest ways to estimate the low-temperature liquid viscosity when no experimental data are available. Since theoretical calculation of liquid viscosity is quite complicated, many empirical methods have been proposed and, among these, Morris' method [15], [19] was chosen for liquid viscosity calculation for surrogate models. The main point is that this method has an advantage on applicability to all compound classes such as alcohols, acids, n-paraffins, iso-paraffins, naphthenes, cycloparaffins, aromatics, heterocyclic amines, aldehydes or multi-halogenated compounds. Also availability of related data and simple numerical evaluation (compared to other methods) are another utilization reasons. Nevertheless, analysis has shown that over other ones (e.g. Thomas' and Orick-Erbar's method), it usually introduces smaller calculation errors than the experimental results [15], [64].

3.1. PHYSICAL PROPERTIES

The calculation of the liquid viscosity for this method is defined as follows:

$$\log_{10} \left(\frac{\eta}{\eta^+} \right) = \sqrt{0.0577 + \sum_i^I (b_i \cdot n_i)} \left(\frac{1}{T_r} - 1 \right)$$

where:

- η^+ [cP] is an empirical constant for each compound class, whose values are shown in the table 3.1.
- T_r is the reduced temperature $\left(T_r = \frac{T}{T_{crit}} \right)$
- b_i is the contribution of each group (determined from table 3.2)
- n_i is the number of times that each group appears in the molecule

Compound classes	η^+ [cP]
Hydrocarbons	0.0875
Halogenated Hydrocarbons	0.1480
Benzene derivatives	0.0895
Halogenated benzene derivatives	0.1230
Alcohols	0.0189
Organic acids	0.1170
Ethers, ketones, aldehydes, acetates	0.0960
Phenols	0.0126
Miscellaneous	0.1000

Table 3.1 Empirical constant for each compound class [15]

Group	b_i [-]	Group	b_i [-]	Group	b_i [-]
CH_3, CH_2, CH	0.0825	I	0.1908	NH_2 adjoining ring	0.7645
Halogenated-subst. CH_3	0.00	Double bond	-0.0742	F, Cl adjoining ring	0.00
Halogenated-subst. CH_2	0.0893	C_6H_4 benzene ring	0.3558	OH for alcohols	2.0446
Halogenated-subst. CH	0.0667	Additional H in ring	0.1446	COOH for acids	0.8896
Halogenated-subst. C	0.00	CH_2 saturated ring	0.1707	C=O for ketones	0.3217
Br	0.2058	CH_{1-3} adjoining ring	0.0520	O=C-O for acetates	0.4369
Cl	0.1470	NO_2 adjoining ring	0.4170	OH for phenols	3.4420
F	0.1344			-O- for ethers	0.1090

Table 3.2 Structural contribution for b_i [15]

Based on the above-given information, the dynamic viscosities of individual components of the surrogate can be calculated. Then, each viscosity should be divided by the density of the relative compound, obtaining the respective kinematic viscosity. Kinematic viscosities of the blend could be calculated using the corresponding mole fractions χ_i and the obtained values of kinematic viscosities of individual components:

$$v_{mix} = \sum_{i=1}^I \chi_i \cdot v_i \quad \text{where} \quad v_i = \frac{\eta_i}{\rho_i} \quad [cSt]$$

where:

- χ_i is the mole fractions of each components in the surrogate mixture
- v_i is the kinematic viscosity of each components in the mixture

• Distillation Curve and Phase Diagram

The distillation curve of a complex fluid is a critically important indicator of the bulk behavior or response of the fluid. For this reason, the distillation curve, usually presented graphically as the boiling temperature against the volume fraction distilled, is often cited as a primary design and testing criterion for liquid fuels, lubricants and other important industrial fluids. While the distillation curve gives a direct measure of fluid volatility fraction by fraction, the information the curve contains can be taken much further; there are numerous engineering and application-specific parameters that can be correlated to the distillation curve. When applied to liquid engine fuels, researchers can estimate engine starting ability, drivability, fuel system icing, vapor lock, fuel autoignition, etc.

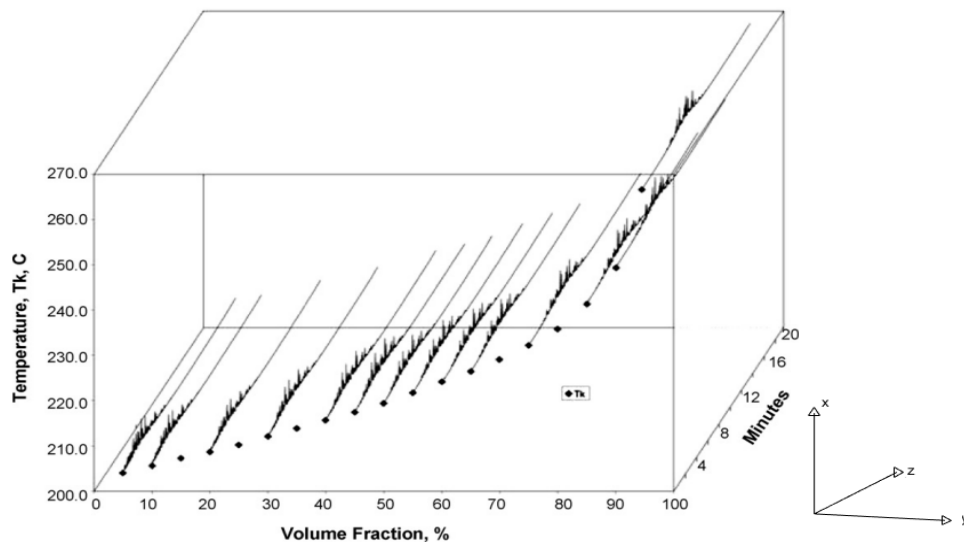


Figure 3.1 A distillation curve showing the temperature of the fluid against volume fraction in the x-y plane and the composition as measured by gas chromatography along the z axis, represented as retention time against peak intensity.

On the other hand, the phase¹ diagram shows, in pressure-temperature space, the lines of equilibrium or phase boundaries between the three phases of solid, liquid and gas. The curves on the phase diagram show the points where the free energy becomes non-analytic. The open spaces, where the free energy is analytic, correspond to single phase regions. Single phase regions are separated by lines where phase transitions, called phase boundaries. The phase diagram is especially important for the atomization and evaporation modeling and thus has to be included in the set of reference properties for surrogate model design. Calculation of phase diagram and distillation curve is based on Soave-Redlich-Kwong (SRK) equation of state, which was developed in 1949.

¹A phase, or state of matter, is a domain within a many-body system within which relevant physical properties are uniform.

The Soave-Redlich-Kwong equation of state is an empirical algebraic equation that relates temperature, pressure and volume of gases. It is generally more accurate than the van der Waals equation and the ideal gas equation at temperatures above the T_{crit} . The equation is formulated as:

$$p = \frac{RT}{V_m - b} - \frac{a}{\sqrt{T}V_m(V_m + b)}$$

where:

- p is the gas pressure [Pa]
- R is the gas constant $\left[\frac{J}{mol \cdot K}\right]$,
- T is temperature [K],
- V_m is the molar volume $\left[\frac{V}{n}\right]$,
- a is a constant that corrects for attractive potential of molecules
- b is a constant that corrects for volume

The constants are up to the which gas which is being analyzed and they could be generally calculated from the critical point data of the gas:

$$a = \frac{1}{9\left(\sqrt[3]{2}-1\right)} \frac{R^2 T_{crit}^{2.5}}{p_{crit}} \quad b = \frac{\sqrt[3]{2}-1}{3} \frac{RT_{crit}}{p_{crit}}$$

where T_{crit} and p_{crit} refer to the critical point (CP).

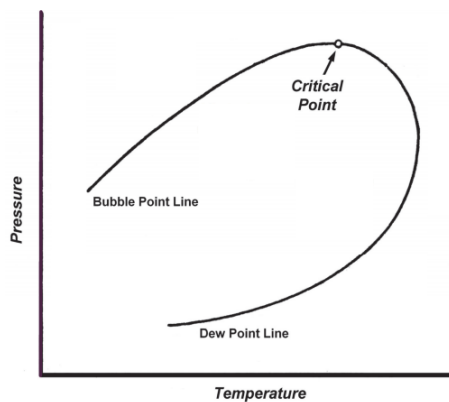


Figure 3.2 Typical hydrocarbons' system phase diagram

In figure 3.2, the following points are evident:

- critical point: the end point of the pressure-temperature curve that designates conditions under which a liquid and its vapor can coexist. At higher temperatures, the gas can't be liquefied by pressure alone
- bubble point line: the bubble point is the temperature (at a given pressure) where the first bubble of vapor is formed when heating a liquid consisting of two or more components
- dew point line: it is the temperature to which air must be cooled to become saturated with water vapor. When further cooled, the airborne water vapor will condense to form liquid water (dew)

• Boiling Temperature T_{boil}

The boiling behavior of chemical substances are described by the following equation:

$$T_{boil,mix} = \sum_{i=1}^I \chi_i \cdot T_{boil,i} \quad [K]$$

where:

- χ_i is the mole fractions of each components in the surrogate mixture
- $T_{boil,i}$ is the boiling temperature of each components involved

Estimation techniques for T_{boil} , when data are no available, are all empirical. Some of the most promising are reported in the following list [15]:

- Watson method: Watson [61] related the boiling temperature with the liquid volume. He obtained the following equation:

$$T_{boil} = \frac{\theta}{V_{boil}^{0.18}} \exp \left(\frac{2.77 V_{boil}^{0.18}}{\theta} - 2.94 \right)$$

where the variable θ can be obtained starting from the molecule structure. Furthermore, the low exponent on V_{boil} makes the estimation of T_{boil} relatively insensitive to possible errors in V_{boil} .

- Ogata and Tsuchida method: [62] They employed the linear relation:

$$T_{boil} = py + q$$

In this equation, y is determined from the hydrocarbon radical type and p and q from the functional group.

- Somayajulu and Palit method: [63] they suggested a method of comparable accuracy:

$$T_{boil} = a (\sum Z)^c + b$$

The constants a , b and c are listed for homologous series. The term $\sum Z$ is the atomic-number sum.

• Formation Enthalphy

Formation enthalpy of the individual species of the surrogate mixtures could be calculated using the additivity rule, also known as the Benson's method [15], [16]. According to this theory, the formation enthalpy Δh_f^0 of each species is given as:

$$\Delta h_f^0 = \sum_{i=1}^I n_i \cdot h_{f,i}^0 \quad \left[\frac{kJ}{mol} \right]$$

where:

- n_i is the number of times the group occurs in a molecule
- $h_{f,i}^0$ is the formation enthalpy of the compounds group

If data are not available, good solutions are given by empirical relations:

- Verma and Doraiswamy: they suggested a linear relation:

$$\Delta h_f^0 = A + BT$$

where A and B contributions are given for each group. This relation could be used in the temperature range $300 \leq T \leq 1500$ K and it gives back good results (there is a difference of $\pm 5 \frac{\text{kcal}}{\text{g mole}}$)

- Souders, Matthews and Hurd's method: they developed an additive-group estimation technique for Δh_f^0 that fully reflects the characteristics of the reference hydrocarbons:

$$\Delta h_{f,T}^0 = \Delta h_{f,298}^0 + \left[\int_{298}^T \sum C_{p_{\text{vibrational}}}^0 dT - \frac{n}{2} \int_{298}^T C_{p_{H_2}}^0 dT + \dots \right. \\ \left. \dots - m \int_{298}^T \sum C_{p_{\text{carbon}}} dT \right]_I + \left(\int_{298}^T \sum C_{p_{\text{internalrotation}}}^0 dT \right)_{II} + 4R(T - 298)$$

where:

- $C_{p_{H_2}}^0$ is the heat capacity of hydrogen at standard state
- $C_{p_{\text{carbon}}}$ is the heat capacity of solid graphite (standard state)
- m, n are the numbers of atoms of carbon and hydrogen in the molecule
- $C_{p_{\text{vibrational}}}^0$ is the vibrational contribution to heat capacity and it is function of the chemical structure
- $C_{p_{\text{internalrotation}}}^0$ is the internal rotational contribution to heat capacity and it is function of the chemical structure

• Combustion Enthalpy

The previous calculations are essential to evaluate the combustion enthalpy of mixture's chemical reactions [65], [66], according to the relation:

$$\Delta_c H^0 = \sum_{i=1}^I w_i \cdot \Delta h_{f,i}^0 \quad \left[\frac{\text{kJ}}{\text{mol}} \right]$$

where:

- w_i is the stoichiometric coefficient of the i -th reactant in the reaction
- $\Delta h_{f,i}^0$ is the formation enthalpy of each reactant

• Specific Energy

Specific energy can be calculated from the combustion energy [65], [66], according to the formula:

$$E_{S,mix} = \sum_{i=1}^I \chi_i \cdot \left(\frac{-\Delta_c H_i^0}{MW_i} \right) \quad \left[\frac{\text{kJ}}{\text{kg}} \right]$$

where:

- χ_i is the mole fractions of each component in the surrogate mixture
- $\Delta_c H_i^0$ is the combustion enthalpy of each molecule involved
- MW_i is the molecular weight of each molecule in the surrogate

3.1. PHYSICAL PROPERTIES

Compound (gas)	Formula	Heat of formation Δh_f^0	Heat of combustion $-\Delta H_c^0$
		$\left[\frac{\text{kcal}}{\text{mol}}\right]$	$\left[\frac{\text{kcal}}{\text{mol}}\right]$
Ethene (ethylene)	C_2H_4	$+12.496 \pm 0.066$	337.234 ± 0.072
Propene (propylene)	C_3H_6	$+4.879 \pm 0.122$	491.987 ± 0.129
1- Butene	C_4H_8	$+0.280 \pm 0.196$	649.757 ± 0.204
cis-2-Butene	C_4H_8	-1.362 ± 0.196	648.115 ± 0.204
trans-2-Butene	C_4H_8	-2.405 ± 0.196	647.072 ± 0.204
2-Methylpropene (isobutene)	C_4H_8	-3.343 ± 0.182	646.134 ± 0.191
1-Pentene	C_5H_{10}	-5.00 ± 0.43	806.85 ± 0.44
cis-2-Pentene	C_5H_{10}	-6.51 ± 0.26	805.34 ± 0.27
trans-2-Pentene	C_5H_{10}	-7.59 ± 0.26	804.26 ± 0.27
2-Methyl-1-butene	C_5H_{10}	-8.68 ± 0.23	803.17 ± 0.24
3-Methyl-1-butene	C_5H_{10}	-6.92 ± 0.22	804.93 ± 0.23
2-Methyl-2-butene	C_5H_{10}	-10.17 ± 0.22	801.68 ± 0.23
1-Hexene	C_6H_{12}	-9.96 ± 0.44	964.25 ± 0.45
cis-2-Hexene	C_6H_{12}	-11.56 ± 0.53	962.66 ± 0.54
trans-2-Hexene	C_6H_{12}	-12.56 ± 0.53	961.66 ± 0.54
cis-3-Hexene	C_6H_{12}	-11.56 ± 0.53	962.66 ± 0.54
trans-3-Hexene	C_6H_{12}	-12.56 ± 0.53	961.66 ± 0.54
2-Methyl-1-pentene	C_6H_{12}	-13.56 ± 0.56	960.66 ± 0.57
3-Methyl-1-pentene	C_6H_{12}	-11.02 ± 0.46	963.20 ± 0.47
4-Methyl-1-pentene	C_6H_{12}	-11.66 ± 0.47	962.56 ± 0.48
2-Methyl-2-pentene	C_6H_{12}	-14.96 ± 0.56	959.26 ± 0.57
cis-3-Methyl-2-pentene	C_6H_{12}	-14.32 ± 0.55	959.90 ± 0.56
trans-3-Methyl-2-pentene	C_6H_{12}	-14.32 ± 0.55	959.90 ± 0.56
cis-4-Methyl-2-pentene	C_6H_{12}	-13.26 ± 0.56	960.96 ± 0.57
trans-4-Methyl-2-pentene	C_6H_{12}	-14.26 ± 0.56	959.96 ± 0.57
2-Ethyl-1-butene	C_6H_{12}	-12.92 ± 0.55	961.30 ± 0.56
2,3-Dimethyl-1-butene	C_6H_{12}	-14.78 ± 0.27	959.44 ± 0.28
3,3-Dimethyl-1-butene	C_6H_{12}	-14.25 ± 0.28	959.97 ± 0.29
2,3-Dimethyl-2-butene	C_6H_{12}	-15.91 ± 0.27	958.31 ± 0.28
1-Heptene	C_7H_{14}	-14.89 ± 0.44	1121.69 ± 0.45
1-Octene	C_8H_{16}	-19.82 ± 0.45	1279.13 ± 0.46
1-Nonene	C_9H_{18}	-24.74 ± 0.46	1436.59 ± 0.48
1-Decene	$C_{10}H_{20}$	-29.67 ± 0.48	1594.02 ± 0.50
1-Undecene	$C_{11}H_{22}$	-34.60 ± 0.50	1751.46 ± 0.52
1-Dodecene	$C_{12}H_{24}$	-39.52 ± 0.52	1908.91 ± 0.55
1-Tridecene	$C_{13}H_{26}$	-44.45 ± 0.56	2066.35 ± 0.59
1-Tetradecene	$C_{14}H_{28}$	-49.38 ± 0.59	2223.79 ± 0.62
1-Pentadecene	$C_{15}H_{30}$	-54.31 ± 0.62	2381.23 ± 0.66
1-Hexadecene	$C_{16}H_{32}$	-59.23 ± 0.66	2538.68 ± 0.70
1-Heptadecene	$C_{17}H_{34}$	-64.15 ± 0.70	2696.13 ± 0.74
1-Octadecene	$C_{18}H_{36}$	-69.08 ± 0.75	2853.57 ± 0.79
1-Nonadecene	$C_{19}H_{38}$	-74.00 ± 0.80	3011.01 ± 0.85
1-Eicosene	$C_{20}H_{40}$	-78.93 ± 0.84	3168.45 ± 0.89
Δ for CH_2 ; $n > 5$	$-CH_2-$	-4.296	157.443

Table 3.3 Enthalpies table [67]

3.2 Chemical properties

• Iso-to-Normal Paraffins Ratio

The influence of the iso-to-normal paraffins ratio is considered to reflect the influence of the fuel's molecular structure on autoignition. The importance of this criterion and the influence of the isomer's structure on the fuel ignition is illustrated with data obtained by Ribaucour [68] for 3 pentane isomers: n-pentane, neo-pentane and i-pentane (figure 3.3).

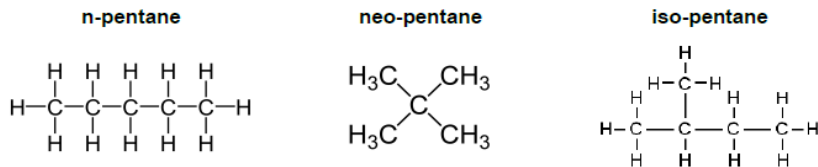


Figure 3.3 Molecular structure of the three pentane isomers

Figure 3.4 shows computed temperatures for each isomer at the same compression temperature and initial pressure. The compression histories are identical but the constant-volume ignition delay times are different.

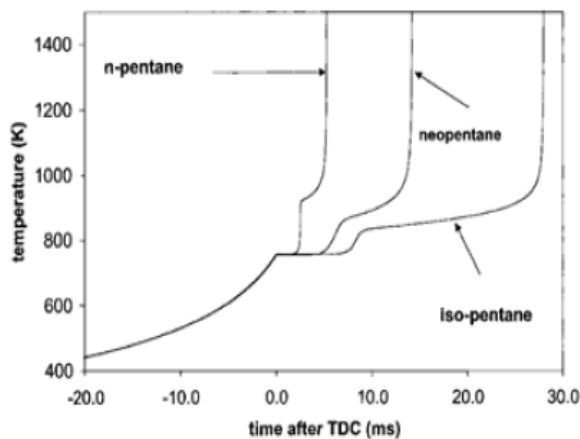


Figure 3.4 Temperature history for pentane isomers

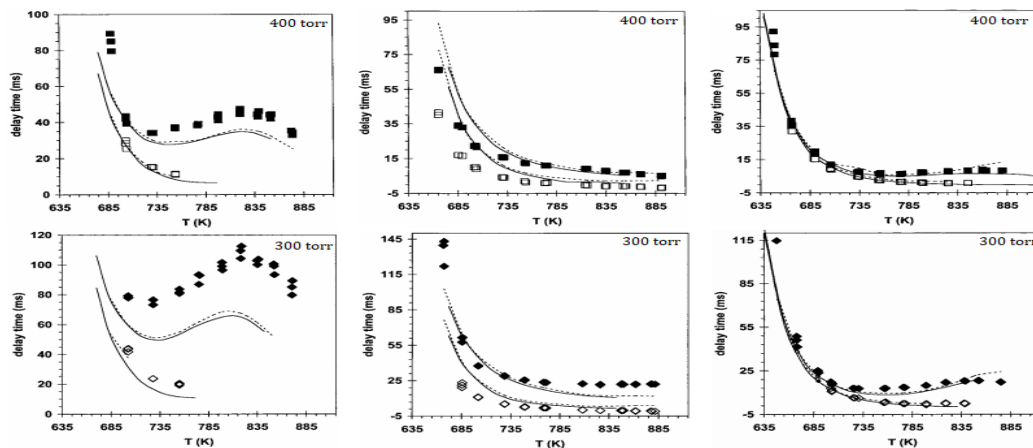


Figure 3.5 Effect of chemical structure on delay times for iso/neo/n-pentane.

- **Cetane Number (CN)**

Cetane numbers for each component are measured using a method developed in the 1930s by the Cooperative Fuel Research (CFR) Committee and later standardized as ASTM D613. Two primary reference fuels (made by a single hydrocarbon) define the cetane number scale:

- n-hexadecane, also called cetane, is characterized by the molecular formula $n-C_{16}H_{34}$ and has very good ignition quality. It was assigned the cetane number of 100
- 1-methylnaphthalene, whose molecular formula is $C_{11}H_{10}$, has a awful ignition quality and then it was assigned a cetane number of 0

In 1962, the low cetane number reference fuel was replaced with isocetane (also called 2,2,4,4,6,8,8-heptamethylnonane or HMN) which had better oxidation stability and was easier to use in the CFR engine. When measured against the two original standards, HMN has a cetane number of 15. When a fuel has the same ignition delay period as a mixture of the two primary reference fuels, its cetane number is derived from the volume percent of cetane and heptamethylnonane as follows:

$$CN = \%cetane + 0.15\%heptamethylnonane$$

Summing up, CN is a significant expression of the quality of a diesel fuel. CN depends on the chemical and the physical fuel properties as well as the molecular structure of fuel hydrocarbons. It can be seen from figure 3.6 [69] that n-paraffins have the highest CNs and that CN tends to grow with the increase of carbon number. The greater the degree of branching, the lower the CN for i-paraffins is. Furthermore, the position of the branch plays a secondary role in the CN. If the branching is only concentrated at one end of the molecule leaving a long chain at the other end, then such i-paraffins tend to have higher CNs [76]. Numerous attempts have been made in the past to correlate the CN with various physical and chemical properties of the fuel [69], [76]. These models are typically empirical and may result restrictive in their application for other fuels. The following relation, proposed by Chosh and Jaffe and based on an explicit and complete representation of the detailed molecular composition of the fuel [76], shows the correlation between the fuels' CN and the pure-component cetane number:

$$CN_{mix} = \frac{\sum_{i=1}^I v_i \beta_i CN_i}{\sum_{i=1}^I v_i \beta_i} \quad [-]$$

where:

- v_i is the volume fraction of each molecule in the fuel
- β_i is the pure-component structure parameter (see table 3.4)
- CN_i is the pure-component CN of each molecule in the fuel

3.2. CHEMICAL PROPERTIES

Molecular class	Molecular structure	β
n-paraffins	from n-C ₅ to n-C ₁₆₊	0.5212
i-paraffins	from i-C ₅ to i-C ₂₅₊ , mono and multi-branched i-paraffins	7.3717
naphthenes	cyclohexane to C ₁₀₊ , naphthenes, decalin to C ₄₊ , decalins	0.0727
aromatics	benzene to C ₁₄₊ , aromatics, naphthalene to C ₁₃₊ , naphthalenes, tetralin to C ₁₅₊ , tetralins	3.1967
olefins/cyclo-olefines	C ₅ to C ₁₈₊ linear olefins, branched olefins and cyclo-olefins	0.3597

Table 3.4 Parameter value β the pure-component structure parameter

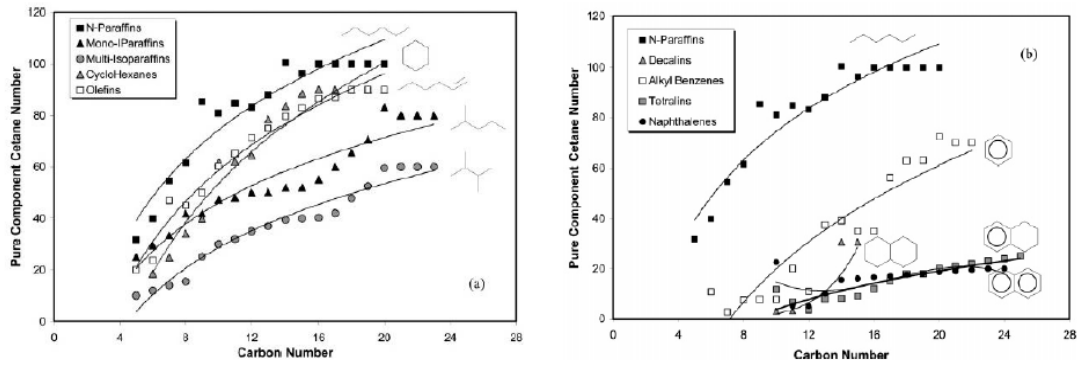


Figure 3.6 Pure-component CNs for different hydrocarbon classes

Fuels with low CN may also increase PM emissions, since combustion begins in the final stage of the expansion cycle when the temperature inside the chamber diminishes, reducing the speed of oxidation, which in turn increases the concentration of unburned hydrocarbons that condense on the surface, causing the mass of particulate matter to increase [70], [71]-[73]. The CN also affects specific fuel consumption, with a tendency for fuel consumption to decrease as the CN increases due to the higher temperature of the combustion process, improving the thermal performance of the engine [74]. Furthermore, as the CN increases the ignition delay time decreases. These features can be summed up in the following image:

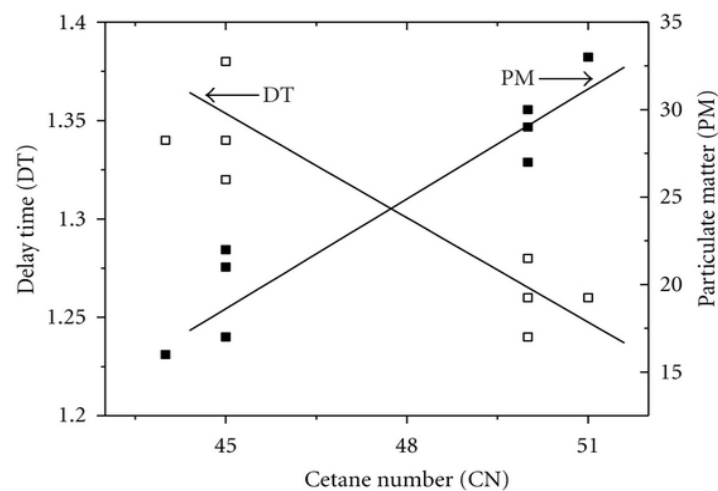


Figure 3.7 Ignition delay time and PM emissions as a function of CN [75]

• Threshold Sooting Index (TSI)

This number is representing the inherent sooting tendency of a compound or a mixture. TSI is used for comparing the experimental studies on the tendency of different fuels to soot. A higher TSI means higher sooting tendency. By analyzing the TSI of the surrogate mixture it is possible to determine the surrogate fuel aromatic composition, which should be very similar to that of the target fuel. This is due to a fact that TSI has been shown to be strongly dependent on aromatic component fraction of the fuel [17]. TSI is an empirical index based on the smoke point. The smoke point is the maximum height of a smoke free laminar diffusion flame and depends on molecular weight of the fuel [17], [77]-[81]. For premixed flames, hypothetical hydrocarbon fuels are considered with very different molecular weights or C/H ratios (both of which are responsible for producing soot) when fuel is burned at critical equivalence ratio Φ_c . Thus, TSI for premixed flames is defined as [17], [77]-[81]:

$$TSI = c - d\Phi_c \quad \text{where } \Phi_c \text{ is defined as: } \Phi_c = \frac{\left(\frac{O}{F}\right)_{stoic}}{\left(\frac{O}{F}\right)} = \frac{\left(\frac{m_{oxid}}{m_{fuel}}\right)_{stoic}}{\left(\frac{m_{oxid}}{m_{fuel}}\right)}$$

For diffusion flames, the TSI is defined as [17]:

$$TSI = a \left(\frac{MW}{h} \right) + b$$

where:

- $a \left[\frac{mol \cdot mm}{g} \right]$, constant of a specific experimental setup
- $b [-]$, constant of a specific experimental setup
- $h [mm]$, critical height of the flame, referred to the smoke point at which the soot is first observed

The TSI of a mixture can be calculated according to the linear mixture formula (Gill & Olson [53]), defined as:

$$TSI_{mix} = \sum_{i=1}^I \chi_i TSI_i \quad [-]$$

where:

- χ_i is the mole fractions of each component involved
- TSI_i is the TSI of each component in the surrogate mixture

Nevertheless, they proposed another non-linear formula for its calculus:

$$(1.1)^{TSI_{mix}} = \sum_i \chi_i (1.1)^{TSI_i} \quad [-]$$

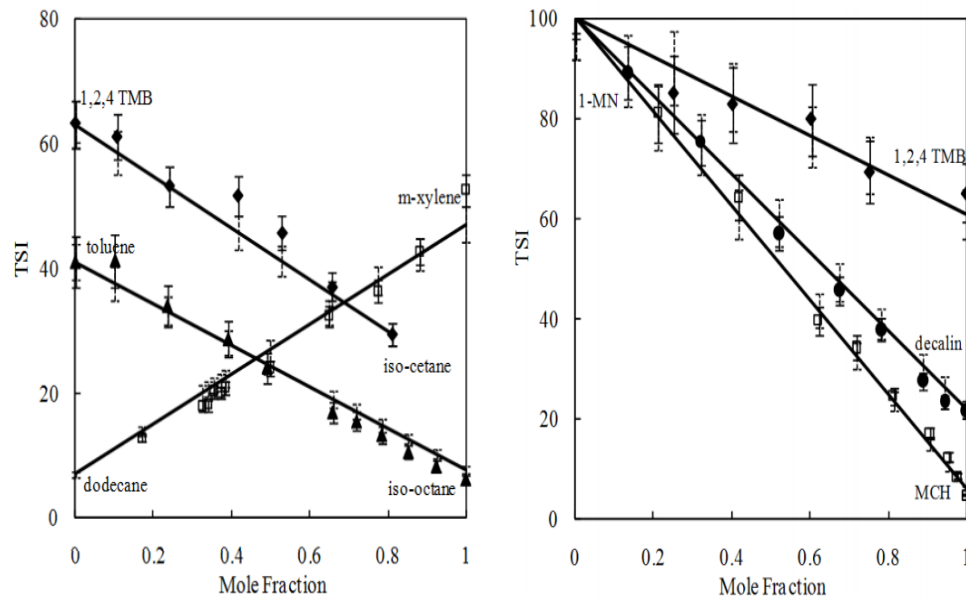


Figure 3.8 Mixture's TSI evaluation

• CH Ratio

This value can be calculated from the average molecular formula which describes the average size of the molecules of a fuel. The higher the average molecular formula, the greater the proportion of large paraffins is which leads to soot formation. Through a global parameter, the carbon/hydrogen ratio reflects the diversity of molecular structure. The densities of hydrocarbon fuels are correlated with their CH values; if the hydrocarbon fuel has a low CH, then the fuel has a low density. Similar perspective could be applied to fuel's viscosity, flash point temperature and net weight heating value. In contrast, a decrease in CH ratio magnitude provokes a decrease of net volumetric heating value [82]. Furthermore, even the combustion enthalpy, the adiabatic flame temperature, flame velocity and the overall radical population are strongly dependent on CH [46].

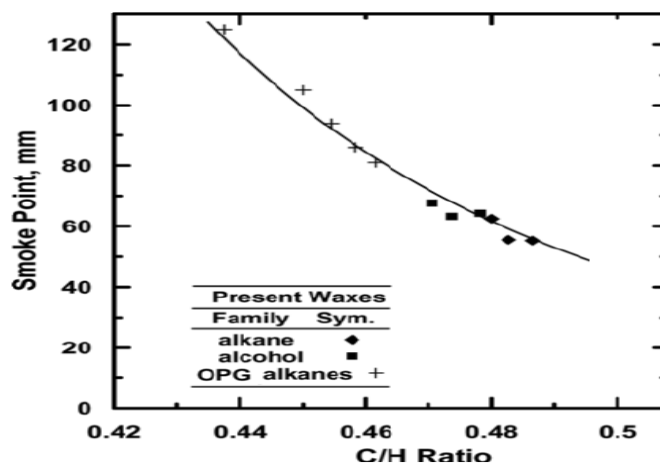


Figure 3.9 CH ratio effect of smoke point

3.3 Experimental estimation methods of fuel properties

- **CH Ratio**

One of the most promising way to evaluate the CH ratio of a blend is the direct collaboration between the atomic spectrometry and the capillary gas chromatography (GC), which creates a system with high separation power as well as high selectivity [84]. The well-defined and identifiable electron transitions in excited atoms or ions render atomic spectroscopy the best element selective method available to the analyst. Its utilization started in the early 1990s after the successful introduction of an atomic emission detector (AED), which was compatible with GC, and so became the tool of many organic environmental and analytical chemists. This tool's robustness and wideranging usefulness have been amply demonstrated. GC–AED provides simultaneous multi-channel detection with excellent limits of detection (LOD). A rewarding aspect of AED detection is the so-called universal or compound-independent calibration principle. The high temperature of the plasma causes a complete breakdown of analyte molecules into their constituent atoms. Consequently, the response per mass unit of an element is independent of the structure of the analyte of interest. Then elemental ratios can be calculated and used to estimate molecular formulas.

- **Cetane Number**

In the ASTM D613 test, the cetane number of a diesel fuel is determined by comparing its ignition delay in the standard CFR (Cooperative Fuel Research) test engine with those for blends of reference fuels of known cetane number. The compression ratio is varied by adjusting a calibrated hand wheel to obtain the same ignition delay for the sample and for each of two bracketing reference fuels, permitting interpolation of cetane number in terms of the hand wheel readings [83]. The ISO 5165 method, the international counterpart to ASTM D613, is essentially the same test using the same engine. In Europe, a similar method, DIN 51773, uses a standard BASF (Badische Anilin- und Soda Fabrik) engine for determining cetane number. Both the CFR and BASF methods vary effective compression ratios, thus varying the available energy to start combustion, but in different ways. The Waukesha CFR engine varies the physical volume of the combustion chamber, thereby changing the compression ratio of the engine and changing the amount of energy available for initiating combustion. The BASF engine, however, varies the amount of air allowed to enter the cylinder while maintaining the same physical compression ratio.

- **Threshold Sooting Index**

According the ASTM D1322, The TSI index is calculated through the Seta Smoke Point Apparatus. The principle of the method is burnign the sample in an enclosed wick-fed lamp that is calibrated against pure hydrocarbon blends of known smoke point and determining the maximum height of flame that can be achieved by the test fuel without smoking.

- **Combustion Enthalpy and Formation Enthalpy**

They are evaluated through the Differential Scanning Calorimetry, or DSC, which is a thermal analysis technique that looks at how a material's heat capacity (C_p) is changed by temperature. A sample of known mass is heated or cooled and the changes in its heat capacity are tracked as changes in the heat flow. This allows the detection of transitions such as melts, glass transitions, phase changes and curing. Because of this flexibility, DSC is used in many industries, including pharmaceuticals, manufacturing and electronics. The biggest advantage of DSC is the ease and speed with which it can be used to see transitions in materials. The basic principle underlying this technique is that when the sample undergoes a physical transformation, more or less heat will need to flow to it than the reference to maintain both at the same temperature. For these reasons, DSC is the most common thermal analysis technique and is found in many analytical, process control, quality assurance and R&D laboratories.

- **Viscosity**

There are several different methods that could be used to evaluate the viscosity of a fluid. The most used ones are:

- Ostwald viscometer: also known as U-tube viscometer or capillary viscometer, it is a device used to measure the viscosity of the liquid with a known density. The method of determining viscosity with this instrument consists of measuring the time for a known volume of the liquid (the volume contained between the upper and the lower mark) to flow through the capillary under the influence of gravity. The instrument must first be calibrated with materials of known viscosity such as deionized water. Knowing the value of viscosity of one liquid, one can calculate the viscosity of other liquid according the relation:

$$n_1 = n_2 \cdot \frac{\rho_1 t_1}{\rho_2 t_2}$$

where n_1 , n_2 are viscosity coefficients of the liquid and water, ρ_1 , ρ_2 are the densities and t_1 , t_2 are the flow time, respectively. This tool was named after the German chemist Wilhelm Ostwald (1853-1932).

- Zahn cup: it is commonly a stainless steel cup with a tiny hole drilled in the center of the bottom of the cup. There is also a long handle attached to the sides. There are five cup specifications, labeled Zahn cup #n, where n is the number from one to five. Large number cup sizes are used when viscosity is high, while low number cup sizes are used when viscosity is low. To determine the viscosity of a liquid, the cup is dipped and completely filled with the substance. After lifting the cup out of the substance, the user measures the time until the liquid streaming out of it breaks up, this is the corresponding efflux time. One can convert efflux time to kinematic viscosity by using an equation defined for each cup specification number.

- Falling sphere viscometer: the falling sphere viscometer is based on the measuring principle by H  ppler for simple but precise dynamic viscosity measurement of transparent Newtonian fluids. The basic concept is to measure the elapsed time required for the ball to fall under gravity through a sample-filled tube inclined at an angle (the most used angles are 50  , 60  , 70   and 80  ). The tube is mounted on a pivot bearing which quickly allows rotation of the tube of 180  , thereby allowing a repeat test to run immediately. Three measurements are taken and the average time it takes for the ball to fall is the result. A conversion formula turns the time reading into a final viscosity value. The falling sphere viscometer is used for quality control in various industries as well as in academic institutions to illustrate scientific method. The ease of use and straightforward method for recording time measurements ensures meaningful test results.
- Rotational viscometer: they use the idea that the torque required to turn an object in a fluid is a function of the viscosity of that fluid. Then, they measure the torque required to rotate a disk or bob in a fluid at a known speed.
- Vibrational viscometer: they date back to the 1950s Bendix instrument, which belongs to a tools's family that operates by measuring the damping of an oscillating electromechanical resonator immersed in a fluid whose viscosity is to be determined. The resonator generally oscillates in torsion or transversely (as a cantilever beam or tuning fork). The higher the viscosity, the larger the damping imposed on the resonator. The resonator's damping may be measured by one of several methods:
 - * measuring the power input necessary to keep the oscillator vibrating at a constant amplitude. The higher the viscosity, the more power is needed to maintain the amplitude of oscillation
 - * measuring the decay time of the oscillation once the excitation is switched off. The higher the viscosity, the faster the signal decays
 - * measuring the frequency of the resonator as a function of phase angle between excitation and response waveforms. The higher the viscosity, the larger the frequency change for a given phase change

Currently, many industries around the world consider these viscometers to be the most efficient system with which to measure the viscosities of a wide range of fluids. Furthermore, rotational viscometers require more maintenance, are unable to measure clogging fluid, and require frequent calibration after intensive use. Vibrating viscometers have no moving parts, no weak parts and the sensitive part is very small. Even very basic or acidic fluids can be measured by adding a protective coating or by changing the material of the sensor.

- **Average Molecular Weight**

There are several different methods that could be used to evaluate the average molecular weight of a blend. The most used ones are:

- Vapour pressure osmometry: it is an experimental technique for the determination of a polymer's average molecular weight, MW . It works by taking advantage of the decrease in vapor pressure that occurs when solutes are added to pure solvent. A typical vapor phase osmometer consists of:
 1. two thermistors, one with a polymer-solvent solution droplet adhered to it and another with a pure solvent droplet
 2. a thermostated chamber with an interior saturated with solvent vapor
 3. a liquid solvent vessel in the chamber
 4. an electric circuit to measure the bridge output imbalance difference between the two thermistors

The voltage difference is an accurate way of measuring the temperature difference between the two thermistors, which is a consequence of solvent vapor condensing on the solution droplet (the solution droplet has a lower vapor pressure than the solvent). Then, the average molecular weight for a polymer sample is given by the relation:

$$MW_{mix} = \frac{K}{\lim_{c \rightarrow 0} \left(\frac{\Delta V}{c} \right)}$$

where:

- * K is a calibration constant
- * ΔV is the bridge imbalance output voltage
- * c is the polymer-solvent solution concentration

It is necessary to calibrate a vapor phase osmometer and it is important to note that K is found for a particular solvent, operational temperature and type of commercial apparatus. A calibration can be carried out using a standard of known molecular weight. Some possible solvents for VPO include toluene, tetrahydrofuran or chloroform. Once the experiment is performed, concentration and output voltage data can be graphed on a plot of $\left(\frac{\Delta V}{c} \right)$ versus c. The plot can be extrapolated to the y-axis in order to obtain the limit of $\left(\frac{\Delta V}{c} \right)$ as c approaches zero. The equation above can then be used to find K.

- Freezing-point depression: it is the decrease of the freezing point of a solvent on the addition of a non-volatile solute. Examples include salt in water or alcohol in water.
- Boiling point elevation: it describes the phenomenon that the boiling point of a liquid (a solvent) will be higher when another compound is added, meaning that a solution has a higher boiling point than a pure solvent.

- Gel permeation chromatography: GPC is a type of size exclusion chromatography that separates analytes on the basis of size. The technique is often used for the analysis of polymers. GPC separates relying on the size or hydrodynamic volume (radius of gyration) of the analytes. This differs from other separation techniques which depend upon chemical or physical interactions to separate analytes. Separation occurs via the use of porous beads packed in a column. The smaller analytes can enter the pores more easily and therefore spend more time in these pores, increasing their retention time. These smaller molecules spend more time in the column and therefore will elute last. Conversely, larger analytes spend little if any time in the pores and are eluted quickly. All columns have a range of molecular weights that can be separated. Analytes that are not retained are eluted with the free volume outside of the particles (V_o), while analytes that are completely retained are eluted with volume of solvent held in the pores (V_i). The total volume is obtained by the following equation, where V_g is the volume of the polymer gel and V_t is the total one:

$$V_t = V_o + V_i + V_g$$

As can be inferred, there is a limited range of molecular weights that can be separated by each column and therefore the size of the pores for the packing should be chosen according to the range of molecular weight of analytes to be separated. For polymer separations, the pore sizes should be on the order of the polymers being analyzed.

- **Density**

With regard to the density, the main existing method for its evaluation is the oscillating tube (or vibrating tube) densimetry. It is a technique to determine the density of liquids and gases based on an electronic measurement of the frequency of oscillation, from which the density value is calculated. This measuring principle is based on the mass-spring model. The sample is filled into a container with oscillation capacity. The eigenfrequency of this container is influenced by the sample's mass. This container with oscillation capacity is a hollow, U-shaped glass tube (oscillating U-tube) which is electronically excited into undamped oscillation. The two branches of the U-shaped oscillator function as its spring elements. The direction of oscillation is normal to the level of the two branches. The oscillator's eigenfrequency is only influenced by the part of the sample that is actually involved in the oscillation. The volume involved in the oscillation is limited by the stationary oscillation knots at the bearing points of the oscillator. If the oscillator is at least filled up to its bearing points, the same precisely defined volume always participates in the oscillation, thus the measured value of the sample's mass can be used to calculate its density.

N	Chemical Formula	Compounds Name	MW	T_{boil}	T_{crit}	T_r	P_{crit}	TSI	$\Delta h_{f,298}^0$	$\Delta_c H_{298}^0$	S_{298}^0	$\rho_{L,298}$	η_{298}	V_{298}
			$\frac{kg}{kmol}$	[K]	[K]	[-]	[atm]	[-]	$\left[\frac{kJ}{mol}\right]$	$\left[\frac{kJ}{mol}\right]$	$\left[\frac{J}{mol \cdot K}\right]$	$\frac{kg}{m^3}$	[cP]	$\left[\frac{m^2}{s}\right]$
n-Paraffines														
1	n- C_5H_{12}	n-Pentane	72.15	309.22	469.70	0.539	33.70	1.3	-173.50	-3508.80	263.47	626.00	0.33766	5.39404E-07
2	n- C_6H_{14}	n-Hexane	86.17	341.88	507.60	0.499	30.25	2.5	-198.70	-4162.90	296.06	659.00	0.48800	7.40526E-07
3	n- C_7H_{16}	n-Heptane	100.20	371.57	540.20	0.469	27.40	2-7	-225.90	-4529.20	328.57	684.00	0.69881	1.02166E-06
4	n- C_8H_{18}	n-Octane	114.23	398.8	568.80	0.445	24.50	3.2	-208.60	-5511.60	361.20	703.00	0.99676	1.41787E-06
5	n- C_9H_{20}	n-Nonane	128.25	423.97	594.60	0.426	22.90	4.1	-274.70	-6124.80	393.67	718.00	1.40386	1.95525E-06
6	n- $C_{10}H_{22}$	n-Decane	142.28	447.30	617.70	0.410	21.10	4.3	-250.02	-6829.32	425.89	726.14	1.96789	2.71008E-06
7	n- $C_{11}H_{24}$	n-Undecane	156.30	469.08	639.00	0.396	19.80	4.3	-327.20	-7430.90	458.15	740.00	2.75731	3.72610E-06
8	n- $C_{12}H_{26}$	n-Dodecane	170.33	489.48	658.00	0.385	18.20	4.8	-352.10	-8085.30	490.66	748.00	3.77628	5.04851E-06
9	n- $C_{13}H_{28}$	n-Tridecane	184.36	508.63	675.00	0.375	16.80	5.2	-377.70	-8739.00	522.87	756.00	5.17435	6.84438E-06
10	n- $C_{14}H_{30}$	n-Tetradecane	198.38	526.76	693.00	0.365	15.70	5.4	-403.30	-9392.70	555.43	763.00	7.20842	9.44748E-06
11	n- $C_{15}H_{32}$	n-Pentadecane	212.41	543.83	708.00	0.358	14.80	-	-428.80	-10046.50	587.52	769.00	9.61395	1.25019E-05
12	n- $C_{16}H_{34}$	n-Hexadecane	226.44	559.98	723.00	0.350	14.00	-	-456.10	-10698.50	586.18	773.00	13.2384	1.71261E-05
i-Paraffines														
13	i- C_4H_{10}	Iso-Butane	58.12	261.34	407.85	0.621	36.40	2.2	-134.39	-1439.61	200.79	594.00	0.20990	3.53372E-07
14	i- C_5H_{12}	Iso-Pentane	72.15	300.99	460.39	0.550	33.81	1.6	-190.30	-3492.00	216.81	620.00	0.31845	5.13633E-07
15	i- C_6H_{14}	2-Methy-Pentane	86.17	333.4	497.50	0.509	29.70	2.9	-175.88	-4185.72	290.58	653.00	0.45620	6.98622E-07
16	i- C_7H_{16}	2-Methyl-Hexane	100.20	363.18	530.10	0.478	27.30	3.2	-229.80	-4525.30	323.34	679.00	0.64918	9.56084E-07
17	i- C_8H_{18}	3-Ethyl 2-Methyl-Pentane	114.23	388.81	567.00	0.446	27.00	-	-249.70	-5470.50	342.60	719.00	0.98701	1.37276E-06
18	i- C_8H_{18}	Iso-Octane	114.23	372.39	543.90	0.465	25.70	5.6	-237.42	-5483.22	328.00	692.00	0.72273	1.04442E-06
19	i- C_9H_{20}	2-Methyl-Octane	128.25	416.43	587.00	0.431	23.10	3.8	-238.01	-6161.49	357.18	713.40	1.32728	1.86051E-06
20	i- C_9H_{20}	3,4-Di-Methyl-Heptane	128.25	413.55	591.10	0.428	24.50	3.5	-246.71	-6152.79	-	731.40	1.37250	1.87654E-06
21	i- $C_{10}H_{22}$	2,7-Di-Methyl-Octane	142.28	433.14	574.00	0.441	21.11	4.3	-267.42	-6811.92	-	736.8	1.35806	1.84319E-06

22	i-C ₁₀ H ₂₂	2- Methyl-Nonane	142.28	440.02	589.7	0.429	21.02	-	-58.72	-6820.08	420.1	726.3	1.55780	2.14485E-06
23	i-C ₁₀ H ₂₂	2,4,5-Tri-Methyl-Heptane	142.28	429.65	606.90	0.417	22.70	-	-276.12	-6802.68	-	737.30	1.13833	1.54393E-06
24	i-C ₁₁ H ₂₄	2,3,3-Tri-Methyl-Octane	156.30	455.15	630.28	0.402	19.89	-	-278.84	-7479.26	-	754.70	2.18576	2.89621E-06
25	i-C ₁₁ H ₂₄	2-Methyl-Decane	156.30	462.40	629.9	0.402	19.20	4.3	-279.43	-7479.26	578.3	726.4	2.53190	3.48563E-06
26	i-C ₁₁ H ₂₄	2,2,3- Tri-Methyl-Octane	156.30	465.82	638.00	0.407	20.30	-	-299.55	-7458.55	585.0	737.0	2.345904	3.18305E-06
27	i-C ₁₂ H ₂₆	2-Methyl-Undecane	170.33	483.15	648.37	0.390	18.35	-	-275.65	-8161.75	-	745.80	4.6812E-06	4.6812E-06
28	i-C ₁₃ H ₂₈	2-Methyl-Dodecane	184.36	500.28	670.00	0.378	17.29	-	-320.85	-8795.85	-	757.00	4.91310	6.49023E-06
29	i-C ₁₆ H ₃₄	2,2,4,4,6,8,8-Hepta-Methyl-Nonane (HMN)	226.44	520.25	693.00	0.365	15.7	-	-443.34	-10711.26	-	793.00	6.18765	7.80284E-06
Cycloparaffines														
30	cy C ₆ H ₁₂	Cyclohexane	84.16	353.93	553.50	0.457	40.73	3.2	-156.40	-3930.00	204.00	779.00	0.66888	8.58641E-07
31	cy C ₇ H ₁₄	Cycloheptane	98.18	391.90	589.00	0.430	36.70	3.3	-157.50	-4597.60	242.55	811.00	0.99652	1.22876E-06
32	cy C ₇ H ₁₄	n-Metyl-Cyclohexane	98.18	374.09	572.19	0.442	34.71	4.4	-190.20	-4565.29	247.90	774.00	0.88749	1.14664E-06
33	cy C ₈ H ₁₆	Cyclooctane	112.21	424.31	647.20	0.391	35.70	5.9	-169.40	-5265.70	262.00	834.00	1.82606	2.18953E-06
34	cy C ₈ H ₁₆	n-Ethyl-Cyclohexane	112.21	405.00	609.00	0.416	32.07	4.6	-213.00	-5222.60	280.91	788.00	1.35302	1.71704E-06
35	cy C ₉ H ₁₈	n-Propyl-Cyclohexane	126.24	429.90	639.00	0.396	27.70	4.3	-195.09	-5719.06	311.88	793.00	1.69539	1.96227E-06
36	cy C ₁₀ H ₂₀	n-Butyl-Cyclohexane	140.26	454.10	667.00	0.380	31.10	-	-215.18	-6577.20	344.97	818.00	2.37145	2.99049E-06
37	cy C ₁₁ H ₂₂	n-Pentyl-Cyclohexane	154.29	476.85	669.00	0.378	22.10	-	-233.8	-7238.50	-	803.70	3.50708	4.28739E-06
38	cy C ₁₂ H ₂₄	n-Hexyl-Cyclohexane	168.32	497.93	679.00	0.373	19.20	-	-251.82	-7899.78	-	807.60	4.22959	5.26265E-06
39	cy C ₁₃ H ₂₆	n-Heptyl-Cyclohexane	182.34	518.14	694.00	0.365	17.70	-	277.93	-8552.97	-	810.90	5.35862	6.63530E-06
Aromatics														
40	C ₆ H ₆	Benzene	78.11	353.24	562.05	0.450	48.95	31	48.70	-3273.00	173.26	885.00	0.17000	1.92000E-07
41	C ₇ H ₈	Toluene	92.14	383.79	591.75	0.428	41.08	50	12.00	-3920.00	220.96	867.00	0.00800	8.95000E-09
42	C ₈ H ₁₀	Ethyl-Benzene	106.16	409.36	617.15	0.410	36.09	59	-12.50	-4567.00	255.01	867.00	0.00700	8.27000E-09
43	C ₈ H ₁₀	m-Xylene	106.16	412.34	617.00	0.410	35.41	51	-25.40	-4549.00	253.80	864.00	0.23100	2.67340E-07
44	C ₉ H ₁₂	Propyl-Benzene	120.19	432.35	638.35	0.397	32.00	47	-38.40	-5218.24	287.78	862.00	0.00700	8.03120E-09
45	C ₉ H ₁₂	1,2,4-Tri-Methyl-Benzene	120.19	442.50	649.10	0.390	32.32	47	-61.90	-5194.80	283.38	880.00	0.28300	3.22230E-07
46	C ₁₀ H ₁₂	Tetralin	132.20	480.75	720.00	0.352	36.50	56	-28.60	-5621.54	251.46	973.00	0.0560	5.75539E-05
47	C ₁₁ H ₁₀	1-Methyl-Naphthalene	142.20	517.84	772.00	0.328	36.00	89	56.20	-5814.00	254.81	990.00	0.04500	4.52540E-08

Table 3.5 Physical properties of the main hydrocarbons

Chapter 4

Brute-Force Search Algorithm

The various modules of this code have been developed starting from the second month of internship, since the first one was devoted to the study of the previously corresponding algorithms. These studies were carried out to determine the starting point of the research, trying also to define which were the strengths (features that could have been further considered in the developing process) and the weaknesses of these codes. Since the previous ones and their relative database were written in MATLAB language, in order to simplify the work of thesis, the code is carried out in the same software environment. Moreover, the choice of this option proved to be appropriate, since MATLAB is build in the C language, that was designed to be compiled using a relatively straightforward compiler, to provide low-level access to memory, to provide language constructs that map efficiently to machine instructions and to require minimal runtime support. Because of algorithm's computational heaviness, in order to run the code in his totality, the memory capacity of a normal personal computer (or a common university's workstation) wasn't enough, but it was necessary to use the university Clusters, whose hardware properties are shown in the next table:

TUM	
Hardware	
number of nodes	148
cores for node	64
hyperthreads per core	4
core nominal frequency	1.3 GHz
memory (DDR4) per node	96 GB (Bandwidth 80.8 $\frac{GB}{s}$)
High Bandwidth Memory per node	16 GB (Bandwidth 460 $\frac{GB}{s}$)
bandwidth to interconnect per node	25 $\frac{GB}{s}$ (2 Links)
number of Omnipath switches (100SWE48)	10+4 (je 48 Ports)
bisection bandwidth of interconnect	1.6 $\frac{TB}{s}$
latency of interconnect	2.3 μs
peak performance of system	394 $\frac{TFlops}{s}$
Software (OS and development environment)	
operating system	SLES12 SP2 Linux
MPI	Intel MPI 2017 or OpenMPI
compilers	Intel icc, icpc, ifort 2017
performance libraries	MKL, TBB, IPP
tools for performance and correctness analysis	Intel Cluster Tools

Politecnico di Torino	
Hactar technical specification	
architecture	Linux Inniband-QDR MIMD Distributed Shared-Memory Cluster
node interconnect	Inniband QDR 40 $\frac{GB}{s}$
Service Network Gigabit	Ethernet 1 $\frac{GB}{s}$
CPU model	2x Xeon E5-2680 v3 2.50 GHz (turbo 3.3 GHz) 12 cores
GPU node	2x Tesla K40-12 GB-2880 CUDA cores
performance	20.18 TFLOPS (June 2018)
computing cores	696
number of nodes	29
total RAM Memory	3.7 TB DDR4 REGISTERED ECC
OS	CentOS 7.4 - OpenHPC 1.3.4
Scheduler	SLURM 17.11

Storages technical specification	
home storage	140 TB on RAID 6, throughput near 200 $\frac{MB}{s}$
lustre storage	87 TB, throughput greater than 2.2 $\frac{GB}{s}$
storage interconnect	Ethernet 10 $\frac{Gb}{s}$

Table 4.1 Clusters features

The description of the algorithm process is matched with his block scheme depiction, in order to clarify the line of reasoning employed in the code's run. This process is divided into four main sub-modules, which can be summed up as the main operation they carry out:

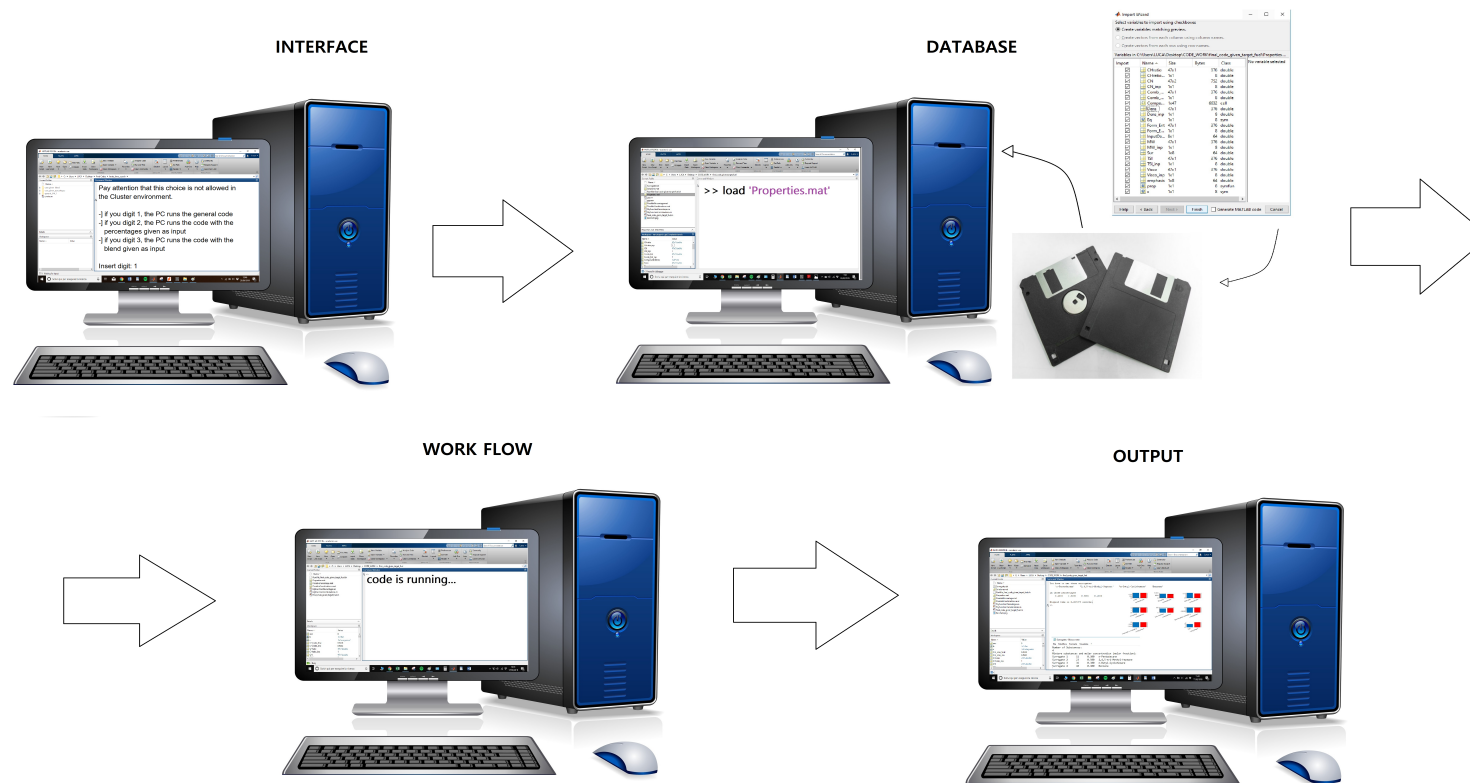


Figure 4.1 Block scheme of the algorithm

4.1 Interface



Figure 4.2 First block of the scheme

The code starts with the algorithm choice on the MATLAB command window (as shown in figure 4.2). By this selection, the user can decide to run a certain code, choosing it out of three possibilities:

- I. The first option refers to the most general code, where the user knows only the physical and chemical properties of the target fuel, without any ideas about which hydrocarbons and percentages could assure them. The user is asked to submit to the code the chemical division of hydrocarbons and the desired refinement for the percentages' range (e.g. table 4.2).

	n-paraffines	iso-paraffines	cycloparaffines	aromatics
hydrocarbons_input	1	2	2	1
single_step	0.01			

Table 4.2 Example

In general, for jet fuels, the combinations of the hydrocarbons could be quite variable, but chemical family's profile is almost constant:

- iso/n-paraffines \simeq 60-70%
- cycloparaffines \simeq 15-20%
- aromatics \simeq 15-25%

According to these technical specifications, the number of percentages combinations is limited to those who meet the requirements. Each of them is matched with all the possible blends, allowing the code to evaluate chemical and physical properties for every surrogate. Then, results are compared with the input ones, finding out the relative error.

4.1. INTERFACE

The output of the code is the IFS, i.e. the combination of hydrocarbons and percentages that minimizes the total relative error. A visual representation of the (simplified) algorithm is shown in table 4.3.

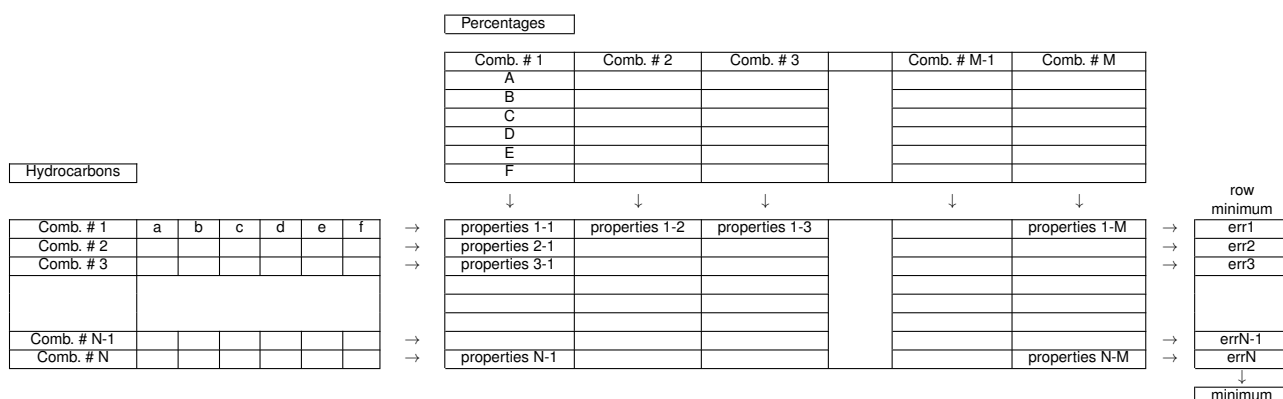


Table 4.3 Simplified algorithm depiction. Model design 1

- II. The second one refers to the case where the user has as input the fuel properties and a certain percentages combination to observe. The output of the code is the best blend of hydrocarbons to meet the requests.

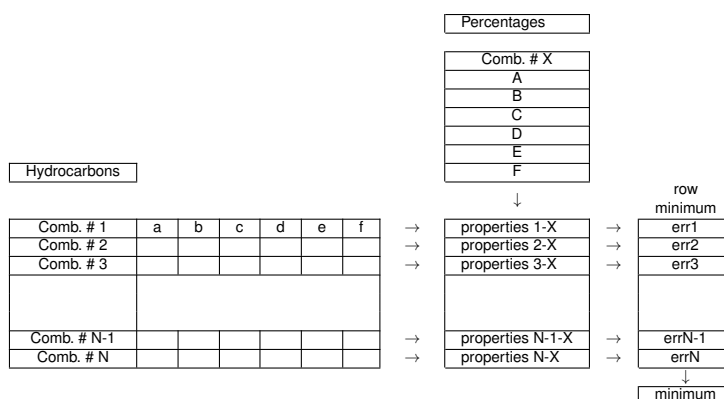


Table 4.4 Simplified algorithm depiction. Model design 2

- III. The last one is the case where the user knows the fuel properties and has, as a input, the hydrocarbon blend to observe. In this case, the output of the code will be the best combinations of percentages to fulfill the requests (the chemical families limitations of the first case still apply).

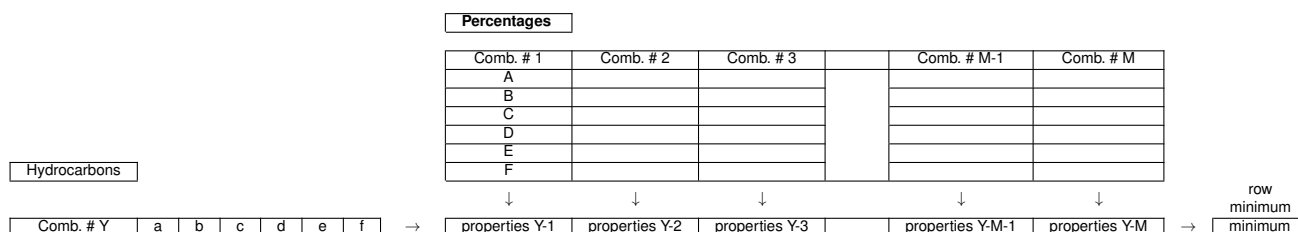


Table 4.5 Simplified algorithm depiction. Model design 3

It is important to note that these possibilities have different computational weight; while the first one demands for a huge storage capacity, the other two are much lighter, lacking the additional recursions present in model design 1.

4.2 Database

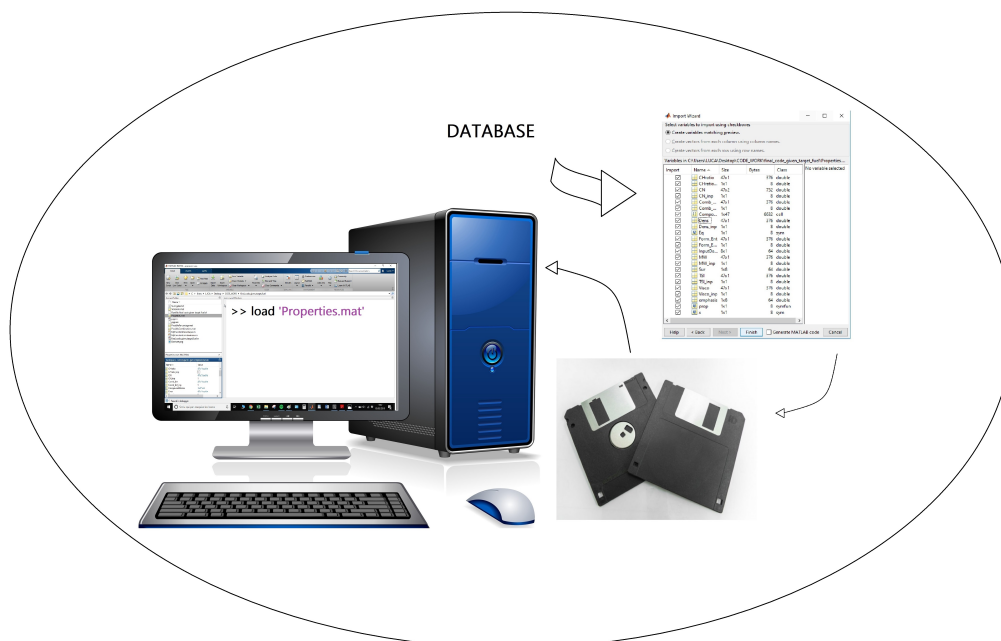


Figure 4.3 Second block of the scheme

The second block of the scheme is dedicated to the upload of hydrocarbons data. In this database are gathered all the chemical and physical properties of the forty-seven hydrocarbons available for the research, whose index is shown in the table 4.8. A small sum up of this file is shown in the following lines:

- **CHratio**: the ratio, on a molecular basis, of carbon-to-hydrogen ratio in each hydrocarbons. It is dimensionless, [-]. Because of their structure, while aromatic hydrocarbons have the highest CH ratio indices, the chemical family of cyclo-paraffins shows a constant value of 0.500.
- **CHratio_inp**: CH_ratio of the input fuel. The user provides it to the code.
- **CN**: it is the cetane number of a molecular components. It is dimensionless, [-]. Because of their chemical meaning, in the input file CN shows a double value column. In the first one are reported the CN values of each hydrocarbon, in the second one the β values, necessary for the final surrogate's cetane number calculation (the differentiation for each chemical family follows the directives proposed in section 3.2). The range of the CN values is relatively wide, starting from numbers almost nil for aromatics arriving to the biggest values, i.e. the n-paraffine family's ones.
- **CN_inp**: CN of the input fuel. It is given as input from the keyboard.
- **Comb_Ent**: it is the enthalpy change when one mole of a substance burns (combines with oxygen) under standard state conditions. Sometimes called "heat of combustion", it has always a negative value (since burning always releases heat) and its unit of measurement is $\left[\frac{\text{kJ}}{\text{mol}}\right]$. Finally, it is important to note that the most reactive hydrocarbons are those characterized by a higher average *MW*.

- **Comb_Ent_inp**: $\Delta_c H^0$ of the input fuel. The user provides it to the code.
- **CompoundsName**: the correlation between the name of the molecular species and their number in the file. They are reported under IUPAC's specifications.
- **Dens**: the density of the species taken in account for the research. They are reported in $\left[\frac{kg}{m^3}\right]$. For the record, it's important to remind that the densest hydrocarbons belong to the aromatic family.
- **Dens_inp**: density of the input fuel and it is provided from the keyboard.
- **Eq**: it is a symbolic variable, useless for the code developed in this thesis.
- **Form_Ent**: it is the enthalpy change for a reaction in which exactly one mole of a pure substance is formed from free elements in their most stable states under standard state conditions. Its unit of measurement is $\left[\frac{kJ}{mol}\right]$ and it has, generally, a negative value involving a process exothermic (the only hydrocarbons that don't follow this feature are n-Heptyl-Cyclohexane, Benzene and Toluene). On average, the most exothermic hydrocarbons belong to the n-paraffine family ($\Delta h_f^0 \simeq -306.36 \left[\frac{kJ}{mol}\right]$) while the least ones refer to the aromatic family ($\Delta h_f^0 \simeq -6.24 \left[\frac{kJ}{mol}\right]$).
- **Form_Ent_inp**: Δh_f^0 of the input fuel. The user provides it to the code.
- **InputData**: it is a vector pre-allocated with the input fuel data, useless for the code developed in this thesis.
- **MW**: it is the molecular weight of the hydrocarbons. Since the *MW* increase with the number of atoms involved in the molecule, high-branched structures shows higher *MW*. It is measured in $\left[\frac{kg}{kmol}\right]$.
- **MW_inp**: *MW* of the input fuel and it is provided to the code by the user.
- **Sur**: it is a vector that contains the combination of the eight surrogates which could simulate the chemical and physical properties of the input fuel. Intended to be updated every calculation's loop, it's useless for the code developed in this thesis.
- **TSI**: this number is representing the inherent sooting tendency of a compound or a mixture. While many hydrocarbons of the first three family show a value equal to 0, aromatics have an index variable for 31 to 89 (this is a reason of their limited usage in fuel surrogates). It is dimensionless $[-]$.
- **TSI_inp**: TSI index of the input fuel. It is provided by the user.
- **Visco**: dynamic viscosity is a property of fluids characterized by their internal resistance against flowing. Generally, the viscosity of hydrocarbons tends to increase according to the molecular weight of the compound. It is interesting to note that, while for the first three family the viscosity values lay on the same magnitude, aromatic family's viscosity show values about 10-to-100 fold lower. It is measured in $[cP]$.
- **Visco_inp**: η of the input fuel. The user provides from the keyboard.
- **emphasis**: it is a vector that contains parameters about the relevance of each properties of the fuel. It is chosen by default as a vector of all ones.
- **prop**: symbolic variable, useless for the code developed in this thesis.
- **x**: symbolic variable, useless for the code developed in this thesis.

Import	Name	Size	Bytes	Class
[✓]	CHratio	47x1	376	double
[✓]	CHratio_inp	1x1	8	double
[✓]	CN	47x2	752	double
[✓]	CN_inp	1x1	8	double
[✓]	Comb_Ent	47x1	376	double
[✓]	Comb_Ent_inp	1x1	8	double
[✓]	CompoundsName	1x47	6632	cell
[✓]	Dens	47x1	376	double
[✓]	Dens_inp	1x1	8	double
[✓]	Eq	1x1	8	sym
[✓]	Form_Ent	47x1	376	double
[✓]	Form_Ent_inp	1x1	8	double
[✓]	InputData	8x1	64	double
[✓]	MW	47x1	376	double
[✓]	MW_inp	1x1	8	double
[✓]	Sur	1x8	64	double
[✓]	TSI	47x1	376	double
[✓]	TSI_inp	1x1	8	double
[✓]	Visco	47x1	376	double
[✓]	Visco_inp	1x1	8	double
[✓]	emphasis	1x8	64	double
[✓]	prop	1x1	8	symfun
[✓]	x	1x1	8	sym

Table 4.6 Input file

#	CHratio	Comb_Ent	CN		Dens	MW	Spec_Ent ¹	TSI	Visco	Visco_St ¹
			CN	β						
1	0.4160	-3508.8	30	0.5212	626	72.15	48632.0	1.3	0.338	0.539
2	0.4280	-4162.9	40	0.5212	659	86.17	48310.3	2.5	0.488	0.741
3	0.4375	-4529.2	55	0.5212	684	100.2	45201.6	4.5	0.699	1.022
4	0.4440	-5511.6	60	0.5212	703	114.23	48250.0	3.2	0.997	1.418
.										
.										
.										
45	0.75	-5194.8	7	3.1967	880	120.19	43221.6	47	0.283	0.322
46	0.833	-5621.5	6	3.1967	973	132.2	42523.0	56	0.056	0.058
47	1.111	-5814.0	20	3.1967	990	142.2	40886.1	89	0.045	0.045

Table 4.7 Input data

¹ These data are not available on the database but they have been evaluated according to the following formulas, derived from chapter 3:

$$\text{Spec_Ent} = -1000 \cdot \frac{\text{Comb_Ent}}{\text{MW}} \quad \text{Visco_St} = 1000 \cdot \frac{\text{Visco}}{\text{Dens}}$$

n-paraffines		i-paraffines	
1	n-Pentane	13	Iso-Butane
2	n-Hexane	14	Iso-Pentane
3	n-Heptane	15	2-Methyl-Pentane
4	n-Octane	16	2-Methyl-Hexane
5	n-Nonane	17	3-Ethyl-2-Methyl-Pentane
6	n-Decane	18	Iso-Octane
7	n-Undecane	19	2-Methyl-Octane
8	n-Dodecane	20	3,4-Di-Methyl-Heptane
9	n-Tridecane	21	2,7-Di-Methyl-Octane
10	n-Tetradecane	22	2-Methyl-Nonane
11	n-Pentadecane	23	2,4,5-tri-Methyl-Heptane
12	n-Hexadecane	24	2,3,3-tri-Methyl-Octane
		25	2-Methyl-Decane
		26	2,2,3-Tri-Methyl-Octane
		27	2-Methyl-Undecane
		28	2-Methyl-Dodecane
		29	2,2,4,4,6,8,8-HMN

cyclo-paraffines		aromatics	
30	Cyclohexane	40	Benzene
31	Cycloheptane	41	Toluene
32	n-Methyl-Cyclohexane	42	Ethyl-Benzene
33	Cyclooctane	43	m-Xylene
34	n-Ethyl-Cyclohexane	44	Propyl-Benzene
35	n-Propyl-Cyclohexane	45	1,2,4-Tri-Methyl-Benzene
36	n-Butyl-Cyclohexane	46	Tretalin
37	n-Pentyl-Cyclohexane	47	1-Methyl-Naphthalene
38	n-Hexyl-Cyclohexane		
39	n-Heptyl-Cyclohexane		

Table 4.8 Family division of hydrocarbons

Hydrocarbons names are reported according to IUPAC nomenclature ².

2



Figure 4.4 IUPAC logo

The IUPAC nomenclature of organic chemistry is a systematic method of naming organic chemical compounds as recommended by the International Union of Pure and Applied Chemistry (IUPAC). It is published in the Nomenclature of Organic Chemistry. Ideally, every possible organic compound should have a name from which an unambiguous structural formula can be created.

4.3 Software



Figure 4.5 Third block of the scheme

The three options shown in the section 4.1 cannot be debated as a one, since they differentiate themselves both for the input and for the central algorithm. In order to give a more general (and, as much as possible, better) explanation of the code, the following section is focused on the discussion of the interface's first option³. It is possible to divide the main code in three different sub-modules, each characterized by the specific function it is intended to fulfill:

- The first sub-module refers to the calculus of all possible combinations of hydrocarbons (blends), up to their chemical family's division
- The second one is based on the calculus of all possible combinations of percentages for the hydrocarbons
- The third and last sub-module is the leading part of the code, the one which returns the user the effective results. It can be summed up as the definition of the optimized Input Formula of Surrogate (IFS) (i.e. which hydrocarbons and how much of them are necessary for the surrogate)

³ For the other module design the treatise is almost fully equivalent. The only differences are based on a lightening of the code's computational weight, since there is no more need to find specific solutions. The features are shown in the following table:

	Combinations	Percentages	Main step	
Model design 1	v	v	v	v = evaluated
Model design 2	v	x	v	x = not evaluated
Model design 3	x	v	v	

Table 4.9 Models design

4.3.0 MATLAB's version conformity check

Because of the usage of some specific MATLAB's functions released starting from the R2018b version, if the user tried to run the code with a previous software's update, he would incur in some fatal error during the process. The version check is fulfilled by an auxiliar function, named *MyFunctionVersion.m*, which compares the used version with the reference one and gives back a flag if the required condition is not satisfied.

4.3.1 First sub-module

The first module, whose whole block diagram is shown in figure 4.6, represents the processes accomplished to obtain the hydrocarbon combinations matrix (more properly, blends matrix). The code starts with the manual input of the compounds quantity the users wants to utilize to simulate a given fuel, according to the respective chemical family (n-paraffins, iso-paraffins, cyclo-paraffins and aromatics). Once defined the vector of the desired hydrocarbons, is possible to calculate the sum of its components. At this point, the code loads the *Properties.mat* file, which, among other things, includes the chemical and physical properties of the compounds. Their total number is 47, divided up to their chemical family as shown in table 4.8. Therefore, the code, in order to evaluate all the possible blends, utilizes the MATLAB *nchoosek* function. It represents the binomial coefficient of k variables out n numbers⁴, where k is the chosen number of compounds of each family and n is the family's hydrocarbons number. Once obtained the matrices of the four families, the code exploits the MATLAB function *ndgrid* in order to rearrange them in the final blends matrix (the various functions are better explained on sections C.1, C.2). In the end, it's possible to save the results in the *PossibleCombinations.mat* file. These calculations are mainly performed in a support function, named *MyFunctionCombinations.m*, in order to fast the computational time of the code. If the users choosed to use the Model design 3, all these processes would be exluded, since the hydrocarbons required are already available.

⁴ In mathematics, the binomial coefficients are the positive integers that occur as coefficients in the binomial theorem. Commonly, a binomial coefficient is indexed by a pair of integers $n \geq k \geq 0$ and is written $\binom{n}{k}$. It is the coefficient of the x^k term in the polynomial expansion of the binomial power $(1+x)^n$, and it is given by the formula:

$$\binom{n}{k} = \frac{n!}{k! \cdot (n-k)!} = \frac{n \cdot (n-1) \cdot \dots \cdot (n-k+2) \cdot (n-k+1)}{k!}$$

4.3. SOFTWARE

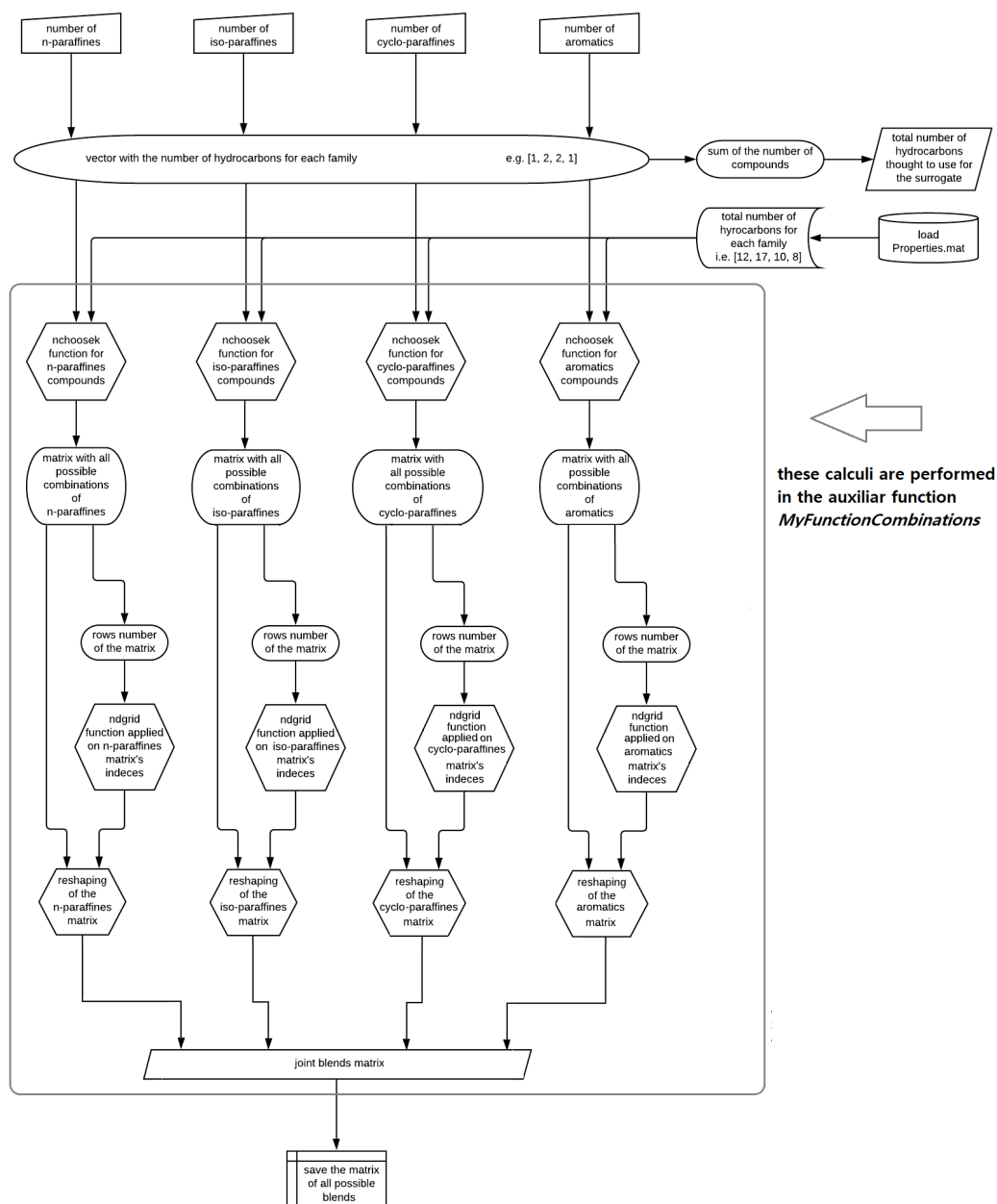


Figure 4.6 First sub-module of the algorithm

4.3.2 Second sub-module

The second sub-module can be summed up as the percentage block, since it is devoted to the calculation of the matrix containing all the valid percentages combinations for the hydrocarbons, according to the family division given as input. It starts with the manual input of the boundary function, whose aim is to set the inferior limit of the possible percentages range. The chosen function is an hyperbola, described by the equation (a) (the parameter *constant* is given as input from keyboard). Once found the minimum percentage, the code evaluates the maximum percentage theoretically achievable by each single compound, according to the relation (b).

$$\min = f(\text{const}, \# \text{hyd}) = \frac{\text{const}}{\# \text{hyd}} \quad \max = 1 - \sum_{i=1}^{\# \text{hyd}-1} (\min) = 1 - (\# \text{hyd} - 1) \cdot \min$$

(a) (b)

Unfortunately, these results are assumed to be partial, since they do not respect the typical jet fuels compositions constraints (figure 4.7). Referring to section 4.1, it's evident the necessity to further limit the possible percentages ranges. This process is accomplished in the *MyFunctionPercentages.m* auxiliar function, which gives back the final percentages matrix. Then, thanks to the *ndgrid* MATLAB function (see C.2), it is possible to couple together all the hydrocarbon's range, checking the ones that fulfill the physical constraints of surrogate's total unity. In the end, the final results are saved in the specific *PossiblePossiblePercentage.mat* file and in three different figures, printed in order to clarify the family division (figure 4.8, 4.9). In case the users choosed the second option, all these processes would be exluded, since the percentages are already available.

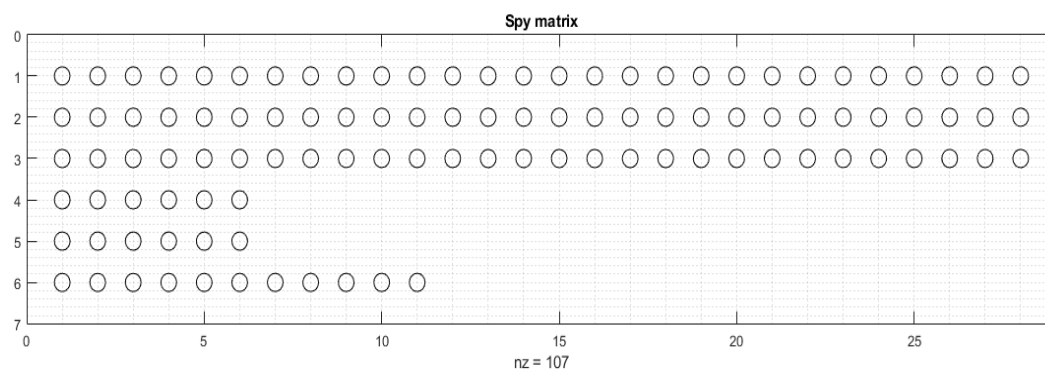


Figure 4.7 First refinement of percentages

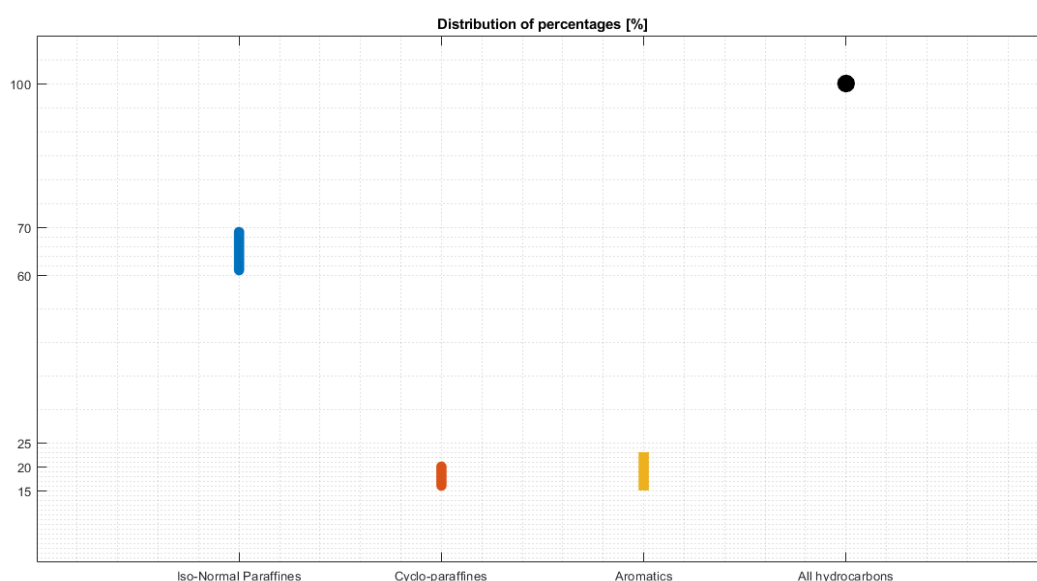


Figure 4.8 Final distribution of percentages according to the chemical family

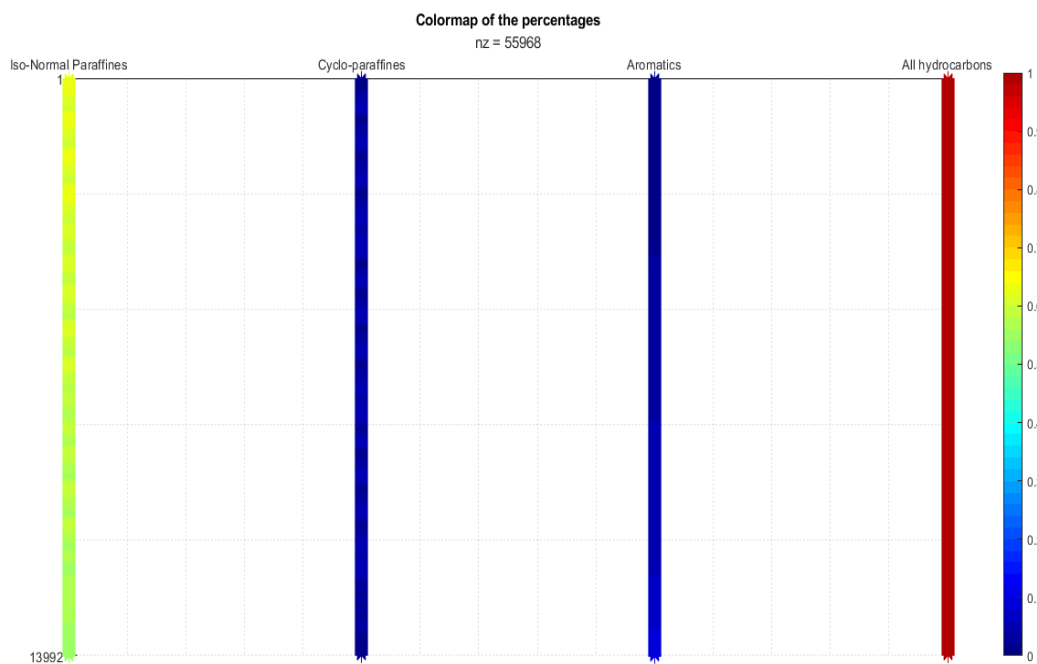


Figure 4.9 Colormap of figure 4.8

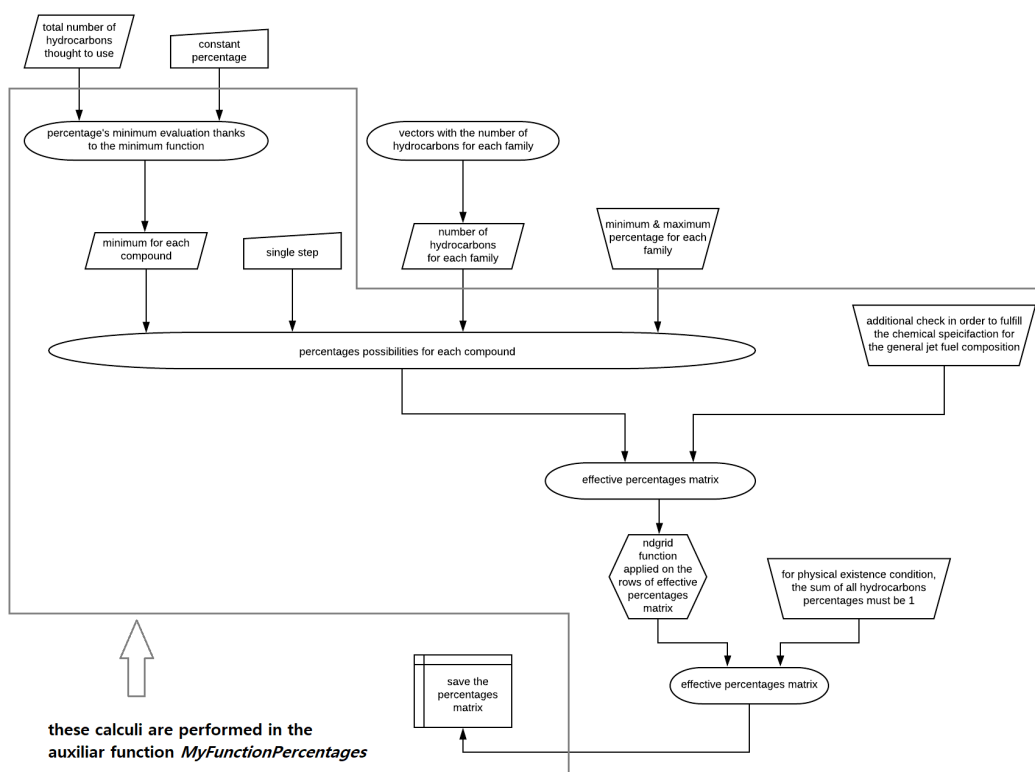


Figure 4.10 Second sub-module of the algorithm

4.3.3 Third sub-module

The third and last module concerns about the main portion of the code, i.e. the one that leads to the solutions of the problem. It starts with the initial setup of the value vector and of the data matrix to zeros, in order to fast the progressive allocation of the each component inside. The allocation takes place thanks to two nested loops; while the external one (a *parfor* loop, see section C.3), is limited by the dimensions of the blends matrix, the internal one (a common *for* loop) follows the percentages matrix geometry. Before the inner loop, there is the initial setup of the error relative vectors to empty cells (pre-allocation process); then, after loading the chemical and physical properties of the hydrocarbons, the code starts the recursive operations which evaluate the features of each surrogate. The calculated values (molecular weight (MW), density (ρ), CH ratio, viscosity (ν), cetane number (CN), specific energy and threshold sooting index (TSI)) are then compared to the input targets and each relative error is saved in the respective support vector's cell. Thanks to the goodness of the input file, most of the properties vector do not need to be further modified for the operations. Unfortunately, this feature does not last for the kinematic viscosity and for the specific energy, that have to be evaluated for every surrogate. Once found the necessary properties, they are compared with the reference ones, giving back the total relative error calculated according to the formula:

$$\varepsilon_{rel} = \sqrt{\sum_j^J \left(\frac{(\sum_i^I \chi_i y_{i,j}) - Y_j}{Y_j} \right)^2} \quad \text{where} \quad \begin{cases} \chi_i & \text{is the molar percentage of the } i\text{-th compound} \\ y_i & \text{is the } j\text{-th property of the } i\text{-th hydrocarbon} \\ Y_j & \text{is the } j\text{-th reference property} \\ i & \text{index goes from 1 to } I, \text{ the total hydrocarbons number} \\ j & \text{index goes from 1 to } J, \text{ the total properties number} \end{cases}$$

These errors are then saved in the value vector's cells; its minimum represents the best percentage combinations for that hydrocarbon combination. It is important to recall that all these chemical and physical properties are assumed to be extensive, so the equivalent quantity of the mixture is given by the direct sum of each reagent with equal emphasis. Repeating the calculations for all the external *parfor* loop, the code returns the final data matrix. Then, the code searches its minimum (using the default command *min*) and gives back the user the correctly defined IFS (the process is summed up in table 4.10).

	percentages 1	percentages 2		percentages J-1	percentages J
generic blend	x	x		x	x
	↓ min()				
	min 1	[blend 1]		[best percentages]	
	min 2	[blend 2]		[best percentages]	
blend ↓	min i	[blend i]		[best percentages]	
	min I-1	[blend I-1]		[best percentages]	
	min I	[blend I]		[best percentages]	
	min() ↓				
	total minimum	IFS			

Table 4.10 Brief depiction of main algorithm

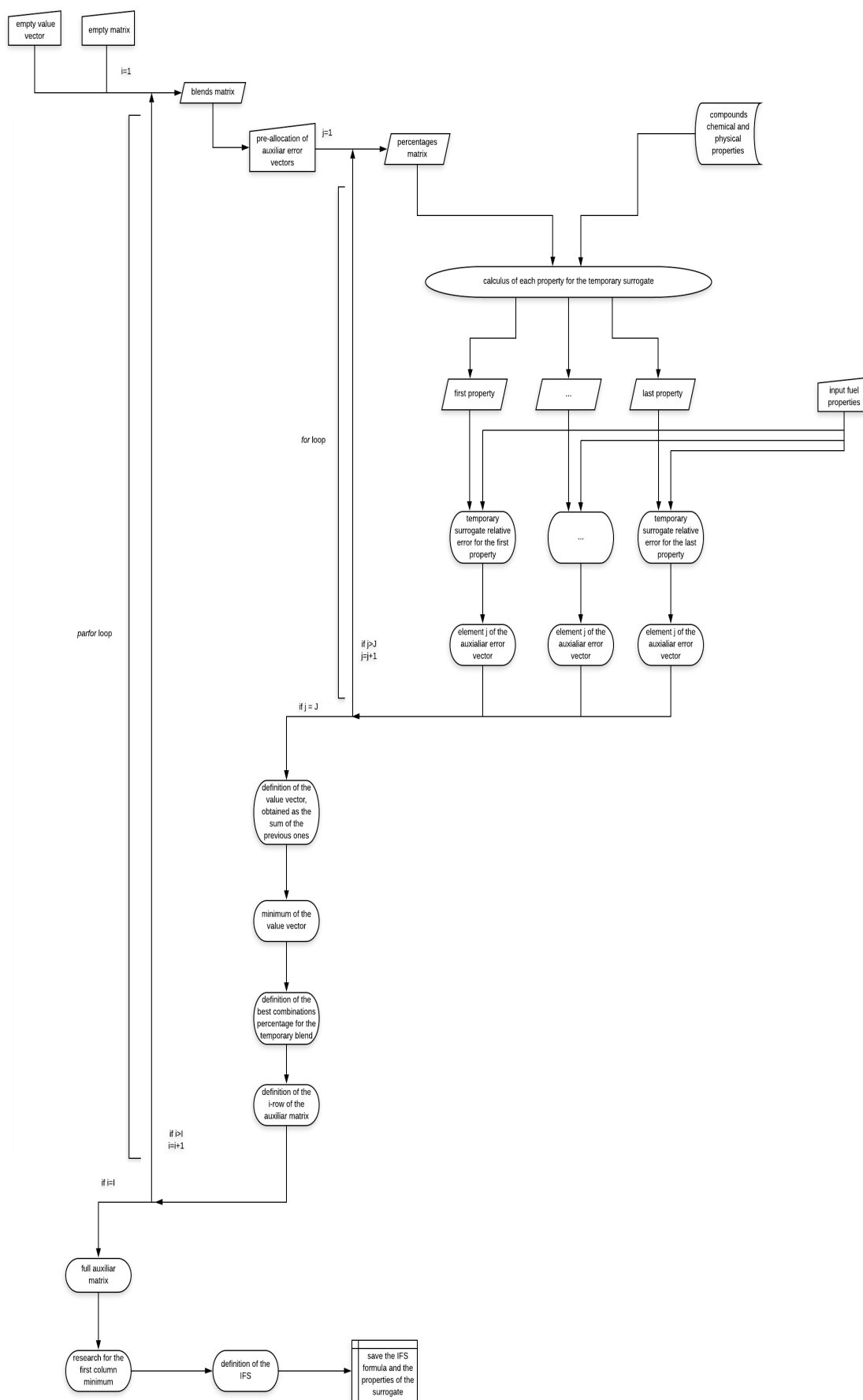


Figure 4.11 Last block of the algorithm

4.4 Output

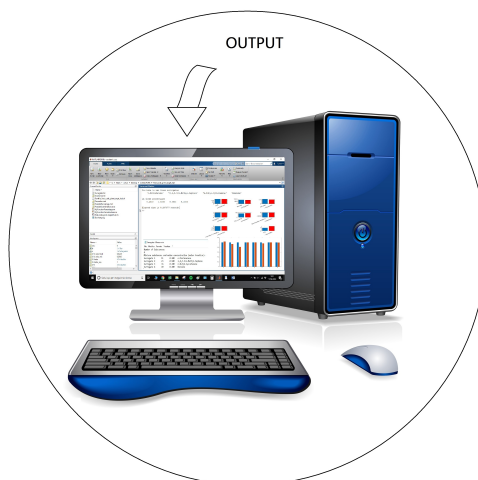


Figure 4.12 Last block of the scheme

The fourth and last block of the code is dedicated to the saving and the exhibition of the results obtained from the subsection 4.3.3. Once found the coordinates of the total minimum in the data matrix, since every index corresponds to specific blend and percentages combination, the code gives back the IFS; then, using the relative indices, it calculates and restitutes the surrogate chemical and physical properties. Each of these result is then compared to the input one:

- in figure 4.13, with the use of a bar chart, is shown the magnitude comparison between the various properties
- in figure 4.14 the normalized values are depicted thanks to another auxiliar bar chart (the properties are normalized with respect to the input ones)

In order to separate the various, an external folder is automatically generated, which is intended to contain the following output data:

#	name	extension
i	compared_magnitude	.png
ii	distribution_percentages	.png
iii	distribution_percentages_colormap	.png
iv	Hydrocarbons	.txt
v	license	.txt
vi	output_command_window	.txt
vii	PossibleCombinations	.mat
viii	PossiblePercentages	mat
ix	relative_magnitude	.png
x	Solutions	.mat
xi	spy_matrix	.png

Table 4.11 Brief sum up of the output files

4.4. OUTPUT

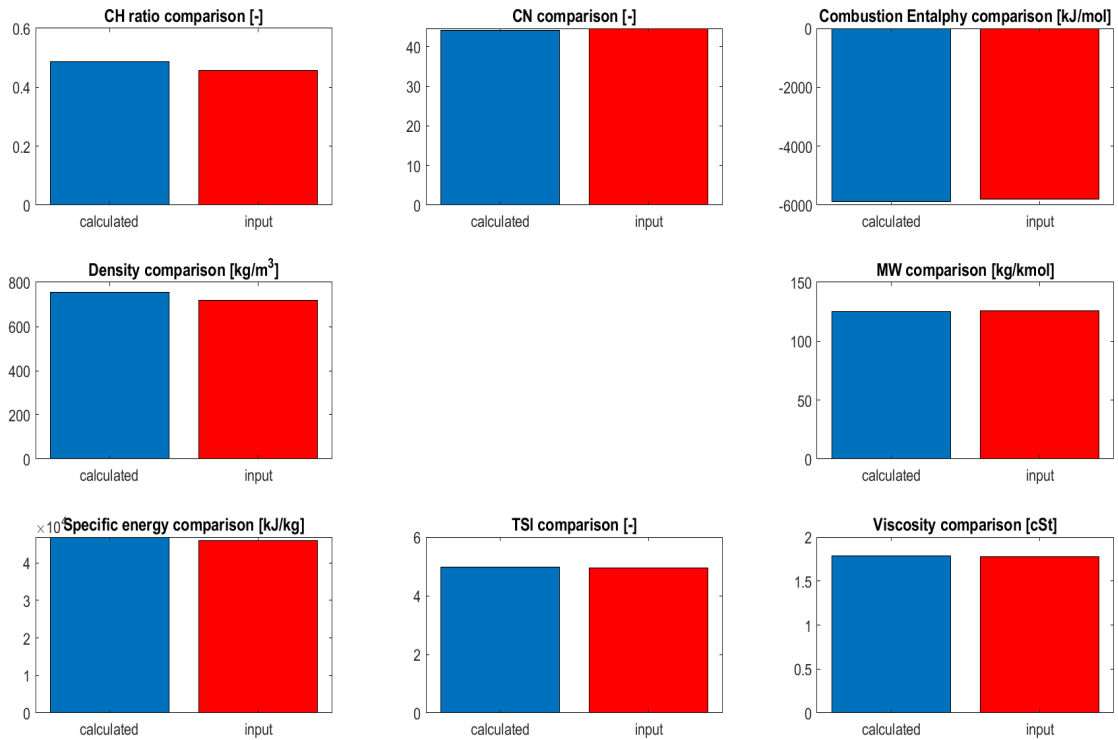


Figure 4.13 Compared magnitude of the input values and the calculated ones

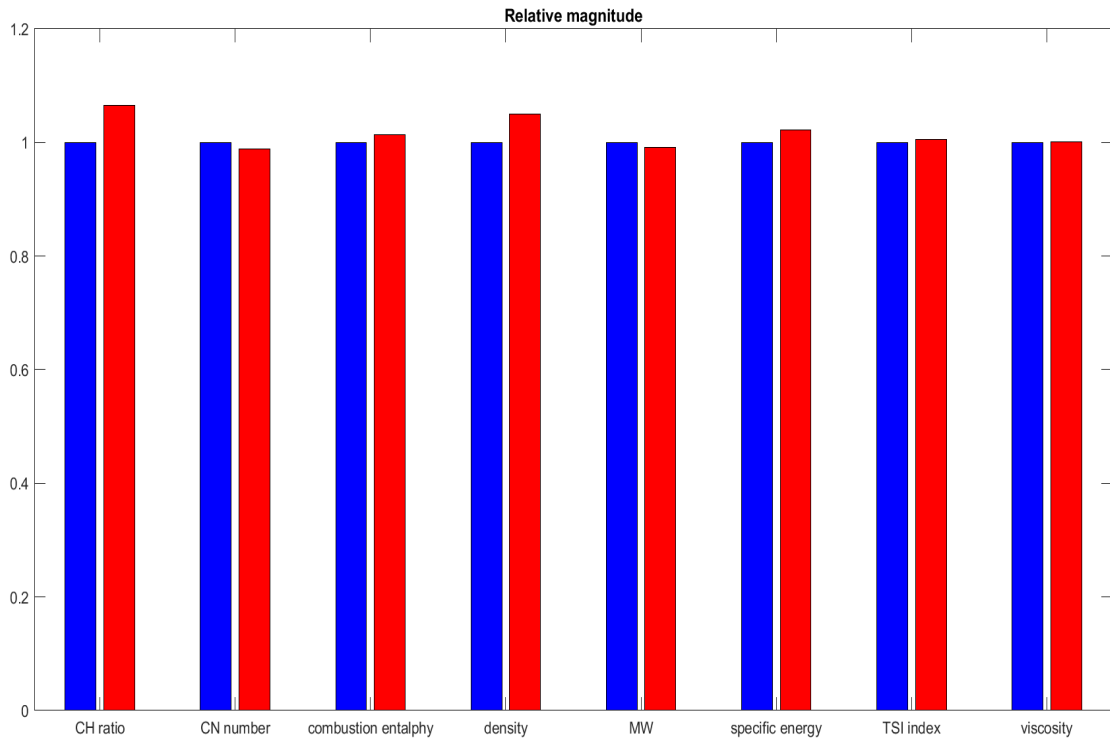


Figure 4.14 Relative magnitude of the input values and the calculated ones

4.4. OUTPUT

Anyway, the codes give two further information, whose aim is to report the problem solutions. The first one is the output on the MATLAB command window:

```
You have to use these hydrocarbons
'n-Hexane'      '2-Methyl-Nonane'
'n-Butyl-Cyclohexane'  'Benzene'
```

```
in these percentages
0.1300    0.5700    0.1500    0.1500
```

and the second one an auxiliary .txt file where, after being remembered the total number of surrogates, the results are shown in the following format:

Mixture compounds and molar fraction:

Hydrocarbon #	index in the database file	percentage	name
---------------	----------------------------	------------	------

and then a small sum up of the main properties of the two fuel:

Number of Substances: 4

Mixture substances and molar concentration (molar fraction):

Surrogate 1	02	0.130	n-Hexane
Surrogate 2	22	0.570	2-Methyl-Nonane
Surrogate 3	36	0.150	n-Butyl-Cyclohexane
Surrogate 4	40	0.150	Benzene

The input data are:

CH ratio=0.4566 CN=44.6200 combustion enthalpy=-5790.1692 density=719.5200
MW=126.1200 specific energy=45910.0000 TSI=4.9500 viscosity=1.7800

while the calculated ones are:

CH ratio=0.4863 CN=44.0857 combustion enthalpy=-5867.9523 density=755.1110
MW=125.0572 specific energy=46922.1470 TSI=4.9750 viscosity=1.7825

with a relative error of: 0.0861

(the formation enthalpy and the combustion enthalpy
are not involved in the error calculation)

Chapter 5

PSO Directly Optimized Algorithm

In addition to the previous one, in the last two months of the thesis another possible code has been developed in order to propose a valid alternative to the first algorithm, trying to overcome its huge computational weight. This code, which shows the same input operations to the first one, differs for the best percentages and blend research. Indeed, they are calculated thanks to two MATLAB functions, *fmincon* (section C.4) and *particleswarm* (section C.5), mainly developed for the direct optimization algorithms. Furthermore, in order to clarify the comparison between the codes results, the output function is kept constant. Since there is no more need of the percentages combination family (because of the different approach), the automatically created Output folder will not have some of the previous figures (fig. 4.7, 4.8 and 4.9), but it will include an additional image, which displays the objective function value against the iterations number, and a further .txt file with the *fmincon* function results. Then, the content of the folder can be summed up in the next table:

#	name	extension
i	compared_magnitude	.png
ii	Hydrocarbons	.txt
iii	iterations_function_objective	.fig
iv	license	.txt
v	output_command_window	.txt
vi	relative_magnitude	.png
vii	results_fmincon	.txt
viii	Solutions	.mat

Table 5.1 Brief sum up of the output files

It is important to remind that this family of algorithms, namely heuristics algorithms, are designed to solve a problem in a faster and more efficient manner than traditional methods by sacrificing optimality, accuracy, precision or completeness in favor of speed. Therefore, theoretically, the minimum value found for the objective found could refer to a local minimum, circumstance unfavourable for the research. However, this pessimistic option has been excluded thanks to the code's results validation through the *GlobalSearch* MATLAB function.

5.1 Particle Swarm Optimization

In computational science, Particle Swarm Optimization, abbreviated as PSO, is a computational method that optimizes a problem by iteratively trying to improve a candidate solution of the input objective function according to a given measure of quality [85]. It solves the input problem by having a population of candidate solutions, dubbed particles, and moving these particles around in the multi-dimensional search-space according to the physical formulas over the particle's position and velocity. Each particle's movement is influenced by its local best known position, but is also guided toward the best known position in the search-space, which is updated as better position and could be found by any other particle in the swarm. In short, it's like every particle adjusts its flying according to its own flying experience (personal cognition) as well as the flying experience of other particles (social cognition). This idea, after due iterations, is expected to move the swarm toward the best solutions. PSO, attributed to the researches of Kennedy, Eberhart and Shi and developed from 1995, was first intended for simulating social behaviour, as a stylized representation of the movement of a bird flock or fish school (figure 5.1 and figure 5.2).



Figure 5.1 Bird flock



Figure 5.2 Fish school

PSO could be defined as a metaheuristic population-based algorithm, since it makes few or no assumptions about the problem being optimized and can search very large spaces of candidate solutions. However, metaheuristics such as PSO do not guarantee an optimal solution is ever found. Moreover, PSO does not use the gradient of the problem being optimized, which means it does not require the optimization problem to be differentiable as is required by classic optimization methods such as gradient descent and quasi-Newton methods. In past several years, PSO has been successfully applied in many research and application areas since it is demonstrated that PSO gets better results in a faster, cheaper way compared with other methods. Compared to the Genetic Algorithm (generally abbreviated as GA, is another valid population-based algorithm), the advantages of PSO are that the first one is easier to implement and there are just few parameters to adjust. The most important reason why PSO is chosen to be implemented into the code is that with this algorithm is easy to realize calculation parallelization (see *parfor* in section C.3).

A basic variant of the PSO algorithm works by having a population of candidate solutions. These particles are moved around in the search-space according to a few simple formulas. The movements of the particles are guided by their own best known position in the search-space as well as the entire swarm's best known position. When improved positions are being discovered these will then come to guide the movements of the swarm. The process is repeated and by doing so it is hoped, but not guaranteed, that a satisfactory solution will eventually be discovered. Formally, let $f : \mathbb{R}^n \rightarrow \mathbb{R}$ be the objective function which is desired to be minimized (in case the user chose to search for the maximum of the same f function, he has to use the auxiliary function $h = -f$, where $h : \mathbb{R}^n \rightarrow \mathbb{R}$). The function takes a candidate solution as an argument in the form of a vector of real numbers, whose dimensions are linked to the dimensions of the search-space, and produces a real number as output which indicates the objective function value of the given candidate solution. The gradient of f is not known and, most importantly, not necessary. The goal is to find a solution a for which $f(a) \leq f(b) \quad \forall b \in \mathbb{R}^n$, which would mean a is the function's global minimum. All these relations can be summed up in the following system:

$$\begin{cases} \mathbf{v}_i^{t+1} = \omega_i^t \cdot \mathbf{v}_i^t + c_1 \cdot \text{rand}_1[] (\mathbf{x}_{p,i,\text{best}} - \mathbf{x}_i^t) + c_2 \cdot \text{rand}_2[] (\mathbf{x}_{g,\text{best}} - \mathbf{x}_i^t) \\ \mathbf{x}_i^{t+1} = \mathbf{x}_i^t + \mathbf{v}_i^{t+1} \cdot d_i^{t+1} \end{cases}$$

which represents, in the most general way, the required equations for the problem. The variables of the the equations are summarized in the following list:

- t : generic iteration of the algorithm. It varies from 1 to T
- i : generic particle of the swarm. It varies from 1 to I
- \mathbf{x} : vectorial position of the particle
- \mathbf{v} : vectorial velocity of the particle
- $\mathbf{x}_{p,\text{best}}$: vectorial position of each particle that gives back its minimum objective function value
- $\mathbf{x}_{g,\text{best}}$: vectorial position of the particle that show the minimum objective function value
- ω : inertial weight factor of the particle
- c_1 : cognitive parameter. It represents how much the particle trusts its own past experience (personal influence)
- c_2 : social parameter. It represents the importance the particles give to the swarm best (social influence)
- $\text{rand}_1, \text{rand}_2$: they are random numbers
- d : is a deceleration factor

The most used parameters of PSO algorithm are considered as follows:

- Inertial weight factor ω : 0.9 to 0.4
- c_1 and c_2 parameters: 2 to 2.05. In general, experience has shown that the best results have been obtained with $c_1 + c_2 = 4$
- population size (swarm size) I : 10 to 100
- maximum iterations T : 500 to 10000
- initial velocity $\simeq 10\%$ of the initial position

5.1. PARTICLE SWARM OPTIMIZATION

Referring to the previous notation, is then possible to introduce the PSO common algorithm, showing its most important features and steps:

Algorithm 5.1: PSO algorithm

- 1: Set parameters ω , c_1 , c_2 and d
 - 2: Initialize population of particles having positions \mathbf{x} and velocities \mathbf{v}
 - 3: Set iteration $t = 1$
 - 4: Calculate fitness of particles $F_i^1 = f(\mathbf{x}_i^1), \forall i$, and find the index of the best fitness value b ($b \rightarrow f(\mathbf{x}_{g,best}) \rightarrow F_b$)
 - 5: Find the best position of each particle's path $\mathbf{x}_{p,i,best}$ (that, obviously, for this first iteration will be the same starting position) and the best swarm position at the first iteration $\mathbf{x}_{g,best}$
 - 6: **for** $t = 2:T$
 - 7: Update the velocities and the positions for each particle according the vectorial formulas shown in the previous page ($\rightarrow \mathbf{v}_i^t$ and \mathbf{x}_i^t)
 - 8: Evaluate fitness $F_i^t = f(\mathbf{x}_i^t), \forall i$
 - 9: If the conditions are met, update the required data:
 - if** $F_i^t < F_i^{t-1}$
 - $\mathbf{x}_{p,i,best} = \mathbf{x}_i^t$
 - end**
 - if** $F_i^t < F_b$
 - $\mathbf{x}_{g,best} = \mathbf{x}_i^t$
 - $F_b = f(\mathbf{x}_{g,best})$
 - end**
 - 10: **end**
 - 11: Show the final $\mathbf{x}_{g,best}$, which is assumed to be the solution of the problem
-

The algorithm can be further shown with its relative block diagram:

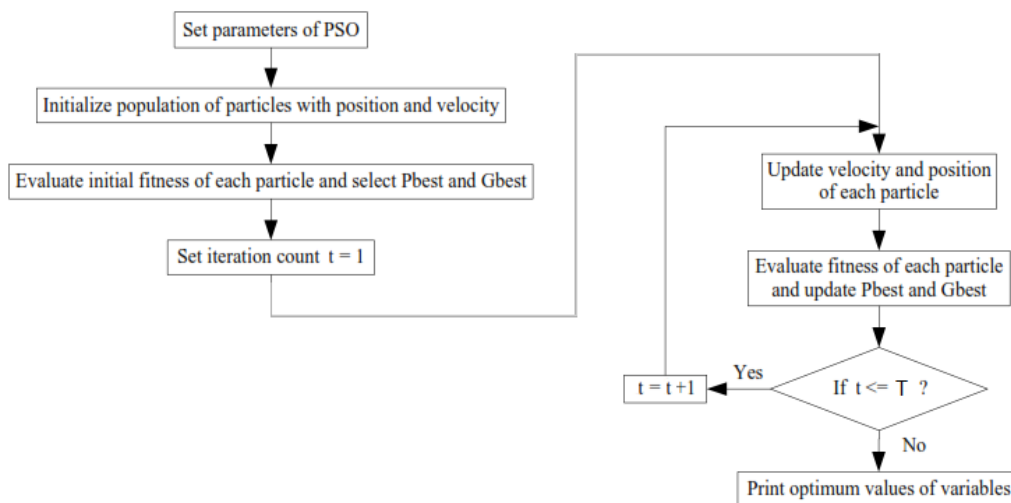


Figure 5.3 Basic PSO block diagram

5.1. PARTICLE SWARM OPTIMIZATION

In the end of this PSO introduction, it's important to focus on the parameter's effect on the computational iter to the solution:

- ω : while large inertia weight facilitates global exploration, small one facilitates local exploration. Generally ω is selected constant or smoothly decreasing over the run
- c_1, c_2 : c_1 parameter represents the importance given to the personal best to the research of the objective function's minimum; c_2 represents the importance given to the whole swarm best. Pluriannual experience showed that the best results are obtained when their sum is $\simeq 4$, but there is no further reason than mere empiricism
- \mathbf{v} : one of the most important for the convergence of the algorithm is the maximum velocity reached by a particle. In fact, it determines the fineness with which the space-search regions are fathomed:
 - if too high, the particle can fly past optimal solutions. The algorithm may become unstable
 - if too low, the particle can get stuck in local minima. The algorithm may become too slow.

These different approaches are made clear in the following image, which displays the region spaced by the velocity at each iteration. It is then evident their undeniable importance for the algorithm's convergence.

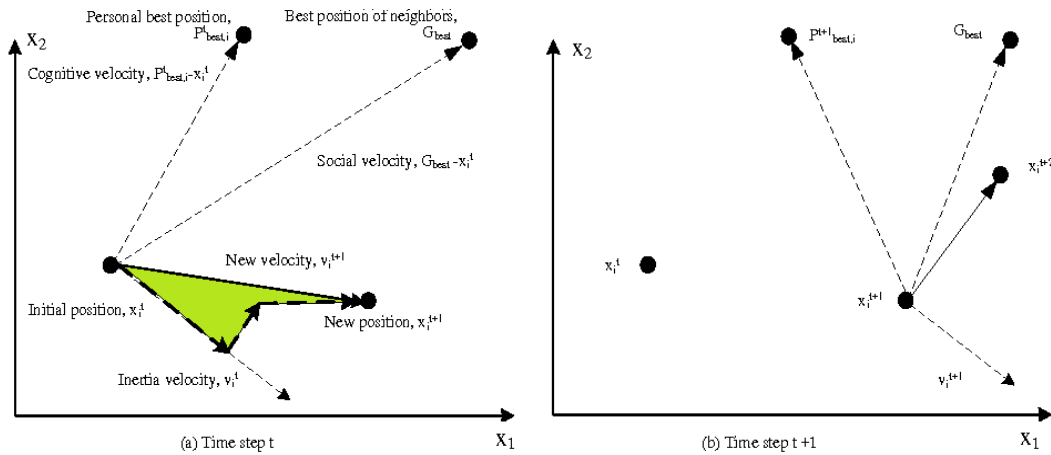


Figure 5.4 Spaced region by particle's velocity

Despite its easy implementation, it has been proven that PSO need some modification to guarantee to find a local optimum. This means that determining convergence capabilities of different PSO algorithms and parameters therefore still depends on empirical results. Many different variants have been proposed to overcome this problem. For example, there are different ways to initialize the particles and velocities (e.g. start with zero velocities instead), how to dampen the velocity, updating $\mathbf{x}_{p,i,best}$ and $\mathbf{x}_{g,best}$ after the entire swarm has been updated, etc. These possibilities, which have been widely debated and studied, have begun to give back promising results for the researches.

5.2 Software

Being most of the auxiliar functions used by the optimizer equal to the ones exploited in the 4.3 section, their treatise is abandoned in order to leave more space to the main parts' ones. The main module, after activating the parallel computing toolbox, receives in input the *GS* function developed in the homonym module, which, given a certain hydrocarbons blend and using the default MATLAB function *fmincon*, gives back the blend's percentages which minimize the relative error. The error, whose formula is the same as in subsection 4.3.3, refers to the input properties. Entering slightly more into the details, the *GS* function, after a small handling of the input vector, defines the percentages' physical constraints. They are reported in auxiliar vectors and matrices, which are intended to be used by the *fmincon* operator (see section C.4). The output error of the function is then refreshed for three times. This attention, associated with new random starting coordinates x_0 , allows the user to be sure that the found value is the global minimum and not a local one. With these operations, the code finds the optimal blend for the given fuel; thanks to a second *GS* function call, the best combination of percentages is provided. The results are then processed with the *Output* function explained above (see section 4.4). In the end, the additional figure of the iteration-objective function curve is moved to the Output folder. It makes aware the users about the error evolution in the particle swarm operations and could be useful to understand the convergence behaviour of the model. A possible example of this curve is shown in the next figure:

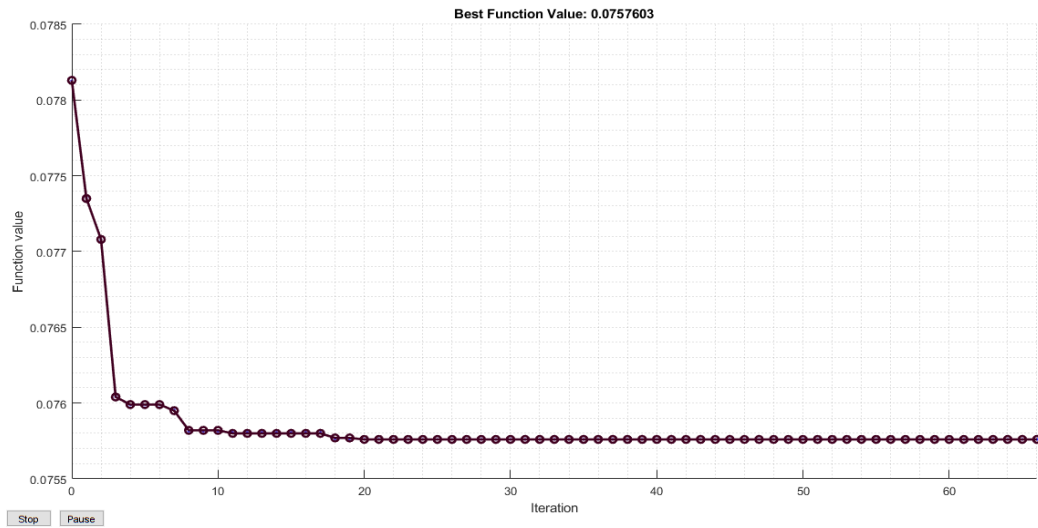


Figure 5.5 Example of iteration-objective function curve

Referring to the previous image, users could wrongly think to limit the iterations because of the simil-asymptote reached after 15 iterations; this idea could reveal itself to be dangerous for the model convergence, since the particle swarm optimization operates in a stochastic process and a premature interruption could lead the code to neglect a better solution.

Chapter 6

Results

6.1 Saibov's Thesis Validation

Before getting to the heart of this thesis, it is important to verify the mathematical tools used in the work, checking the validity of the model. The surrogates taken as reference are the ones proposed by the Ph. D. student Emin Saibov for his final dissertation in 2012 [86]. In this work, in fact, the student developed three different surrogates, named, respectively, SPK-1, SPK-2 and SPK full, which were thought to mimic the blend 3 fuel, a kerosene made up of three commercial solvents according the following percentages: 2% of Shellsol T, 32% of Shellsol DCS and 66% of Bintulu. In order to overcome the complicated composition of the fuel (which counts more than a hundred compounds), the surrogates are defined to be composed by only few components:

SPK-1		
Name	Formula	%
n-decane	$n-C_{10}H_{22}$	36
iso-octane	$i-C_8H_{18}$	49
n-propyl-cyclohexane	$cy-C_9H_{18}$	15

SPK-2		
Name	Formula	%
n-decane	$n-C_{10}H_{22}$	36
iso-octane	$i-C_8H_{18}$	17
2- methyl-decane	$i-C_{11}H_{24}$	32
n-propyl-cyclohexane	$cy-C_9H_{18}$	15

SPK full		
Name	Formula	%
n-decane	$n-C_{10}H_{22}$	36
2,7-di-methyl-octane	$i-C_{10}H_{22}$	17
2- methyl-decane	$i-C_{11}H_{24}$	32
n-propyl-cyclohexane	$cy-C_9H_{18}$	15

Table 6.1 SPK composition

Aiming to validate these surrogates' properties, the numerical models developed in this thesis are intended to work with the same database, same input percentages and same compounds. Theoretically, the obtained results should equal the reference one, admitting eventual minima rounding errors, function of internal operations between the input properties.

6.1. SAIBOV'S THESIS VALIDATION

Comparing the results of the SPK surrogates to the obtained ones, the deriving features are shown in the following tables:

SPK full				
INPUT	CALCULATED	lin. err.	quad. err.	
CH ratio [-]	0.46147	0.46823	1.46587	0.02149
Cetane Number [-]	45.21	43.633	3.48772	0.12164
Combustion Entalphy $\left[\frac{kJ}{mol}\right]$	-6894.63	-6861.00	0.48790	0.00238
Density $\left[\frac{kg}{m^3}\right]$	738.99	738.06	0.12525	0.00016
Molecular Weight $\left[\frac{kg}{kmol}\right]$	144.36	144.36	0.00028	0.00000
Specific Energy $\left[\frac{kJ}{kg}\right]$	47760	47526.85	0.48817	0.00238
TSI index [-]	4.28	4.300	0.46729	0.00218
Viscosity [cSt]	2.7	2.725	0.92593	0.00857

Table 6.2 Check SPK full

SPK-1				
INPUT	CALCULATED	lin. err.	quad. err.	
CH ratio [-]	0.45662	0.45628	0.07562	0.00006
Cetane Number [-]	44.62	43.865	1.69130	0.02860
Combustion Entalphy $\left[\frac{kJ}{mol}\right]$	-5790.17	-6003.25	3.68006	0.13543
Density $\left[\frac{kg}{m^3}\right]$	719.52	719.44	0.01106	0.00000
Molecular Weight $\left[\frac{kg}{kmol}\right]$	126.12	126.13	0.00753	0.00000
Specific Energy $\left[\frac{kJ}{kg}\right]$	45910	47595.93	3.67225	0.13485
TSI index [-]	4.95	4.937	0.26263	0.00069
Viscosity [cSt]	1.78	1.808	1.57782	0.02490

Table 6.3 Check SPK-1

SPK-2				
INPUT	CALCULATED	lin. err.	quad. err.	
CH ratio [-]	0.46083	0.46720	1.38240	0.01911
Cetane Number [-]	18.69	47.580	154.572	238.926
Combustion Entalphy $\left[\frac{kJ}{mol}\right]$	-6668.18	-6637.32	0.46271	0.00214
Density $\left[\frac{kg}{m^3}\right]$	730.53	730.45	0.01117	0.00000
Molecular Weight $\left[\frac{kg}{kmol}\right]$	139.56	139.59	0.02286	0.00001
Specific Energy $\left[\frac{kJ}{kg}\right]$	47780	47548.05	0.48545	0.00236
TSI index [-]	4.53	4.521	0.19868	0.00039
Viscosity [cSt]	2.60	2.589	0.41362	0.00171

Table 6.4 Check SPK-2

Looking at the previous tables, it can be said that, in general, the proposed model shows good agreement (error < 1.5-2%) with the reference one, except for few properties. Then, it is important to understand the reasons of these inconsistencies, which are all limited to four derived quantities (CH ratio, cetane number, combustion enthalpy and specific energy). Starting from the SPK full surrogate, after a brief control, a transcription error in the CN calculus in Saibov's work has been revealed, since he reported the n-undecane's CN number instead of the n-decane's one. A minimum discrepancy has been also found in the CH ratio; it should be due to the fact that the reported number is the inverse of the reference one and the error could have propagated. A similar perspective can be applied to the SPK-2 surrogate, where the same errors are present. While the CH ratio shows a similar magnitude to the first case (symptom of equivalent behaviour), the calculated CN is extremely large, creating a miscalculation of $\simeq 154\%$. After many attempts, a possible motivation of this trouble has been explained as a slip-up from Saibov, since he could have missed a contribution in the property's evaluation. This possibility has been further validated by the comparison with the typical range for jet fuel, which is provided in 1.7 and shows a working range from 40 to $\simeq 55$. Regarding the SPK-2 surrogate, in Saibov's thesis the cetane number has been calculated according to weird components, absolutely not corresponding to the input ones. In fact, while in the input formula he used three compounds (one normal, one iso and one cycloparaffine), in the CN calculus he added one iso-paraffines, without explaining the reasons of this choice (see table 6.5). Furthermore, other motivations of discrepancies have to be attribute to the specific energy and, since it is calculated directly from the previous property, to the combustion enthalpy. Besides having reported a wrong value of the combustion enthalpy for the n-propyl-cyclohexane (instead of $\Delta_c H^0 = -5719.06 \frac{kJ}{mol}$, he set $\Delta_c H^0 = -5919.06 \frac{kJ}{mol}$), in the evaluation many other calculation error are present. On the other hand, the properties not yet discussed show nearly the same values that the input ones. Concluding this validation section, it can be summed up that the numerical model developed in this thesis, showing good agreement with the reference data, can be thought to be relatively accurate and, generally, valid for eventual further researches. Nonetheless, many doubts about the goodness of the numerical model chapter in the Saibov's thesis still remain. A possible motivation of its sloppiness could be due to the not-centrality in the dissertation of this specific chapter or, more likely, to a physiological lack of attention on performing repetitive calculations.

Molecular lumps	N-paraffins			I-paraffins			Naphthenes		
	v_i	β_i	CN_i	v_i	β_i	CN_i	v_i	β_i	CN_i
SPK full									
C_9	-	-	-	-	-	-	15	0.0727	14
C_{10}	-	-	-	17	7.4	40	-	-	-
C_{11}	36	0.52	84.7	32	7.4	45	-	-	-
SPK-2									
C_8	-	-	-	49	7.4	15.5	-	-	-
C_{10}	36	0.52	80.9	-	-	-	15	0.0727	14

Table 6.5 CN calculation table as shown in [86]

6.2 Saibov's Thesis Continuation

This work of thesis has been initially developed aiming to continue the work that the Ph. D. student Emin Saibov made in 2012 for his final dissertation at the Institute of Combustion Technology for Aerospace Engineering in Stuttgart (Institut für Verbrennungstechnik der Luft- und Raumfahrt). Recalling the percentages shown in the previous section, it's evident, since they do not respect the average percentages shown in section 4.1, that they are supposed not to be adequate for actual fuels simulation and then that it's necessary to extend the number of the input's hydrocarbons, divided properly according their chemical family. The chosen division is given by a single n-paraffin, two i-paraffines, 2 cyclo-paraffines and one aromatic hydrocarbon. In order to validate the new surrogates against the previous ones, the comparison of section 4.3 is conducted, trying to minimize the margin of relative error.

6.2.1 Premise

Before showing the results obtained thanks to the developed codes, it's important to note the high error of uncertainty associate with the reference percentages. In this context, the error propagation theory set serious limitations on their validity. In fact, being evident the low level of detail of these numbers, restricted to the second digit after the decimal place, each compound carries around its personal error, evaluable through the relation:

$$\text{given the number } x, \text{ where } x = \bar{x} + \partial x, \text{ the error of uncertainty is: } \frac{\partial x}{\bar{x}}$$

where: • \bar{x} is the best estimated value • ∂x is the number's uncertainty

In case of a multi-variables function, the total error is given by the linear sum of the uncertainties (if the main function had inside additions or subtractions) or of the uncertainty's error (if are present multiplications or divisions). With these relations, it is then possible to calculate the error that afflicts each surrogate. However, beacuse of the lack of information about the validity of the database, in these calculations it is assumed that they are error-free, being aware about the partial validity of the results. In the end, the conclusive table of the uncertainty errors is reported, showing the huge levels of distrust of the input data:

SPK-1		SPK-2		SPK full	
Formula	$\frac{\partial x}{\bar{x}}$	Formula	$\frac{\partial x}{\bar{x}}$	Formula	$\frac{\partial x}{\bar{x}}$
n-C ₁₀ H ₂₂	2.78	n-C ₁₀ H ₂₂	2.78	n-C ₁₀ H ₂₂	2.78
i-C ₈ H ₁₈	2.04	i-C ₈ H ₁₈	5.88	i-C ₁₀ H ₂₂	5.88
cy-C ₉ H ₁₈	6.67	i-C ₁₁ H ₂₄	3.13	i-C ₁₁ H ₂₄	3.13
		cy-C ₉ H ₁₈	6.67	cy-C ₉ H ₁₈	6.67
Sum	11.49	Sum	18.46	Sum	18.46

Table 6.6 Uncertainty errors

6.3 Results

Chapter 7

Further Developments

Bibliography

- [1] American Council International
https://aci.aero/Media/9d12ed0c-e36b-48da-9b9f-8ec4640d5821/iM0Zyg/Statistics%20and%20Data/Infographics/Infographic_ACI_World_Airport_Traffic_Forecasts%202017%E2%80%932040.pdf.
- [2] Boeing
https://public.tableau.com/profile/theboeingcompany#!/vizhome/CMO_1/GlobalOverview
- [3] Airbus
<https://www.airbus.com/aircraft/market/global-market-forecast.html>
- [4] Embraer
https://www.embraermarketoutlook2018.com/wp-content/uploads/2018/07/Embraer_MarketOutlookBook_2018_DownloadablePDF_A4.pdf
- [5] Bombardier
https://businessaircraft.bombardier.com/sites/default/files/2018-03/market_forecast_en.pdf
- [6] S.A. de Jong
GREEN HORIZONS. 1991
- [7] J. Hrbek
"Aviation Biofuels through Biomass Gasification". 2016
- [8] Pratt & Whitney
https://www.faa.gov/about/office_org/headquarters_offices/apl/research/aircraft_technology/clean/reports/media/PW_Amyris_Final.pdf
- [9] J. S. Heyne, M. Colket, M. Gupta, A. Jardines, J. Moder, J. T. Edwards, W. M. Roquemore, C. Li, M. Rumizen.
"Year 2 of the National Jet Fuels Combustion Program: Moving Towards a Streamlined Alternative Jet Fuels Certification Process". January 2017
- [10] N. A. Slavinskaya, A. Zizin, M. Aigner.
"On Surrogate Fuel Formulation". June 2009
- [11] J. I. Hileman, R. W. Stratton
"Alternative jet fuel feasibility". 2014

- [12] F. Cheng, C.E. Brewer
"Producing jet fuel from biomass lignin: potential pathways to alkyl-benzenes and cycloalkanes". 2017
- [13] J.D. Kinder, T. Rahmes
"Evolution of Bio-Derived synthetic paraffinic kerosenes (Bio-SPK)". 2009
- [14] E. Dybing, P.E. Schwarze, P. Nafstad, K. Victorin, T.M. Penning
"Polycyclic aromatic hydrocarbons in ambient air and cancer". 2015
- [15] R.C. Ried, J.M. Prausnitz, T.K. Sherwood.
"The Properties of Gases and Liquids". 1997
- [16] S.M. Zhorov.
"Termodinamical calculation of Petrochemical Processes". 1985
- [17] H.F. Colcatee, D.M. Manos.
"Effects of Molecular Structure on Incipient Soot Formation". 1983
- [18] C.L. Yaw
"Yaw's Handbook of thermodynamic and physical properties of chemical Compounds". 2003
- [19] P.S. Morris
"Estimation of liquid viscosity from structure". 1964
- [20] T. Edwards, L.Q. Maurice
"Surrogate Mixtures to Represent Complex Aviation and Rocket Fuels". 2001
- [21] C.R. Martel
 ADA186752. November 1987
- [22] C. Moses
"Properties of Russian Jet Fuels". November 2011
- [23] ChevronTexaco
 AVIATION FUELS. 2005
- [24] E.G. Eddings, S. Yan, W. Ciro, A.F. Sarofim
"Formulation of a Surrogate for The Simulation of Jet Fuel Pool Fires". 2005
- [25] K. Mati, A. Ristori, S. Gail, G. Pengolan, P. Dagaut
"The Oxidation of a Diesel fuel at 1-10 atm: Experimetal study in a JSR and detailed chemical kinetic modeling". 2007
- [26] P. Gokulakrishnan, G. Gaines, M.S. Klassen, R.J. Roby, J. Currano
"Experimental and Kinetic Modeling of Kerosene-type Fuels at Gas Turbine Operating Conditions". 2007
- [27] C.K. Westbrook, W.J. Pitz, O. Herbinet, H.J. Curran, E.J. Silke
"A Detailed Chemical Kinetic Reaction Mechanism for n-Alkane Hydrocarbons from n-Octane to n-Hexadecane". 2008

- [28] S.S. Vasu, D.F. Davidson, R.K. Hanson
"Jet Fuel Ignition Delay Times: Shock Tube Experiments over Wide Conditions and Surrogate Model Predictions". 2008
- [29] L.J. Spadaccini, J.A. TeVelde
"Autoignition Characteristics of Aircraft-type Fuels". 1980
- [30] A.J. Dean, O.G. Penyazkov, K.L. Sevruck, B. Varatharajan
"Autoignition of Surrogate Fuels at Elevated Temperatures and Pressures". 2007
- [31] F.L. Dryer, H. Xu, Z. Yang, M. Chaos
"Surrogate Jet Fuel Mixture Formulation and Development of Experimental Databases". 2008
- [32] C.V. Honnet, K. Seshadri, U. Niemann, N. Peters
"A surrogate fuel for kerosene". 2009
- [33] G. Bikas, N. Peters
"Combustion and Flame". 2001
- [34] U. Pfahl, K. Fiewegger, G. Adomeit
"Shock Tube Investigation of Ignition Delay Times of Multicomponent Fuel/Air-Mixtures under Engine Relevant Conditions". 1996
- [35] C.V. Naik, K.V. Puduppakkam, A. Modak, E. Meeks, Y.L. Wang, Q. Feng, T.T. Tsotsis
"Detailed chemical kinetic mechanism for surrogates of alternative jet fuels". 2010
- [36] D.F. Davidson, M.A. Oehlschlaeger, J.T. Herbon, R.K. Hanson
 PROC. COMBUST. 2002
- [37] D.J. Vermeer, J.W. Meyer, A.K. Oppenheim COMBUST. FLAME 1972
- [38] U. Pfahl, K. Fieweger, G. Adomeit PROC. COMBUST. INST. 1996
- [39] V.P. Zhukov, V.A. Sechenov, A.Y. Starikovskii COMBUST. FLAME 2008
- [40] S.S. Vasu, D.F. Davidson, Z. Hong, V. Vasudevan, R.K. Hanson
 PROC. COMBUST. INST. 2009
- [41] A. Zhao, J. Li, A. Kazakov, F.L. Dryer
"Burning Velocities and High Temperature Skeletal Kinetic Model for n-Decane". 2005
- [42] R.P. Lindstedt, L.Q. Maurice
"Detailed Chemical Kinetic Model for Aviation Fuels". 2000
- [43] C. Doute, J.L. Delfau, R. Akrich, C. Vovelle
"Chemical Structure of Atmospheric Pressure Premixed n-Decane and Kerosene Flames". 1995

- [44] S.K. Zeppieri, S.D. Klotz, F.L. Dryer
"Modeling Concepts for Larger Carbon Number Alkanes: A Partially Reduced Skeletal Mechanism for n-Decane Oxidation and Pyrolysis". 2000
- [45] G. Bikas, N. Peters
"Kinetic Modelling of n-Decane Combustion and Autoignition". 2001
- [46] S. Dooley, S.H. Won, M. Chaos, J. Heyne, Y. Ju, F.L. Dryer, K. Kumar, C.J. Sung, H. Wang, M.A. Oehlschlaeger, R.J. Santoro
"A Jet Fuel Surrogate Formulated by Real Fuel Properties". 2010
- [47] S. Dooley, S.H. Won, J. Heyne, T.I. Farouk, Y. Ju, F.L. Dryer, K. Kumar, X. Xin Hui, C.J. Sung, H. Wang, M.A. Oehlschlaeger, V. Iyer, S. Iyer, T.A. Litzinger, R.J. Santoro, T. Malewicki, K. Brezinsky
"The experimental evaluation of a methodology for surrogate fuel formulation to emulate gas phase combustion kinetic phenomena". 2012
- [48] S. Dooley, S.H. Won, M. Chaos, J. Heyne, Y. Ju, F.L. Dryer, K. Kumar, C.Y. Sung, H. Wang, M.A. Oehlschlaeger, R.J. Santoro, T.A. Litzinger
"A Jet Fuel Surrogate Formulated By Real Fuel Properties". 2010
- [49] M.L. Huber, E.W. Lemmon, T.J. Bruno
"Energy Fuels". 2010
- [50] R. Lemaire, A. Faccinetto, E. Therssen, M. Ziskind, C. Focsa, P. Desgroux
"Experimental comparison of soot formation in turbulent flames of Diesel and surrogate Diesel fuels". 2009
- [51] W. Hentschel, K.P. Schindler, O. Haahtela
"European Diesel Research IDEA - Experimental Results from DI Diesel Engine Investigations". 1994
- [52] M. Colket, T. Edwards, S. Williams, N.P. Cernansky, D.L. Miller, F.N. Egolfopoulos, F.L. Dryer, J. Bellan, P. Lindstedt, K. Seshadri, H. Pitsch, A. Sarofim, M. Smooke, W. Tsang
"Identification of Target Validation Data for Development of Surrogate Jet Fuels". 2008
- [53] D.B. Olson, J.C. Pickens, R.J. Gill
"The effects of molecular structure on soot formation II. Diffusion flames". 1985
- [54] Y. Yang, A.L. Boehman, R.J. Santoro
"A study of jet fuel sooting tendency using the threshold sooting index (TSI) model". 2007
- [55] S. Kook, L.M. Pickett
"Combustion and Soot Processes of Conventional and Surrogate Jet Fuels at High-Temperature and High-Pressure Conditions". 2009
- [56] R.H. Natelson, M.S. Kurman, N.P. Cernansky, D.L. Miller
"Experimental investigation of surrogates for jet and diesel fuels". 2008

- [57] U. Steil, M. Braun-Unkhoff, M. Aigner
"An experimental and modeling study on the auto ignition of kerosene and surrogate fuel mixture". 2009
- [58] K.J. Myong, H. Suzuki, J. Senda, H. Fujimoto
"Spray inner structure of evaporating multi-component fuel". 2008
- [59] J.G. Speight *"Handbook of petroleum analysis"*. 2001
- [60] D.L. Katz, A. Firoozabadi PREDICTING PHASE BEHAVIOR OF CONDENSATE/CRUDE OIL SYSTEMS USING METHANE INTERACTION COEFFICIENTS. Journal of Petroleum Technology 1978
- [61] K.M. Watson IND. ENG. CHEM. 1931
- [62] Y. Ogata, M. Tsuchida IND. ENG. CHEM. 1931
- [63] G. R. Somayajulu, S. R. Palit J. CHEM. SOC. 1957
- [64] L.H. Thomas
"The Dependence of the viscosities of liquids on reduced temperature, and a relation of viscosity, density, and chemical constitution". 1946
- [65] J. Kerres
"Introduction to Chemical Reaction Engineering for WASTE-Engineers". 2009-2010
- [66] U. Niekem *"Chemische Reaktionstechnik 1"*. 2006-2007
- [67] E.J. Prosen, F.D. Rossini
"Heats of formation, hydrogenation, and combustion of the monoolefin hydrocarbons through the hexenes, and of the higher i-alkanes, in the gaseous state at 25° C". 1946
- [68] M. Ribacour, R. Minetti, L.R. Sochet, H.J.R Curran, W.J. Pitz, C.K. Westbrook
"Ignition of Isomers of Pentane: An Experimental and Kinetic Modeling Study". 2000
- [69] N. Ladommatos, J. Goacher
"Equations for predicting the Cetane Number of Diesel Fuels from their Physical Properties". 1995
- [70] W. F. Northrop, P. V. Madathil, S. V. Bohac, D. N. Assanis
"Condensational growth of particulate matter from partially premixed low temperature combustion of biodiesel in a compression ignition engine". 2011
- [71] S. Braun, L. G. Appel, M. Schmal
"The pollution from diesel engines - the particulate matter current experiences and future needs". 2004
- [72] E. W. De Menezes, R. Cataluña
"Sampling of particulate matter and of the volatile organic fraction of emissions from a diesel cycle engine without the use of dilution tunnel". 2008

- [73] G.A.S. Schulz, S. Tamborim, G. Cardoso, T. Santos, E. Lissner, R. Cataluña
"Carbon oxidation generated in diesel engines using iron-doped fuel". 2012
- [74] K. Owen, T. Coley AUTOMOTIVE FUELS REFERENCE BOOK. 1990
- [75] R. Cataluña, R. da Silva
"Effect of Cetane Number on Specific Fuel Consumption and Particulate Matter and Unburned Hydrocarbon Emissions from Diesel Engines". 2012
- [76] P. Ghosh, S.B. Jaffe
"Detailed Composition-Based Model for Predicting the Cetane Number of Diesel Fuels". 2006
- [77] V. Iyer, S. Dooley, S. Iyer, F.L. Dryer, T.A. Litzinger, C.J. Mordaunt, R.J. Santoro
"Emulating the Sooting Propensity of JP-8 with Surrogate Fuels from Solvent Mixtures". 2009
- [78] J.C. Street, A. Thomas *"Carbon Formation in Premixed Flames"*. 1955
- [79] D.B. Olson, J.C. Pickens, R.J. Gill
"The Effects of Molecular Structure on Soot Formation II. Diffusion Flames". 1985
- [80] Y. Yang, A.L. Boehman, R.J. Santoro
"A study of jet fuel sooting tendency using the Threshold Sooting Index (TSI) model". 2007
- [81] R. Watson, C. Ness, N. Morgan, M. Kraft
"An Improved Methodology for Determining Threshold Sooting Indices from Smoke Point Lamps". 2011
- [82] Y. Lei, L. Guangqian, H. Guijin, G. Yongsheng, X. Li, F. Wenjun
"Impacts of hydrogen to carbon ratio (H/C) on fundamental properties and supercritical cracking performance of hydrocarbon fuels". 2015
- [83] M.J. Murphy, J.D. Taylor, R.L. McCormick
"Compendium of Experimental Cetane Number Data". 2004
- [84] L.L.P. Van Stee, U.A.T. Brinkman, H. Bagheri
"Gas chromatography with atomic emission detection: a powerful technique". 2002
- [85] A. Pinto, H. Alves, I. Domingues, L. Rocha, S. Cruz
"The Particle Swarm Optimization Algorithm". 2010-2011
- [86] E. Saibov
"In-Depth Characterization of Synthetic GTL Jet Fuel Combustion Performance". April 2012

Appendix A

Physics of Aircraft Engine

The primary function of a fuel is to provide a source of energy to propel the aircraft. The turbine engine converts the chemical energy stored in the fuel into mechanical energy, providing the thrust that powers the flight. More deeply, the chemical energy in the fuel is released by combustion, which is a rapid reaction of fuel with oxygen at high temperature. The energy released during this reaction is called the heat of combustion and it could be represented by two different parameters, higher heating value (HHV) and lower heating value (LHV). LHV has its origin in HHV, after subtraction of the enthalpy of vaporization. After being heated and taking advantage of the turbine pressure drop, air flow is then speed up and it gains mechanical energy (figure A.1).

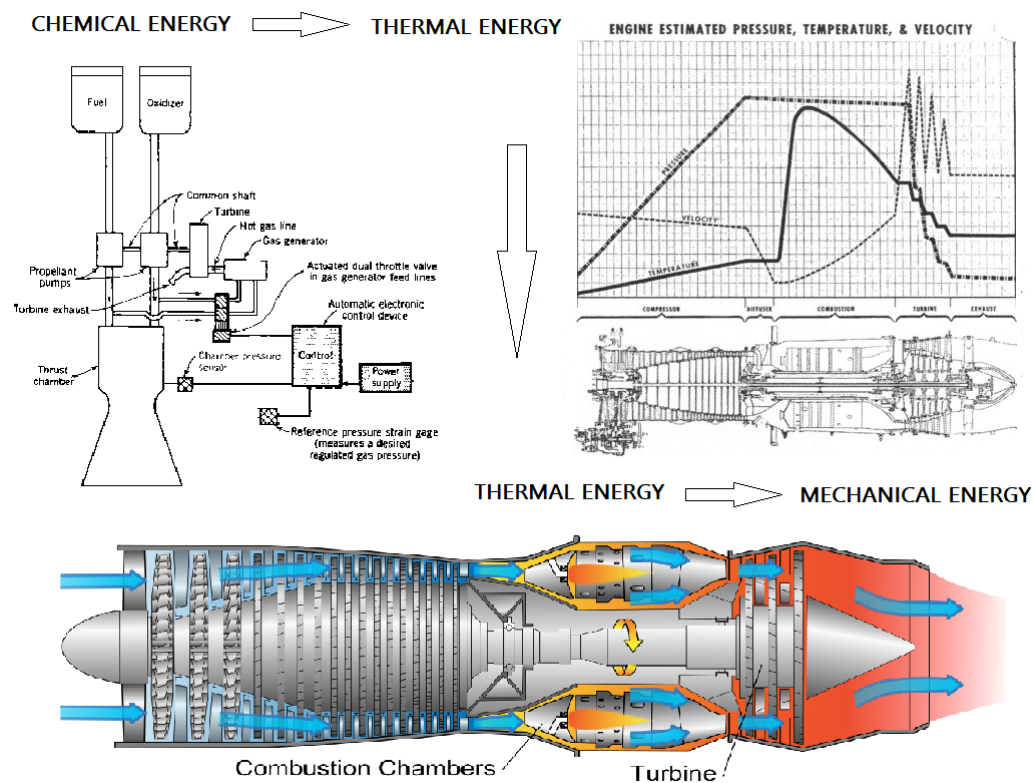


Figure A.1 Fuel properties evolution

The physics of the whole process can be explained thanks to the fundamental equations of continuum mechanics, which are based on the conservation laws. They can be summed up in:

- mass conservation
- momentum conservation (linked to Newton's second law)
- energy conservation (linked to the first law of thermodynamics)
- species transport conservation

The fundamental equations may be obtained by using the finite volume approach, where the fluid flow is divided into a limited number of control volumes and a mathematical description is developed for the finite control volume. The fluid is regarded as a continuum, where properties such as density, pressure, velocity, etc. are defined as averages over fluid elements, neglecting the behavior of individual molecules. In continuum mechanics, conservation laws are fundamentally derived in integral form, taking into consideration the total amount of some property within the control volume. The rate of change of this total amount is equal to the net rate which the property flows across the bounding surface of the control volume, defined "flux", plus the net rate of production (+) or consumption (-) within the control volume, known as "source" or "sink" (in the following lines the quotations marks will be omitted):

$$\{\text{Property time rate of change}\}_V = \{\text{Property net flux}\}_S + \{\text{Source/Sink}\}_V$$

$$\hookrightarrow \iiint_V \frac{\partial \Phi}{\partial t} dV = - \iint_S \Phi (\mathbf{q} \cdot \mathbf{n}) dS + \sum_i Q_i$$

Starting from the integral form, it is possible to obtain the equations in the derivative form, which are much more used because of their easier manipulation. The treatise of the equation starts with the introduction of the control volume, shown in fig. A.2. The bounding surface are assumed to be perpendicular to the incumbent flow (in a general case, the control volume could have any shape), so the respective positive normals are parallel to the flow velocity components and outgoing from the control volume. Furthermore, the flow is generally thought to be generally three-dimensional:

$\mathbf{q} = u\mathbf{i} + v\mathbf{j} + w\mathbf{k}$, where:

- \mathbf{i} is the plane YZ versor
- \mathbf{j} is the plane XZ versor
- \mathbf{k} is the plane XY versor

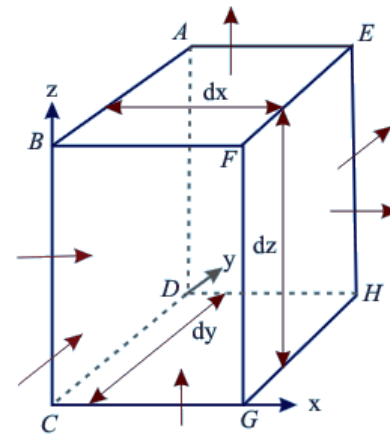


Figure A.2 Control volume

Another important premise concerns the dimensional nature of the equations. Indeed, while the first, the third and the last equation refer to scalar variables (mass, energy and species transport), the second one refers to a vector quantity, possessing a magnitude and a direction in the 3D space; is then possible to convert the vector $\mathbf{p} = m\mathbf{q}$ (and its parent $\hat{\mathbf{p}} = \rho\mathbf{q}$, where ρ is the mass per unit volume) in a set of scalar equations along the three axis (X, Y, Z).

Mass conservation

Starting from the general relation proposed in the previous page, it's possible to define the various components of the equation under examination. Hypothesizing the absence of source or sink ($Q_i = 0$), the total rate of change of the mass is equal to the net flux through the external surface of the control volume. Recalling that the reference property of this case is the density ρ (a scalar variable), the equation becomes:

$$\iiint_V \frac{\partial \rho}{\partial t} dV = - \iint_S \rho (\mathbf{q} \cdot \mathbf{n}) dS$$

Furthermore, using the Gauss divergence¹ theorem, the integral over the bounding surface can be transformed into the volume integral, and then the above equation can be rewritten as:

$$\iiint_V \frac{\partial \rho}{\partial t} dV = - \iiint_V \nabla \cdot (\rho \mathbf{q}) dV \quad \Rightarrow \quad \iiint_V \frac{\partial \rho}{\partial t} dV + \iiint_V \nabla \cdot (\rho \mathbf{q}) dV = 0$$

Being the control volume equal for the two integrals and non-zero, in order to obtain the differential form of the equation, it's possible to rewrite:

$$\iiint_V \left[\frac{\partial \rho}{\partial t} + \nabla \cdot (\rho \mathbf{q}) \right] dV = 0 \quad \Rightarrow \quad \frac{\partial \rho}{\partial t} + \nabla \cdot (\rho \mathbf{q}) = 0$$

Rearranging slightly the found relation and introducing the Lagrangian derivative², the equation becomes:

$$\begin{aligned} \frac{\partial \rho}{\partial t} + \nabla \cdot (\rho \mathbf{q}) &= 0 \quad \Rightarrow \quad \frac{\partial \rho}{\partial t} + \frac{\partial (\rho u)}{\partial x} + \frac{\partial (\rho v)}{\partial y} + \frac{\partial (\rho w)}{\partial z} = 0 \\ \frac{\partial \rho}{\partial t} + \rho \frac{\partial u}{\partial x} + u \frac{\partial \rho}{\partial x} + \rho \frac{\partial v}{\partial y} + v \frac{\partial \rho}{\partial y} + \rho \frac{\partial w}{\partial z} + w \frac{\partial \rho}{\partial z} &= 0 \\ \frac{\partial \rho}{\partial t} + u \frac{\partial \rho}{\partial x} + v \frac{\partial \rho}{\partial y} + w \frac{\partial \rho}{\partial z} + \rho \left[\frac{\partial u}{\partial x} + \frac{\partial v}{\partial y} + \frac{\partial w}{\partial z} \right] &= 0 \\ \frac{\partial \rho}{\partial t} + \mathbf{q} \cdot \nabla \rho + \rho \nabla \cdot \mathbf{q} &= 0 \quad \Rightarrow \quad \frac{D\rho}{Dt} + \rho \nabla \cdot \mathbf{q} = 0 \end{aligned}$$

¹ The divergence theorem states that the outward flux of a tensor field through a closed surface is equal to the volume integral of the divergence over the region inside the surface:

$$\iiint_V \nabla \cdot \mathbf{F} dV = \iint_S \mathbf{F} \cdot \mathbf{n} dS$$

² The Lagrangian derivative describes the time rate of change of a physical quantity subjected to a space-and-time dependent velocity field variations. It can be written as:

$$\frac{D\Phi}{Dt} = \frac{\partial \Phi}{\partial t} + \mathbf{q} \cdot \nabla \Phi$$

Momentum conservation (Newton's second law)

The equation for conservation of momentum can be derived in a similar manner as the equation of mass conservation, as discussed previously. According to Newton's second law, the time rate of change of momentum (the reference property) of a fluid particle is equal to the sum of the volume and surface forces acting on the particle, which, in this case, play the Q_i variables' role. Furthermore, the surface forces can be divided in two sub-categories, i.e normal forces and tangential forces³, which differentiate by the way they operate on the particles. The equation can be written as:

$$\begin{aligned}\iiint_V \frac{\partial(\rho \mathbf{q})}{\partial t} dV &= - \iint_S \rho \mathbf{q} (\mathbf{q} \cdot \mathbf{n}) dS + \mathbf{R} \\ \iiint_V \frac{\partial(\rho \mathbf{q})}{\partial t} dV &= - \iint_S \rho \mathbf{q} (\mathbf{q} \cdot \mathbf{n}) dS + \mathbf{R}_S + \mathbf{R}_V \\ \iiint_V \frac{\partial(\rho \mathbf{q})}{\partial t} dV &= - \iint_S \rho \mathbf{q} (\mathbf{q} \cdot \mathbf{n}) dS - \iint_S p \bar{\mathbf{I}} \cdot \mathbf{n} dS + \iint_S \bar{\mathbf{T}} \cdot \mathbf{n} dS + \iiint_V \rho \mathbf{f} dV\end{aligned}$$

Using the same artifices as in the previous case, the equation can be written as:

$$\begin{aligned}\iiint_V \frac{\partial(\rho \mathbf{q})}{\partial t} dV &= - \iiint_V \nabla \cdot (\rho \mathbf{q} \mathbf{q}) dV - \iiint_V \nabla p dV + \iiint_V \nabla \cdot \bar{\mathbf{T}} dV + \iiint_V \rho \mathbf{f} dV \\ \iiint_V \left[\frac{\partial(\rho \mathbf{q})}{\partial t} + \nabla \cdot (\rho \mathbf{q} \mathbf{q}) \right] dV &= \iiint_V \left[-\nabla p + \nabla \cdot \bar{\mathbf{T}} + \rho \mathbf{f} \right] dV \\ \frac{\partial(\rho \mathbf{q})}{\partial t} + \nabla \cdot (\rho \mathbf{q} \mathbf{q}) &= -\nabla p + \nabla \cdot \bar{\mathbf{T}} + \rho \mathbf{f}\end{aligned}$$

The last equation could be further converted in a set of three scalar equations:

$$\begin{cases} \frac{\partial(\rho u)}{\partial t} + \frac{\partial(\rho uu)}{\partial x} + \frac{\partial(\rho uv)}{\partial y} + \frac{\partial(\rho uw)}{\partial z} = -\frac{\partial p}{\partial x} + \left[\frac{\partial \tau_{xx}}{\partial x} + \frac{\partial \tau_{xy}}{\partial y} + \frac{\partial \tau_{xz}}{\partial z} \right] + \rho f_x \\ \frac{\partial(\rho v)}{\partial t} + \frac{\partial(\rho vu)}{\partial x} + \frac{\partial(\rho vv)}{\partial y} + \frac{\partial(\rho vw)}{\partial z} = -\frac{\partial p}{\partial y} + \left[\frac{\partial \tau_{xy}}{\partial x} + \frac{\partial \tau_{yy}}{\partial y} + \frac{\partial \tau_{yz}}{\partial z} \right] + \rho f_y \\ \frac{\partial(\rho w)}{\partial t} + \frac{\partial(\rho wu)}{\partial x} + \frac{\partial(\rho wv)}{\partial y} + \frac{\partial(\rho ww)}{\partial z} = -\frac{\partial p}{\partial z} + \left[\frac{\partial \tau_{xz}}{\partial x} + \frac{\partial \tau_{yz}}{\partial y} + \frac{\partial \tau_{zz}}{\partial z} \right] + \rho f_z \end{cases}$$

³ Tangential forces are due to the presence of the internal friction. The physical result can be represented by the friction tensor $\bar{\mathbf{T}}$, so defined:

$$\bar{\mathbf{T}} = \begin{bmatrix} \tau_{xx} & \tau_{xy} & \tau_{xz} \\ \tau_{yx} & \tau_{yy} & \tau_{yz} \\ \tau_{zx} & \tau_{zy} & \tau_{zz} \end{bmatrix} \xrightarrow{\text{symmetric matrix}} \bar{\mathbf{T}} = \begin{bmatrix} \tau_{xx} & \tau_{xy} & \tau_{xz} \\ \tau_{xy} & \tau_{yy} & \tau_{yz} \\ \tau_{xz} & \tau_{yz} & \tau_{zz} \end{bmatrix}$$

Energy conservation (First law of thermodynamics)

The energy equation is derived by the physical principle that the amount of energy remains constant and energy is neither created nor destroyed but it could only be converted from one form to another. The rate of energy change equals the sum of the rate of heat addition and the rate of work done on (or by) the particle, which play the role of source/sink and could be further divided up to their physical action (if acting on the surface or on the volume). Then, the equation can be written as:

$$\iiint_V \frac{\partial(\rho E)}{\partial t} dV = - \iint_S \rho E (\mathbf{q} \cdot \mathbf{n}) dS + \mathcal{E}$$

$$\iiint_V \frac{\partial(\rho E)}{\partial t} dV = - \iint_S \rho E (\mathbf{q} \cdot \mathbf{n}) dS + W + A$$

where W refer to Wärme (heat) and A to Arbeiten (work).

$$\iiint_V \frac{\partial(\rho E)}{\partial t} dV = - \iint_S \rho E (\mathbf{q} \cdot \mathbf{n}) dS + W_S + W_V + A_S + A_V$$

$$\begin{aligned} \iiint_V \frac{\partial(\rho E)}{\partial t} dV &= - \iint_S \rho E (\mathbf{q} \cdot \mathbf{n}) dS - \iint_S p (\mathbf{q} \cdot \mathbf{n}) dS + \dots \\ \dots + \iint_S (\bar{\mathbf{T}} \cdot \mathbf{q}) \cdot \mathbf{n} dS + \iiint_V \rho (\mathbf{f} \cdot \mathbf{q}) dV - \iint_S \mathbf{K} \cdot \mathbf{n} dS + \iiint_V \rho \dot{q} dV \end{aligned}$$

Using the same artefices as previously and reminding that $\mathbf{K} = -\lambda \nabla T$ (Fourier's postulate), the equation becomes:

$$\begin{aligned} \iiint_V \frac{\partial(\rho E)}{\partial t} dV &= - \iiint_V \nabla \cdot (\rho E \mathbf{q}) dV - \iiint_V \nabla \cdot (p \mathbf{q}) dV + \dots \\ \dots + \iiint_V \nabla \cdot (\bar{\mathbf{T}} \cdot \mathbf{q}) dV + \iiint_V \rho (\mathbf{f} \cdot \mathbf{q}) dV - \iiint_V \nabla \cdot \mathbf{K} dV + \iiint_V \rho \dot{q} dV \\ \frac{\partial(\rho E)}{\partial t} &= -\nabla \cdot (\rho E \mathbf{q}) - \nabla \cdot (p \mathbf{q}) + \nabla \cdot (\bar{\mathbf{T}} \cdot \mathbf{q}) + \rho (\mathbf{f} \cdot \mathbf{q}) - \nabla \cdot \mathbf{K} + \rho \dot{q} \\ \frac{\partial(\rho E)}{\partial t} &= -\nabla \cdot (\rho E \mathbf{q}) - \nabla \cdot (p \mathbf{q}) + \nabla \cdot (\bar{\mathbf{T}} \cdot \mathbf{q}) + \rho (\mathbf{f} \cdot \mathbf{q}) + \lambda \cdot \nabla^2 T + \rho \dot{q} \end{aligned}$$

Species transport conservation

In case of fuel combustion, the conservation equations for each chemical species of interest have the following form:

$$\frac{\partial(\rho Y_i)}{\partial t} = -\nabla \cdot (\rho \mathbf{q} Y_i) - \nabla \cdot \mathbf{J}_i + R_i + S_i \quad i = 1, \dots, I$$

where Y is the local mass fraction, \mathbf{J} the diffusion flux (linked to Fick's laws of diffusion), R the net rate of production by chemical reaction and S the rate of creation by addition from the dispersed phase plus any defined sources.

Appendix B

Particle Swarm Optimization Example

In order to clarify the PSO algorithm functioning, this chapter, which contains an example of how the PSO algorithm works, has been added. The chosen objective function is a 3D curve, whose formula is:

$$X3 = (X1 - 5)^2 + (X2 - 5)^2 + 30 \cdot [\sin(X1 - 5) + \dots \\ \dots + \sin(X1 + 5) + \cos(X2 - 5) + \cos(X2 + 5)]$$

This function has been chosen since it's very easy, continuous and defined in the whole domain ($f : \mathbb{R}^3 \rightarrow \mathbb{R}$). Furthermore, it shows some local minima around its global minimum (see figure B.1 and figure B.2); this feature makes it perfect to see if the PSO algorithm is valid to find its absolute minimum.

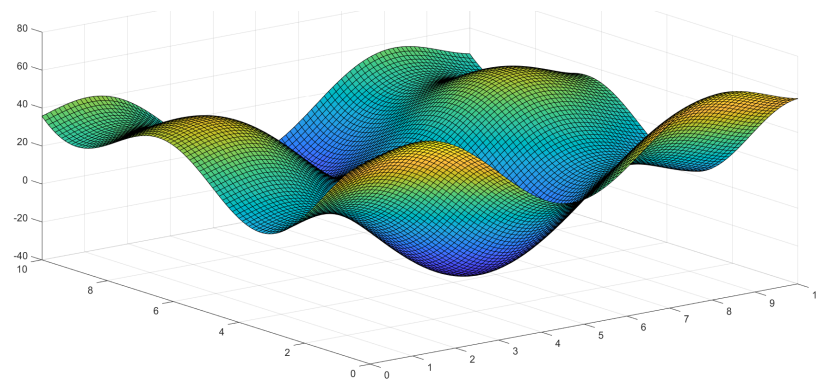


Figure B.1
Function
3D curve

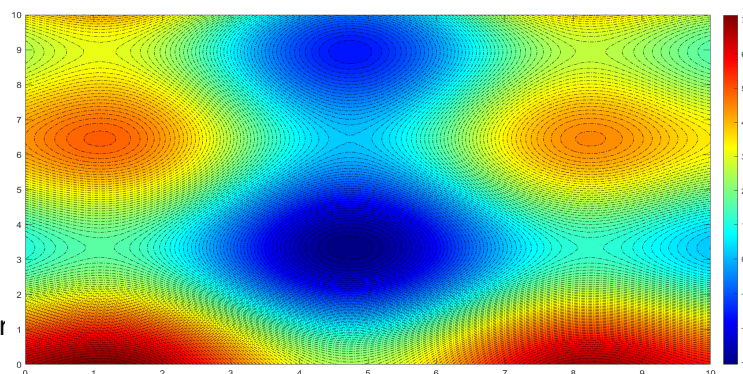


Figure B.2 Contour
lines

Thanks to another optimization MATLAB algorithm (*GlobalSearch*), it's possible to get the certain global minimum of the objective function. This results is then going to be compared with the PSO output, hoping that the two values are equal. For the particle swarm optimization, the parameters shown in table B.1 have been used.

Parameter	Value
Swarm Size	10
Iterations	40
c_1	0.1
c_2	3.9
ω	0.4
d	10
\mathbf{x}_i^1	rand[]
\mathbf{v}_i^1	{0}

Table B.1 Input parameters

The solution process is explained through the following images, which show the first, the second, the eighth and the last iteration:

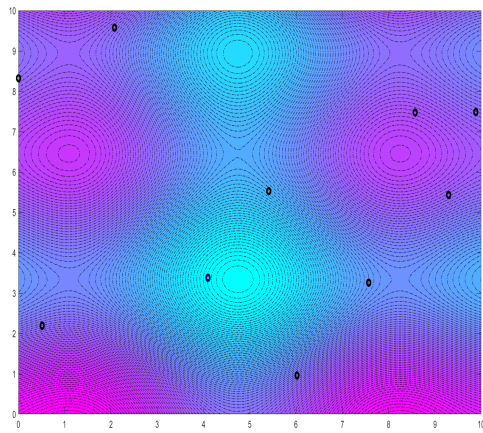


Figure B.3 First PSO iteration

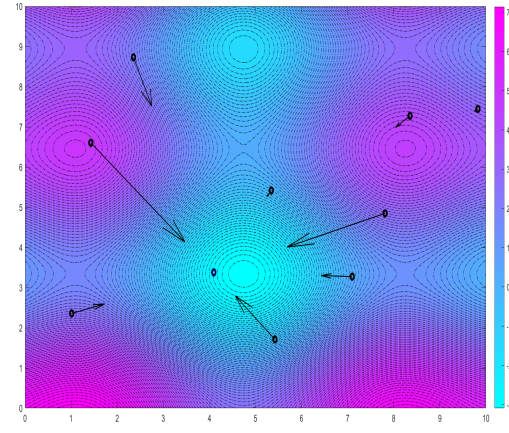


Figure B.4 Second PSO iteration

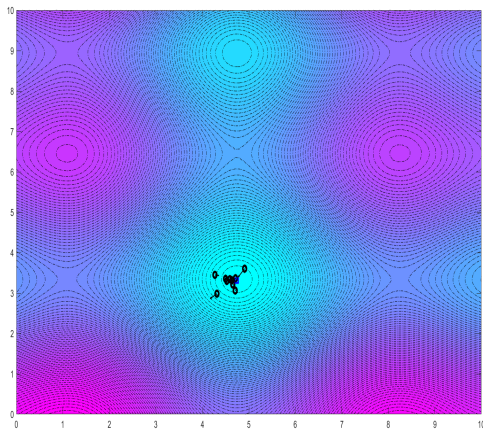


Figure B.5 Eighth PSO iteration

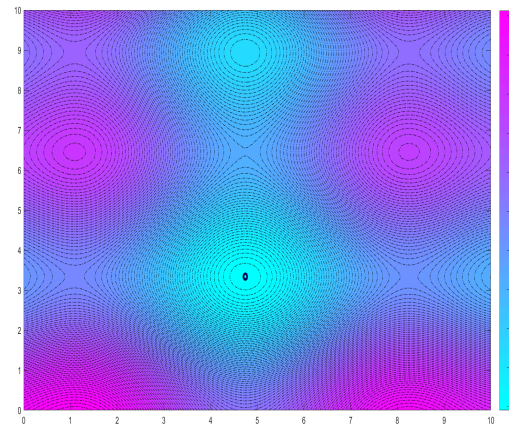


Figure B.6 Last PSO iteration

As shown in the figures, the particles start their journey from random points. In the second iterations, they gain velocity starting to converge to the global minimum point. Despite of the little number of particle, as early as in the 8-th iteration, most of the particles can be found in the surroundings of the best point, which is fully reached at the last iterations (the global minimum point is the same found with the *GlobalSearch* function, i.e. $X1 = 4.7426$ and $X2 = 3.3381$).

Appendix C

MATLAB functions

C.1 *nchoosek*

Binomial coefficient or all combinations.

Syntax

- $b = \text{nchoosek}(n,k)$
- $C = \text{nchoosek}(v,k)$

Description

- $b = \text{nchoosek}(n,k)$ returns the binomial coefficient, defined as $\frac{n!}{(n-k)!k!}$. It is the number of combinations of n items taken k at a time
- $C = \text{nchoosek}(v,k)$ returns a matrix containing all possible combinations of the elements of vector v taken k at a time. Matrix C has k columns and $\frac{n!}{(n-k)!k!}$ rows, where n is $\text{length}(v)$

Example

The command `nchoosek(2:2:10,4)` returns the even numbers from two to ten, taken four at a time:

$$C = \begin{bmatrix} 2 & 4 & 6 & 8 \\ 2 & 4 & 6 & 10 \\ 2 & 4 & 8 & 10 \\ 2 & 6 & 8 & 10 \\ 4 & 6 & 8 & 10 \end{bmatrix}$$

Limitations

This function is only practical for situations where n is about 15-20.

C.2 *ndgrid*

Rectangular grid in ND space.

Syntax

- $[X_1, X_2, \dots, X_n] = \text{ndgrid}(x_1, x_2, \dots, x_n)$
- $[X_1, X_2, \dots, X_n] = \text{ndgrid}(x_g)$

Description

- $[X_1, X_2, \dots, X_n] = \text{ndgrid}(x_1, x_2, \dots, x_n)$ replicates the grid vectors x_1, x_2, \dots, x_n to produce an n-dimensional full grid
- $[X_1, X_2, \dots, X_n] = \text{ndgrid}(x_g)$ specifies a single grid vector x_g to use for all dimensions. The number of output specified arguments determines the dimensionality n of the output

Examples

Create a 2D grid from the vectors $[1, 3, 5, 7, 9, 11, 13, 15]$ and $[2, 4, 6, 8, 10, 12]$.

$[X, Y] = \text{ndgrid}(1 : 2 : 13, 2 : 2 : 12)$

$$X = \begin{bmatrix} 1 & 1 & 1 & 1 & 1 & 1 \\ 3 & 3 & 3 & 3 & 3 & 3 \\ 5 & 5 & 5 & 5 & 5 & 5 \\ 7 & 7 & 7 & 7 & 7 & 7 \\ 9 & 9 & 9 & 9 & 9 & 9 \\ 11 & 11 & 11 & 11 & 11 & 11 \\ 13 & 13 & 13 & 13 & 13 & 13 \end{bmatrix} \quad Y = \begin{bmatrix} 2 & 4 & 6 & 8 & 10 & 12 \\ 2 & 4 & 6 & 8 & 10 & 12 \\ 2 & 4 & 6 & 8 & 10 & 12 \\ 2 & 4 & 6 & 8 & 10 & 12 \\ 2 & 4 & 6 & 8 & 10 & 12 \\ 2 & 4 & 6 & 8 & 10 & 12 \\ 2 & 4 & 6 & 8 & 10 & 12 \end{bmatrix}$$

Input arguments

Grid vectors, specified as vectors containing grid coordinates for each dimension. The grid vectors implicitly define the grid. For example, in 2D:

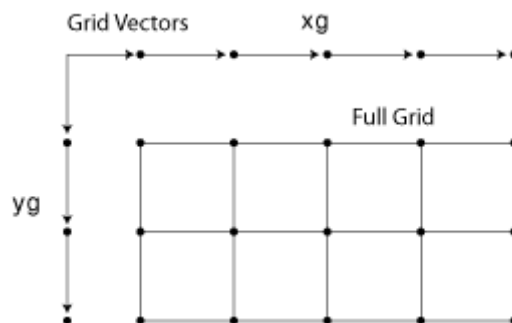


Figure C.1 Input arguments

Tips

The *ndgrid* function is similar to *meshgrid*. However, *ndgrid* supports 1D to ND while *meshgrid* is restricted to 2D and 3D.

C.3 *parfor*

Execute for-loop iterations in parallel on workers.

Syntax

- `parfor loopVar = initVal:endVal; statements; end`
- `parfor (loopVar = initVal:endVal,M); statements; end`
- `parfor (loopVar = initVal:endVal,opts); statements; end`
- `parfor (loopVar = initVal:endVal,cluster); statements; end`

Description

- `parfor loopVar = initVal:endVal; statements; end`
It executes for-loop iterations in parallel on workers in a parallel pool. MATLAB executes the loop body commands in statements for values of `loopVar` between `initVal` and `endVal`. `loopVar` specifies a vector of integer values increasing by 1. If you have Parallel Computing Toolbox™, the iterations of statements can execute on a parallel pool of workers on your multi-core computer or cluster. As with a for-loop, you can include a single line or multiple lines in statements. *parfor* differs from a traditional for-loop in the following ways:
 - Loop iterations are executed in parallel in a non-deterministic order
 - Loop iterations must be consecutive, increasing integer values
 - The body of the *parfor*-loop must be independent. One loop iteration cannot depend on a previous iteration, because the iterations are executed in a nondeterministic order
 - You cannot use a *parfor*-loop inside another *parfor*-loop
- `parfor (loopVar = initVal:endVal,M); statements; end`
It uses `M` to specify the maximum number of workers from the parallel pool to use in evaluating statements in the loop body. `M` must be a non-negative integer. By default, MATLAB uses the available workers in your parallel pool. You can change the number of workers on the Home tab in the Environment section, by selecting Parallel > Parallel Preferences. You can override the default number of workers in a parallel pool by using `parpool`. When no workers are available in the pool or `M` is zero, MATLAB still executes the loop body in a non-deterministic order, but not in parallel. Furthermore, by default, if you execute *parfor*, you automatically create a parallel pool of workers on the cluster defined by your default cluster profile. The default cluster is local. You can change your cluster in Parallel Preferences.

- `parfor (loopVar = initVal:endVal,opts); statements; end`
It uses `opts` to specify the resources to use in evaluating statements in the loop body. Create a set of *parfor* options using the `parforOptions` function. With this approach, you can run *parfor* on a cluster without first creating a parallel pool and control how *parfor* partitions the iterations into subranges for the workers.
- `parfor (loopVar = initVal:endVal,cluster); statements; end`
It executes statements on workers in cluster without creating a parallel pool. This is equivalent to executing
`parfor (loopVar = initVal:endVal,parforOptions(cluster)); statements; end.`

Tips

- Use a *parfor*-loop when:
 - You have many loop iterations of a simple calculation. *parfor* divides the loop iterations into groups so that each thread can execute one group of iterations
 - You have some loop iterations that take a long time to execute
- Do not use a *parfor*-loop when an iteration in your loop depends on the results of other iterations
- When you use *parfor*, you have to wait for the loop to complete to obtain your results. Your client MATLAB is blocked and you cannot break out of the loop early. If you want to obtain intermediate results, or break out of a for-loop early, try *parfeval* instead
- Unless you specify a cluster object, a *parfor*-loop runs on the existing parallel pool. If no pool exists, *parfor* starts a new parallel pool, unless the automatic starting of pools is disabled in your parallel preferences. If there is no parallel pool and *parfor* cannot start one, the loop runs serially in the client session
- You cannot call scripts directly in a *parfor*-loop
- Do not use `clear` inside a *parfor* loop because it violates workspace transparency

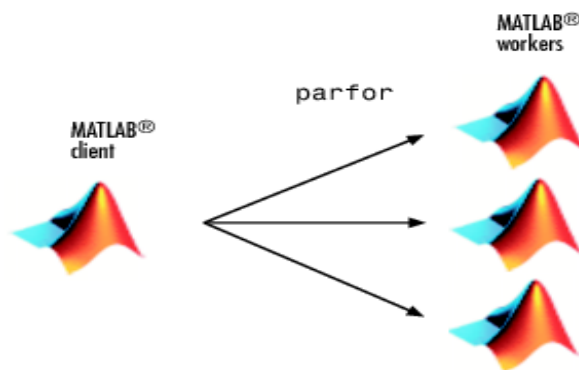


Figure C.2 *parfor* function

C.4 *fmincon*

Find minimum of constrained nonlinear multivariable function.

Nonlinear programming solver.

Finds the minimum of a problem specified by:

$$\min_x f(x) \text{ such that: } \begin{cases} c(x) \leq 0 \\ c_{eq}(x) = 0 \\ A \cdot x \leq b \\ A_{eq} \cdot x = b_{eq} \\ lb \leq x \leq ub \end{cases}$$

b and b_{eq} are vectors, A and A_{eq} are matrices, $c(x)$ and $c_{eq}(x)$ are functions that return vectors, and $f(x)$ is a function that returns a scalar. $f(x)$, $c(x)$ and $c_{eq}(x)$ can be nonlinear functions. x , lb , and ub can be passed as vectors or matrices.

Syntax

- $x = \text{fmincon}(\text{fun}, x_0, A, b)$
- $x = \text{fmincon}(\text{fun}, x_0, A, b, A_{eq}, b_{eq})$
- $x = \text{fmincon}(\text{fun}, x_0, A, b, A_{eq}, b_{eq}, lb, ub)$
- $x = \text{fmincon}(\text{fun}, x_0, A, b, A_{eq}, b_{eq}, lb, ub, \text{nonlcon})$
- $x = \text{fmincon}(\text{fun}, x_0, A, b, A_{eq}, b_{eq}, lb, ub, \text{nonlcon}, \text{options})$
- $x = \text{fmincon}(\text{problem})$
- $[x, fval] = \text{fmincon}(___)$
- $[x, fval, \text{exitflag}, \text{output}] = \text{fmincon}(___)$
- $[x, fval, \text{exitflag}, \text{output}, \text{lambda}, \text{grad}, \text{hessian}] = \text{fmincon}(___)$

Description

- $x = \text{fmincon}(\text{fun}, x_0, A, b)$ starts at x_0 and attempts to find a minimizer x of the function described in fun subject to the linear inequalities $A \cdot x \leq b$. x_0 can be a scalar, vector or matrix.
- $x = \text{fmincon}(\text{fun}, x_0, A, b, A_{eq}, b_{eq})$ minimizes fun subject to the linear equalities $A_{eq} \cdot x = b_{eq}$ and $A \cdot x \leq b$. If no inequalities exist, set $A = []$ and $b = []$.
- $x = \text{fmincon}(\text{fun}, x_0, A, b, A_{eq}, b_{eq}, lb, ub)$ defines a set of lower and upper bounds on the design variables in x , so that the solution is always in the range $lb \leq x \leq ub$. If no equalities exist, set $A_{eq} = []$ and $b_{eq} = []$. If $x(i)$ is unbounded below, set $lb(i) = -\text{Inf}$; if it's unbounded above, set $ub(i) = \text{Inf}$.
- $x = \text{fmincon}(\text{fun}, x_0, A, b, A_{eq}, b_{eq}, lb, ub, \text{nonlcon})$ subjects the minimization to the nonlinear inequalities $c(x)$ or equalities $c_{eq}(x)$ defined in nonlcon . *fmincon* optimizes such that $c(x) \leq 0$ and $c_{eq}(x) = 0$. If no bounds exist, set $lb = []$ and $ub = []$.

- $x = \text{fmincon}(\text{fun}, x_0, A, b, A_{eq}, b_{eq}, lb, ub, \text{nonlcon}, \text{options})$ minimizes with the optimization options specified in *options*. Use *optimoptions* to set these options. If there are no nonlinear inequality or equality constraints, set *nonlcon* = [].
- $x = \text{fmincon}(\text{problem})$ finds the minimum for *problem*, where *problem* is a structure described.
- $[x, fval] = \text{fmincon}(__)$, for any syntax, returns the value of the objective function *fun* at the solution x .
- $[x, fval, \text{exitflag}, \text{output}] = \text{fmincon}(__)$ additionally returns a value *exitflag* that describes the exit condition of *fmincon*, and a structure *output* with information about the optimization process.
- $[x, fval, \text{exitflag}, \text{output}, \text{lambda}, \text{grad}, \text{hessian}] = \text{fmincon}(__)$ additionally returns:
 - *lambda*: structure with fields containing the Lagrange multipliers at the solution x
 - *grad*: gradient of *fun* at the solution x
 - *hessian*: Hessian of *fun* at the solution x . The Hessian for a constrained problem is the Hessian of the Lagrangian. For an objective function f , nonlinear inequality constraint vector c , and nonlinear equality constraint vector c_{eq} , the Lagrangian is:

$$L = f + \sum_i \lambda_i c_i + \sum_j \lambda_j c_{eq_j}$$

where λ_i are Lagrange multipliers. The Hessian of the Lagrangian is:

$$H = \nabla^2 L = \nabla^2 f + \sum_i \lambda_i \nabla^2 c_i + \sum_j \lambda_j \nabla^2 c_{eq_j}$$

***fmincon* algorithms**

fmincon has five algorithm options:

- 'INTERIOR-POINT' (default)
- 'TRUST-REGION-REFLECTIVE'
- 'SQP'
- 'SQP-LEGACY'
- 'ACTIVE-SET'

Use *optimoptions* to set the Algorithm option at the command line.

Use the 'INTERIOR-POINT' algorithm first. To run an optimization again to obtain more speed on small-to-medium sized problems, try 'SQP' next and 'ACTIVE-SET' last. Use 'TRUST-REGION-REFLECTIVE' when applicable. The problem must have: objective function includes gradient, or bounds or linear equality constraints (not both).

C.5 *particleswarm*

Particle swarm optimization.

Syntax

- `x = particleswarm(fun,nvars)`
- `x = particleswarm(fun,nvars,lb,ub)`
- `x = particleswarm(fun,nvars,lb,ub,options)`
- `x = particleswarm(problem)`
- `[x,fval,exitflag,output] = particleswarm(____)`

Description

- `x = particleswarm(fun,nvars)` attempts to find a vector x that achieves a local minimum of fun . $nvars$ is the dimension (number of variables) of fun .
- `x = particleswarm(fun,nvars,lb,ub)` defines a set of lower and upper bounds on the variables in x , so that a solution is found in the range $lb \leq x \leq ub$.
- `x = particleswarm(fun,nvars,lb,ub,options)` minimizes with the default optimization parameters replaced by values in `options`. Set $lb = []$ and $ub = []$ if no bounds exist.
- `x = particleswarm(problem)` finds the minimum for `problem`, where `problem` is a structure.
- `[x,fval,exitflag,output] = particleswarm(____)`, for any input arguments described above, returns:
 - A scalar $fval$, which is the objective function value $fun(x)$
 - A value $exitflag$ describing the exit condition
 - An *output* containing information about the optimization process

Stopping Option	Stopping Test	Exit Flag
MaxStallIterations and FunctionTolerance	Relative change in the best objective function value g over the last MaxStallIterations iterations is less than FunctionTolerance	1
MaxIterations	Number of iterations reaches MaxIterations	0
OutputFcn or PlotFcn	OutputFcn or PlotFcn can halt the iterations	-1
ObjectiveLimit	Best objective function value g is less than or equal to ObjectiveLimit	-3
MaxStallTime	Best objective function value g did not change in the last MaxStallTime seconds	-4
MaxTime	Function run time exceeds MaxTime seconds	-5

Table C.1 *exitflag* table